A TUNNELING INVESTIGATION OF SUPERCONDUCTIVITY

A TUNNELING INVESTIGATION OF THE MECHANISMS DETERMINING SUPERCONDUCTIVITY IN SIMPLE METALS AND ALLOYS

by

ROBERT CARR DYNES, B.Sc., M.Sc.

A Thesis

Submitted to the Faculty of Graduate Studies

in Partial fulfilment of the Requirements

for the Degree

Doctor of Philosophy

McMaster University

May 1968

DOCTOR OF PHILOSOPHY (1968)
(Physics)

McMASTER UNIVERSITY
Hamilton, Ontario

TITLE: A Tunneling Investigation of the Mechanisms Determining Superconductivity in Simple Metals and Alloys

AUTHOR: Robert Carr Dynes, B.Sc. (University of Western Ontario)
M.Sc. (McMaster University)

SUPERVISOR: Professor C. K. Campbell

NUMBER OF PAGES: vii, 167

SCOPE AND CONTENTS:

The present knowledge of lattice dynamics in particular solids is applied to the theory of strongly coupled superconductors. From existing phonon data, the product function $\alpha^2(\omega)F(\omega)$ is determined in various materials, where $\alpha^2(\omega)$ is the electron-phonon coupling term, and $F(\omega)$ is the phonon density of states of that material. The Eliashberg gap equations are solved for these particular materials using this product function and predictions of the superconducting energy gap $\Delta(\Delta_o)$ and tunneling electron density of states $N_T(\omega)$ are made.

Tunneling experiments are performed on selected Tℓ-Pb-Bi alloys where this phonon information is available and comparisons are made both of the predicted and obtained $\Delta(\Delta_o)$ and the tunneling density of states $N_T(\omega)$.

PREFACE

This Thesis is based on a program carried out over the past three years on the topic of electron tunneling between superconductors. Its purpose is two-fold. Firstly, it seeks to investigate what the important properties are which determine whether a material is a superconductor or not. For simple metals this is put on a quantitative basis with encouraging results. Secondly, it attempts to critically analyze the value of tunneling as a method of phonon spectroscopy. It is shown that this method gives excellent agreement with other reliable methods in the location of critical points. The Tℓ-Pb-Bi alloy system, ranging from 3.2 electrons/atom to 4 electrons/atom is studied in this vein.

In many places in this Thesis, both in theoretical descriptions and experimental details, rigour is sacrificed in an effort to preserve clarity and continuity.

Deep gratitude must be expressed to my Supervisor, Professor C. K. Campbell for his tolerance and patient guidance throughout this programme.

It is a pleasure to thank Dr. J. P. Carbotte for sharing with me his inspiration and enthusiasm at darker moments.

The author would also like to express his appreciation to the National Research Council of Canada both for personal finance in the form of an N.R.C. Studentship and a grant-in-aid to Dr. Campbell in support of the project.

In addition, thanks must be extended to Professor B. N. Brockhouse and his neutron scattering group, particularly Dr. S. C. Ng for valuable discussions and data prior to publication. For valuable discussions and impetus, acknowledgments are due to Drs. J. Shewchun, C. V. Stager, D. W. Taylor and E. J. Woll.

Finally, I should like to thank my wife, Christel, whose contribution was inestimable.

TABLE OF CONTENTS

CHAPTER I

INTRODUCTION

1.1 HISTORICAL INTRODUCTION:

Since the discovery of the seemingly unnatural disappearance of all d-c resistivity in mercury below 4.2°K by Onnes[1] in 1911, many investigators have expended much time and effort in an attempt to explain and describe many of the curious traits associated with this phenomenon of superconductivity[2]. Since that time, it has been discovered that many metals, alloys[3], and even some semiconductors[4,5], experience this transition to a completely non-resistive state. In this Chapter, the basic development of the thoughts and theories of the more prominent investigators will be traced from the first macroscopic phenomenological descriptions, some of which display amazing insight, to the present day microscopic explanations. In conjunction with these theories, the results of certain key experiments which have inspired this trail will be presented.

1.2 PHONOMENOLOGICAL THEORIES:

One of the first successful models proposed to incorporate the reversibility of the process in a correct thermodynamic treatment, was the two-fluid model of Gorter and Casimir[6]. It was suggested that below a certain critical temperature, T_c, the electrons available for conduction could be divided into two classes. Firstly, a fraction of these, ϕ,

remained unchanged and remained "normal" while the others $(1 - \phi)$, it was postulated, slipped into some sort of "superconducting" state in such a manner that at

$$T = T_c, \qquad \phi = 1$$

$$\text{and at} \qquad T = 0^{\circ}K, \qquad \phi = 0$$

By using this suggestion, and fitting results wherever possible to experimental knowledge, a minimization of the free energy of the electrons at a given T yielded the result:

$$\phi = (T/T_c)^4$$

Hence, the proportion of superconducting to normal electrons is seen to increase very rapidly below T_c.

This model leads to rather good quantitative agreement in predicting the electronic specific heat in the superconducting state, as well as to an expression for the critical magnetic field (the applied field required to drive the superconductor into the normal state) as a function of temperature.

$$H_c = H_o\left(1 - \left(\frac{T}{T_c}\right)^2\right)$$

where H_o = critical field at $T = 0^{\circ}K$

This agreement was not overly surprising since the theory was originally based on experimental results and is consequently not much more than a description.

In 1933 Meissner and Ochsenfeld discovered another curious property of the superconducting state. A magnetic field impressed onto the

material penetrates only a few hundred angstroms into the bulk. In addition, a magnetic field penetrating the material in the normal state is completely expelled as the sample is cooled through the transition temperature.

This experimental fact inspired the development of the phenomenological, and yet very profound London equations[8] by Heinz and Fritz London. These electromagnetic equations described both the infinite conductivity of a superconductor, and its perfect diamagnetic behaviour. It is to be noted, however, that in their original form, the equations were postulated not to explain why superconductivity existed, but simply to describe the phenomenon.

Using these equations, one can also describe the shallow penetration of a magnetic field into a superconductor by:

$$B(x) = B(0)\, e^{-x/\lambda_L}$$

where

$B(0)$ = magnetic field at the surface of the superconductor

x = distance into the superconductor

λ_L = London penetration depth

$$= \left(\frac{mc^2}{4\pi n_s e^2}\right)^{\frac{1}{2}}$$

m = electron mass
c = velocity of light

e = electronic charge

n_s = number of superconducting electrons in the system

Of even more significance in some respects was the introduction by F. London[9] of the concept of the "stiff" wave function to describe the ground state of the many-body superfluid. It is this rigid ground state wave function with respect to small perturbations, suggesting that a finite energy is required to create excitations in the system, that gave the first hint of the existence of an energy gap in the excitation spectrum.

Utilizing these concepts one can describe many of the phenomena associated with superconductors, including the Meissner effect, zero resistivity, frequency dependence[10], and the recently observed quantization of flux[11,12].

Pippard[13] suggested a modification to the London equations in order to explain certain experimental results. His non-local extension implied that more than simple nearest neighbour interactions need be considered and that the superconducting electron is "aware" of events occuring over a rather large spatial range ($\approx 10^{-4}$ cms). As we shall see later,this non-local concept is of central importance in the microscopic theory of superconductivity.

In addition to these developments, there was a growing belief that there was an energy gap[14] in the spectrum of electron excitations in a superconductor. Several different experiments had been performed on various superconductors; thermal conductivity[15], electronic specific heat, ultrasonic and infra red absorption, all of which seemed to indicate the existence of a gap in the energy spectrum.

1.3 DEVELOPMENT OF A MICROSCOPIC THEORY:

In 1950-51 it was found by Maxwell[15] and Reynolds et al[16] that the critical temperature T_c of various isotopes of mercury depended on the atomic mass such that,

$$T_c M^{\alpha} = \text{constant}$$

where $\alpha \approx \frac{1}{2}$

Similar behaviour was found subsequently in other materials and the obvious conclusion was drawn,namely, that on the microscopic scale, the mechanism responsible for the onset of superconductivity must have something to do with the lattice of the material.

This experimental observation and conclusion inspired a more intensive search between the years of 1950-1957 for the correct model to describe the system. Fröhlich[17] proposed that superconductivity arose from the electron-phonon interaction, and displayed a good correlation between his predicted and observed occurence of superconductivity in the non-transition metals. In attempting to put this prediction on a firmer basis and describe accurately the new state, he was confronted with difficulty when he used a perturbation approach. This independent particle attack, using perturbation methods, could not describe the co-operative features of a superconductor.

Landau[18,19] showed that one could deal with an electron gas by describing excitations from the ground state in terms of "quasiparticles". These quasiparticles were regarded as particles in a self-consistant field of surrounding particles with long lifetimes. Due to the fact that

these are long lived particles, the excitations are very well defined.

Using the results of Fröhlich, Cooper[20] studied the simple problem of a single pair of electrons interacting with each other above the non-interacting Fermi sea - via a two-body potential V first derived by Fröhlich. Using this simple model, Cooper proved that if this potential was attractive, a bound state was formed into which this pair could fall. He suggested that the instability of the normal phase and consequent onset of the superconducting state was due to many pairs of electrons falling into these bound states. A simple summation of all the binding energies involved indicated that this simple pair model was deficient and required the work of Bardeen, Cooper and Schrieffer[21] (hereafter referred to as B.C.S.) to describe accurately the superconducting state. They considered the simple Cooper problem with very strongly overlapping pairs, such that there must be a large coherence between different pairs (dictated simply by the Pauli principle).

Later work by Nambu[22] and Eliashberg[23] and Schrieffer[24] incorporated the sophistication of retardation and lifetime effects which more adequately and quantitatively described the basic interactions.

1.4 SUPERCONDUCTIVE TUNNELING:

One of the natural consequences of the B.C.S. description of a superconductor was the existance of an energy gap for quasiparticle excitations from the superconducting ground state. Indirect evidence of this gap[14] had been accumulated for several years, but it was not until the pioneer experiments of Giaever[25] that the existence of the gap was conclusively confirmed and found to agree very well with the predictions

of B.C.S. By causing electrons to tunnel from a normal metal thin film, through an insulating oxide, into a thin-film superconductor, Giaever was able to measure very accurately, from the current-voltage characteristics of such a device, the energy gap of the superconductor in question.

This breakthrough inspired many experiments on a wide range of superconductive materials, to measure energy gaps and compare these with the predicted B.C.S. values. It was Giaever et al[26] who first noticed slight deviations from the B.C.S. predicted excitation spectrum in lead. These deviations were more extensively investigated by Rowell, Anderson and Thomas[27] and it was noted that there was a close correlation between these deviations and the van Hove critical points in the phonon density of states as determined by inelastic neutron scattering data[28]. A noteworthy description of these deviations[29] - in terms of damping effects and retardation in systems with strong electron-phonon coupling - lead to an inversion of this method[30], whereby using data obtained from a tunneling experiment, a calculation was made of the product function $\alpha^2(\omega)F(\omega)$

where $F(\omega)$ = phonon density of states

$\alpha^2(\omega)$ = electron-phonon coupling function

This calculation opened the possibility of using this tunneling technique as a valuable tool in phonon spectroscopy.

1.5 SCOPE OF THESIS:

It is hoped that this Thesis will bring an experimentalist closer to an understanding of the fundamental theoretical concepts in the field of superconductivity. Where the derivations are tedious and void of any

physical insight results are simply quoted.

Chapter II provides a simple description of electrons in solids, of lattice vibrations, and how these interact.

Chapter III is a brief outline of the B.C.S. theory of superconductivity mainly as it is applied to the description of the energy gap. The fundamental concepts are discussed at the expense of rigour.

In the next Chapter, a description of how one incorporates lifetime effects into the electron-phonon-electron interaction is outlined and the very important results of this incorporation are stressed.

In Chapter V, tunneling theory is discussed as it is applied to electrons tunneling between superconductors, and it is shown how one can, by employing this experimental technique, extract information about the energy gap, as well as the phonon density of states.

The apparatus used in the experimental portion of this Thesis is described in Chapter VI. Only where the techniques differ from standard ones, or are new, is any attempt made to describe the systems in any detail. Appropriate references are cited for situations where the methods are indeed standard.

In Chapter VII, results of calculations of $\alpha^2(\omega)F(\omega)$ for sodium, potassium, aluminum and selected alloys of the thallium-lead-bismuth alloy system are reported and the predicted superconducting nature of these materials, derived from these calculations is discussed. Tunneling experiments on these alloys are also reported and the comparison of the results of predictions and experiments is striking. The validity of the tunneling method as a spectroscopic tool to probe phonon densities of states is outlined and its limitations are pointed out.

Finally, in an Appendix, an outline of some of the calculations performed is presented and the theory behind such calculations is described.

CHAPTER II

ELECTRONS AND PHONONS

In order to gain insight into any physical phenomenon, it is first necessary to study, in some detail, the underlying constituents of that phenomenon, and the interaction of these constituents. Only then can one acquire any knowledge or understanding of the phenomenon and develop predictions of a reliable nature.

Such is the case of superconductivity. In order to understand and explain many of the properties associated with a superconductor, we must critically examine the mechanisms responsible for these characteristics. From the isotope effect[15,16], and from electron tunneling experiments[27,29,30], it is now generally believed that, at least in simple metals, the basic mechanism responsible for the superconducting state is the electron-phonon interaction. Hence, it is essential, before one investigates the properties and characteristics of a superconductor, that one first consider the "bare" constituents of this effect and how they interact to produce the macroscopic result.

2.1 BARE PHONONS:

Let us consider a three dimensional lattice which contains N atoms, the equilibrium position of the ℓ^{th} atom in that lattice given by $R(\overset{0}{\ell})$. Suppose that the excursion of that atom from its equilibrium

position is given by $u(\ell)$ such that the actual position of the ℓ^{th} atom is given by:

$$\underline{r}(\ell)=\underline{R}(\overset{0}{\ell}) + \underline{u}(\ell) \qquad \text{------(2-1)}$$

and that the interaction between two atoms ℓ and ℓ' is given by

$$V(\underline{r}(\ell) - \underline{r}(\ell'))$$

We can very simply describe the Hamiltonian of such a system as the sum of the kinetic energy of the atoms and the potential energy summed over all combinations of atoms.

$$H = \sum_{\ell=1}^{N} \frac{p^2(\ell)}{2M} + \sum_{\substack{\ell,\ell' \\ \ell\neq\ell'}}^{N\,N} \frac{1}{2} V(\underline{r}(\ell) - \underline{r}(\ell')) \qquad \text{--(2-2)}$$

In all of this discussion it is assumed that the primitive unit cell of the lattice contains only one atom. Using a Taylor expansion, this potential term can be expanded about the equilibrium point of the ion positions to obtain to second order

$$V = V_o + \sum_{\ell\alpha} \frac{\partial V}{\partial u_\alpha(\ell)} u_\alpha(\ell) + \sum_{\ell\ell'\alpha\beta} \frac{\partial^2 V}{\partial u_\alpha(\ell)\partial u_\beta(\ell')} u_\alpha(\ell)u_\beta(\ell') + \ldots\ldots \qquad \text{------(2-3)}$$

where the summations are over atomic positions and over the three directions $\alpha = 1, 2, 3$.

In truncating this expansion at second order we are making the so-called harmonic approximation. In order to describe effects such as thermal expansion it is necessary to retain more terms, but for our

purposes the harmonic approximation is adequate. Since we are near the equilibrium point $R(\ell)$, the second term in this expansion goes to zero and the constant term V_o is unimportant in this context.

In the harmonic approximation, the classical equation of motion for the ℓ'^{th} ion is given by:

$$- M \frac{d^2 u_\alpha(\ell)}{dt^2} = \sum_{\ell'\beta} \Phi_{\alpha\beta}(\ell,\ell')\, u_\beta(\ell') \qquad \text{------(2-4)}$$

where $u_\alpha(\ell)$ is the α-direction component of the excursion from equilibrium of the ℓ^{th} ion and $\Phi_{\alpha\beta}(\ell\ell')$ is the force in the α^{th} direction on this ion due to a unit displacement of the ℓ'^{th} ion in the β direction:

$$\Phi_{\alpha\beta}(\ell,\ell') = \left(\frac{\partial^2 V}{\partial u_\alpha(\ell)\, \partial u_\beta(\ell')} \right) \qquad \text{------(2-5)}$$

Clearly, from the definition of these force tensors:

$$\Phi_{\alpha\beta}(\ell,\ell') = \Phi_{\beta\alpha}(\ell',\ell) \qquad \text{------(2-6)}$$

Also, by the symmetry of the lattice, we expect:

$$\Phi_{\alpha\beta}(\ell,\ell') = \Phi_{\alpha\beta}(\ell-\ell', 0) \qquad \text{------(2-7)}$$

From eqn. (2-4), we see that the motion of any ion in the system is coupled to the motion of every other ion in the system. By using a standard mechanical technique of obtaining the normal co-ordinates of a system with 3N degrees of freedom, these equations can be decoupled by a

transformation to these normal co-ordinates $Q(\underline{k}, \lambda)$. This k^{th} normal mode has phonon frequency $\omega(\underline{k}, \lambda)$ and polarization $\underline{\varepsilon}(\underline{k}, \lambda)$, where to get all possible solutions it is sufficient to restrict $\underline{k}$ to the first Brillouin zone, and λ is a branch index.

We can write a solution for $u_\alpha(\ell)$ to satisfy equation (2-4) in the form

$$u_\alpha(\ell) = \frac{1}{(MN)^{\frac{1}{2}}} \sum_{\underline{k},\lambda} Q(\underline{k},\lambda)\, \underline{\varepsilon}_\alpha(\underline{k}, \lambda)\, e^{i\underline{k}.\underline{R}(\ell)} \qquad \text{------(2-8a)}$$

while the momentum conjugate may be expressed in the form:

$$P_\alpha(\ell) = \left(\frac{M}{N}\right)^{\frac{1}{2}} \sum_{\underline{k},\lambda} p(\underline{k}\lambda)\ \underline{\varepsilon}_\alpha(\underline{k}, \lambda)\, e^{i\underline{k}.\underline{R}(\ell)} \qquad \text{------(2-8b)}$$

where $p(\underline{k}, \lambda)$ is the momentum conjugate of $Q(\underline{k}, \lambda)$.

The justification of such a transformation into normal co-ordinates now becomes apparent, for if we now substitute our solution (2-8a) into the equation of motion (2-4), we can obtain an expression for the Hamiltonian of such a system, in terms of these new co-ordinates, in a very simplified form. The Hamiltonian (2-2) can now be written as:

$$H = \sum_{\underline{k}\lambda} \frac{p^+(\underline{k}, \lambda)p(\underline{k}, \lambda)}{2} + \sum_{\underline{k}\lambda} \omega^2(\underline{k}, \lambda)\, \frac{Q^+(\underline{k},\lambda)Q(\underline{k}\lambda)}{2} \qquad \text{------(2-9)}$$

where $p^+(\underline{k}, \lambda) = p(-\underline{k},\lambda)$

and $Q^+(\underline{k}, \lambda) = Q(-\underline{k}, \lambda)$

as may be deduced from the conditions that $u_\alpha(\ell)$ and $P_\alpha(\ell)$ be real.

This Hamiltonian is now in the very familiar form which describes a harmonic oscillator field as decomposed into independent normal modes. Because this Hamiltonian represents a collection of harmonic uncoupled oscillators, we can quantize the system by imposing the quantization condition for a harmonic oscillator. Following regular procedures[31], we thus require that

$$[P(\ell),\ u(\ell')] = \hbar/i\ \delta_{\ell\ell'}$$

and

$$[P(\ell),\ P(\ell')] = [u(\ell), u(\ell')] = 0 \qquad \text{------(2-10)}$$

Hence it follows from (2-8) that:

$$[p(\underline{k},\ \lambda),\ Q(\underline{k}',\ \lambda)] = \hbar/i\ \delta_{\underline{k}\underline{k}'}$$

$$[p(\underline{k},\ \lambda),\ p(\underline{k}',\ \lambda)] = [Q(\underline{k},\ \lambda), Q(\underline{k}',\ \lambda)] = 0 \qquad \text{--------(2-11)}$$

Finally, in order to make the notation workable, we make one more transformation to an operator notation that will serve to create or annihilate these quantized lattice vibrations (phonons). This transformation is written in the form:

$$p(\underline{k},\ \lambda) = \left(\frac{\hbar\omega(\underline{k}\lambda)}{2}\right)^{\frac{1}{2}} i\ (a^{+}(\underline{k}\lambda) - a(-\underline{k}\lambda)) \qquad \text{------(2-12a)}$$

$$Q(\underline{k},\ \lambda) = \left(\frac{\hbar}{2\omega(\underline{k}\lambda)}\right)^{\frac{1}{2}} (a(\underline{k},\ \lambda) + a^{+}(-\underline{k},\ \lambda) \qquad \text{------(2-12b)}$$

where these new operators $a^{+}(\underline{k}, \lambda)$ and $a(\underline{k}, \lambda)$ act to create or destroy a phonon of wave vector $\underline{k}$ and energy $\hbar\omega$.

The Hamiltonian of the system can now be written in the form:

$$H = \sum_{\underline{k}\lambda} \hbar\omega(\underline{k}, \lambda) \left| a^{+}(\underline{k}, \lambda)\, a(\underline{k}, \lambda) + \frac{1}{2} \right| \qquad \text{------(2-13)}$$

where we can look upon the product $a^{+}(\underline{k}, \lambda)a(\underline{k}, \lambda)$ as simply a number operator determining the number of phonons of wave vector $\underline{k}$ in the λ branch of energy $\hbar\omega(\underline{k}, \lambda)$ we have in the system. The $\frac{1}{2}$ term is a manifestation of the zero point energy--a concept very familiar in simple harmonic oscillator theory.

2.2 BARE ELECTRONS AND THE ELECTRON PHONON INTERACTION:

Having considered the system of phonons, it is now necessary to consider the other constituent of the electron-phonon interaction, namely the electrons.

The common procedure employed here is to consider a system of electrons in a lattice of ions all at their equilibrium positions. The kinetic energy of the electron is combined with the coulomb potential of the electron-ion system and the system is expressed in terms of Bloch waves for a single electron moving in a periodic potential.

Using the formalism of second quantization to treat the conduction electrons, we can represent the electronic part of the total Hamiltonian of the system as:

$$H_{el} = \sum_{\underline{k}s} \varepsilon_{\underline{k}}\, C^{+}_{\underline{k}s}\, C_{\underline{k}s} \qquad \text{------(2-14)}$$

where $C^{+}_{\underline{k}s}$ and $C_{\underline{k}s}$ act to create and annihilate electrons in the Bloch state $\underline{k}$ of energy $\epsilon_{\underline{k}}$ with spin s. These operators satisfy the Fermi anticommutation relations

$$\{C_{\underline{k}s},\ C^{+}_{\underline{k}'s'}\} = \delta_{\underline{k}\underline{k}',ss'} \qquad \text{------(2-15)}$$

and

$$\{C_{\underline{k}s},\ C_{\underline{k}'s'}\} = \{C^{+}_{\underline{k}s},\ C^{+}_{\underline{k}'s'}\} = 0$$

Now that we are in a position to write down the Hamiltonian for the electrons in a system as well as for the phonons in a system, we must consider the manner in which these two excitations in a solid are coupled together. Let us recapitulate and consider the interaction of free electrons with the ions, and denote by $W(R(i) - r(\ell))$ the interaction energy between the i^{th} electron at position $R(i)$ and the ℓ^{th} ion at $r(\ell)$. The contribution to the Hamiltonian can be written in the form:

$$\sum_{i\ell} w\,(\underline{R}(i) - \underline{r}(\ell)) = \sum_{i} W(\underline{R}_i) \qquad \text{------(2-16)}$$

where $W(\underline{R}) = \sum_{\ell} w\,(\underline{R} - \underline{r}(\ell))$

is the electron-ion interaction. But in second quantization notation, a sum of one body electron operators $\sum_i f(\underline{R}(i))$ is transformed into:

$$\int d^3R\ \psi_{\underline{p}'}^{*}(\underline{R})\ f(R)\ \psi_{\underline{p}}(\underline{R})$$

$$= \sum_{pp'\sigma} \langle \underline{p}' \mid f \mid \underline{p} \rangle\ C^{+}_{\underline{p}'\sigma}\ C_{\underline{p}\sigma}$$

Hence the contribution of (2-16) to the total Hamiltonian becomes

$$\sum_{\underline{q}\underline{k}\sigma} \langle \underline{k} + \underline{q} \mid W \mid \underline{k} \rangle \; C^{+}_{\underline{k}+\underline{q}\sigma} \; C_{\underline{k}\sigma} \qquad ---(2\text{-}17)$$

Next, we factor out the matrix element of the electron-ion potential:

$$\langle \underline{k} + \underline{q} \mid W \mid \underline{k} \rangle = \int e^{-i(\underline{k}+\underline{q}).\underline{R}} \sum_{\ell} w(\underline{R} - \underline{r}(\ell)) \; e^{i\underline{k}.\underline{R}} \, d^3\underline{R} \qquad ---(2\text{-}18)$$

Interchanging the sum over ℓ and the integration, and in the ℓ'^{th} term carrying out a linear transformation from $\underline{R} - \underline{r}(\ell)$ to $\underline{R}'$, we obtain:

$$\langle \underline{k}+\underline{q} \mid W \mid \underline{k} \rangle = \left[\frac{1}{N} \sum_{\ell} e^{i\underline{q}.\underline{r}(\ell)}\right] \; N \int e^{-i(\underline{k}+\underline{q}).\underline{R}'} w(\underline{R}') \; e^{i\underline{k}.\underline{R}'} d^3\underline{R}'$$

where we now define;

$$S(\underline{q}) = \frac{1}{N} \sum_{\ell} e^{-i\underline{q}.\underline{r}(\ell)} \qquad ------(2\text{-}19)$$

as the structure factor, while the matrix element $\langle \underline{k} + \underline{q} \mid w \mid \underline{k} \rangle$ is the pseudopotential form factor[33]. Hence we may write the electron-ion Hamiltonian as:

$$H = \sum_{\underline{k}\underline{q}\sigma} S(\underline{q}) \langle \underline{k} + \underline{q} \mid w \mid \underline{k} \rangle \; C^{+}_{\underline{k}+\underline{q}\sigma} \; C_{\underline{k}\sigma} \qquad ------(2\text{-}20)$$

Substituting our expression for the excursion of an ion from its equilibrium $\underline{r}(\ell) = \underline{R}(\ell) + \underline{u}(\ell)$ into the expression for the structure factor (2-19) and expanding the exponential to first order, $S(\underline{q})$ becomes:

$$S(\underline{q}) = \frac{1}{N} \sum_{\ell} e^{-i\underline{q}.\underline{R}(\ell)} \; (1 - i\underline{q}.\underline{u}(\ell))$$

When inserted back into the Hamiltonian (2-20) the first term gives the crystal potential for the perfect lattice at its equilibrium position. The second term gives the electron phonon interaction:

$$H_{ep} = \sum_{\underline{k}\underline{q}\sigma} \frac{1}{N} \sum_{\ell} -i\underline{q}.\underline{u}(\ell) < \underline{k} + \underline{q} \mid w \mid \underline{k} > e^{-i\underline{q}.\underline{R}(\overset{o}{\ell})} C^{+}_{\underline{k}+\underline{q}\sigma} C_{\underline{k}\sigma} \qquad \text{--(2-21)}$$

To further reduce (2-21) it is convenient to substitute the solution for $\underline{u}(\ell)$ from equation (2-8a) namely;

$$\underline{u}(\ell) = \frac{1}{(MN)^{\frac{1}{2}}} \sum_{\underline{k}\lambda} Q(\underline{k}, \lambda) \; \underline{\varepsilon}\,(\underline{k}, \lambda) \; e^{i\underline{k}.\underline{R}(\overset{o}{\ell})}$$

where the sum over $\underline{k}$ extends over the first Brillouin zone and M is the ion mass. Performing this substitution yields;

$$H_{ep} = \frac{1}{\sqrt{MN}} \sum_{\underline{k}\underline{q}\underline{k}'\sigma\lambda} Q(\underline{k}',\lambda)(-i\underline{q}.\underline{\varepsilon}(\underline{k}'\lambda)) <\underline{k}+\underline{q}|w|\underline{k}> x \; \delta_{\underline{k}'-\underline{q}\underline{K}_n} C^{+}_{\underline{k}+\underline{q}\sigma} C_{\underline{k}\sigma} \qquad \text{---(2-22)}$$

where we have used the fact that the sum

$$\frac{1}{N} \sum_{\ell} e^{i(\underline{k}'-\underline{q}).\underline{R}(\overset{o}{\ell})} = \delta_{\underline{k}'-\underline{q},\underline{K}_n} \qquad \text{------(2-23)}$$

where K_n is a reciprocal lattice vector.

Using the properties of a delta function, the sum over $\underline{k}'$ can be carried out in (2-22) to yield

$$H_{ep} = \frac{1}{\sqrt{MN}} \sum_{\underline{k}\underline{q}\sigma\lambda} Q(\underline{q}, \lambda)(-i\underline{q}.\underline{\varepsilon}(\underline{q}\lambda)) x < \underline{k}+\underline{q}|w|\underline{k}> C^{+}_{\underline{k}+\underline{q}\sigma} C_{\underline{k}\sigma} \qquad \text{------(2-24)}$$

where in both the normal co-ordinate Q and the polarization vector $\underline{\varepsilon}$ terms, q is to be read as reduced to the first Brillouin zone. Finally, we use the transformation of the normal co-ordinates into phonon creation and annihilation operators $a^{+}(\underline{k},\lambda)$ $a(\underline{k}, \lambda)$ from equation (2-12b), giving us;

$$H_{ep} = \sum_{\underline{k}\sigma\lambda} g_{\underline{k}+\underline{q},\underline{k},\lambda} C^{+}_{\underline{k}+\underline{q}\sigma} C_{\underline{k}\sigma} \left(a^{+}(-\underline{q},\lambda) + a(\underline{q},\lambda)\right) \qquad \text{------(2-25)}$$

where the electron-phonon coupling term g is given by:

$$g_{\underline{k}+\underline{q},\underline{k}\lambda} = -i \left(\frac{1}{2\omega(\underline{q}\lambda)MN}\right)^{\frac{1}{2}} \underline{q}.\underline{\varepsilon}(\underline{q},\lambda) \; \langle \underline{k}+\underline{q} \,|w|\, \underline{k} \rangle \qquad \text{------(2-26)}$$

Physically, we see that the q^{th} normal mode of (2-25) gives rise to processes in which a phonon $\underline{q}$ is absorbed or a phonon $-\underline{q}$ is emitted and the momentum transfer to the electron is given by $\underline{K}_n + \underline{q}$ where $\underline{K}_n$ is a reciprocal lattice vector.

For the type of scattering (almost elastic from the electron energy point of view), it is clear that the pseudopotential form factor $\langle \underline{k}+\underline{q} \,|w|\, \underline{k} \rangle$ in (2-26) is needed only for both $\underline{k}$ and $\underline{k}+\underline{q}$ on the Fermi surface. Such form factors have been determined in the one orthogonal plane wave (o.p.w) approximation by Harrison[33]. In this work, we shall not in fact make use of the o.p.w. form factors, but employ instead the Heine Abarenkov form[34] as tabulated by Harrison[33], which is expected to be somewhat more reliable--since it is derived somewhat from experimental data rather than worked out entirely from first principles.

2.3 THE ELECTRON-PHONON-ELECTRON INTERACTION:

In anticipation of the basic interaction causing the transition to the superconducting state, let us now briefly consider the electron-electron interaction as mediated by a phonon. Since the interaction between electrons and phonons is so non-linear, we expect that any disturbance in the electrons will alter the distribution of the phonons, and this in turn will affect the distribution of electrons. Consequently,we can look upon this interaction as an electron-electron interaction simply mediated by the phonons. This problem was studied in detail by Fröhlich[35] assuming the interaction to be instantaneous (i.e. the electrons respond instantaneously to a shift in their distributions). Although it turns out to be an elegant and more simple problem to write the theory of superconductivity in terms of an instantaneous reaction, in truth due to the relatively low velocity of a phonon, retardation must be considered. This will be outlined in Chapter IV. Nevertheless, the result obtained by Fröhlich, and later modified by Bardeen and Pines[36] is of great interest physically and was the inspiration for the BCS theory. Fröhlich considered the interaction

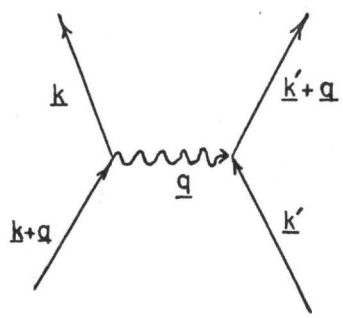

and calculated this new interaction between electrons to be of the form;

$$V = \frac{1}{2} \sum_{\substack{\underline{k},\underline{k}'\underline{q} \\ \lambda\sigma\sigma'}} \frac{g^{*}_{\underline{k}',\underline{k}'+\underline{q},\lambda}\, g_{\underline{k},\underline{k}+\underline{q},\lambda}\, \hbar\omega(\underline{q}\lambda)}{(\varepsilon_{\underline{k}+\underline{q}} - \varepsilon_{\underline{k}})^2 - (\hbar\omega(\underline{q}\lambda))^2} \times C^{+}_{\underline{k}\sigma} C^{+}_{\underline{k}'+\underline{q},\sigma} C_{\underline{k}'\sigma'} C_{\underline{k}+\underline{q},\sigma} \qquad \text{------(2-27)}$$

where g is the coupling term defined by equation (2-26), and $\varepsilon_{\underline{k}}$ is the energy of the Bloch state $\underline{k}$, as contained in equation (2-14).

Probably the most significant contribution of all this work to the theory of superconductivity is the recognition of the fact that in the energy range

$$|\varepsilon_{\underline{k}+\underline{q}} - \varepsilon_{\underline{k}}| < \hbar\omega(\underline{q}, \lambda)$$

this interaction is attractive. Hence, in a certain small energy region about the Fermi surface, the electron-phonon-electron interaction results in an attractive term being added to the total Hamiltonian. This physical result is all important in the theory of superconductivity and is necessary in understanding a basic model for a superconductor.

CHAPTER III

THE BCS THEORY OF SUPERCONDUCTIVITY AS APPLIED TO THE DERIVATION OF AN ENERGY GAP

A very strange effect seems to be unfolding. The electron-phonon interaction, the strength of which determines the resistivity of a material, appears to be the same microscopic mechanism responsible for this transition to a state of zero resistivity. Indeed, in simple metals there seems to be a direct correlation between the resistivity of the material and its superconducting transition temperature. Those pure metals with high conductivities are not likely to have high superconducting transition temperatures if, in fact, they superconduct at all. The solution to this seeming contradiction will become clear in this Chapter as we study the microscopic theory as presented by Bardeen, Cooper and Schrieffer[21], assuming the results of Fröhlich.

3.1 COOPER'S SINGLE PAIR PROBLEM:

The first serious investigation of the microscopic mechanisms responsible for the transition to the superconducting state was performed by Cooper[20] in which he considered a single pair of electrons interacting via some non-retarded potential V above a Fermi sea of non-interacting particles. The Fermi sea serves to block the availability of some states to be scattered into by virtue of the Pauli principle. Cooper studied the scattering problem pictured in Figure 3.1 where we consider scattering from the state $|\underline{k}, -\underline{k}>$ to the state $|\underline{k}', -\underline{k}'>$.

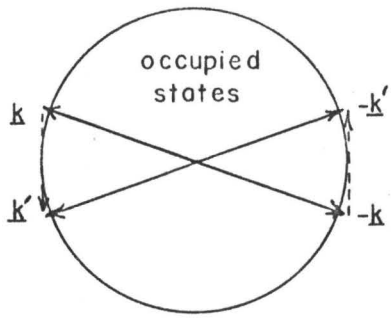

FIGURE 3.1

SCATTERING PROBLEM CONSIDERED BY COOPER

Using the result from the work of Fröhlich, Cooper showed that if this non-retarded potential $V_{\underline{k}\underline{k}'}$, say, is at all attractive for electrons diametrically across the Fermi surface, a bound state will result in which the two electrons are coupled together.

To be more explicit, in this simple two-electron problem, Cooper showed that the binding energy of the $|\underline{k}, -\underline{k}>$ state is given by

$$W = 2\omega_c \,/\, \exp\left[\frac{2}{N(0)V}\right] - 1 \qquad \text{------(3-1)}$$

where $V_{\underline{k}\underline{k}'} = V$ for energies less than ω_c

$= 0$ for energies greater than ω_c

and it is assumed that the density of states $N(\varepsilon_k)$ is slowly varying in the interval $0 < \varepsilon_k < \omega_c$ and may be approximated by $N(0)$.

In the case of strong coupling $(N(0)V >> 1)$

$$W \approx N(0)V\omega_c$$

and in the case of weak coupling $(N(0)V << 1)$

$$W \approx 2\omega_c \exp\left(-\frac{2}{N(0)V}\right)$$

On consideration of this Cooper problem, one immediately sees that a bound state exists for arbitrarily weak interactions insofar as they are attractive. This is an extremely important result as discovered by Cooper. Following this it was suggested that superconductivity could somehow be associated with the forming of many of these bound pairs at the Fermi surface.

In actuality, there is a very great difference between this simple problem considered by Cooper, and a superconductor. Fortunately, this difference can be simply dealt with by means of the notational machinery at our disposal. Contrary to Cooper's assumption of single pairs non-interacting with other pairs, we find that there are, on the average, about 10^6 pairs whose wavefunctions overlap with the wavefunction of any one pair. Consequently, the isolated pair cannot be considered and some coherence effects must be included. This, in essence is why, although the binding energy of any individual non-interacting bound pair is microscopic, in the total system the energy required to destroy any bound pair is macroscopic. Another way of saying this is that the single pair model exhibits an almost continuous spectrum above the ground state, while, if one invokes the Pauli principle restrictions when treating interactions between pairs, a macroscopic energy gap above the ground state results.

3.2 THE GROUND STATE OF A SUPERCONDUCTOR:

We are now in a position to consider the ground state of a superconductor as introduced by BCS. It should be pointed out that in some respects we must display a certain ruthlessness in ignoring certain interactions, although their energies are comparatively high, that are not believed important in the transition to the superconducting state.

As discussed above, we can form a state with lower energy by removing a pair of electrons from the Fermi sea, and allowing them to form a superposition of states above it. The next step, obviously, is to remove more than simply one pair and go to an even lower energy state. If we remove enough of these pairs, however, we will reach the stage where we can no longer treat them as individual, non-interacting pairs. It can be shown by phase-space considerations[37] that when no current is flowing in the superconductor, the greatest possible stability is achieved if the pairs are chosen to have zero total momentum. Hence, we see that the resulting energy is a minimum if we choose pairs of the same value of total momentum (i.e. pairs $\underline{k}$ and $-\underline{k}$). Exchange tends to reduce the pairing interaction energy so that electrons of opposite spin, as well as opposite momentum, are most favourable as partners.

In order to follow as closely as possible the theory as set out by BCS, we shall use the formalism of second quantization. Here the creation and annihilation operators for electrons in Bloch states of a metal are as previously described are given by $C^{+}_{\underline{k}\sigma}$ and $C_{\underline{k}\sigma}$ respectively. Furthermore, as we are considering pairs of electrons of equal and opposite spin and momentum it is convenient to introduce pair creation and annihilation operators;

$$b^{+}_{\underline{k}} = C^{+}_{\underline{k}\uparrow} C^{+}_{-\underline{k}\downarrow}$$

$$b_{\underline{k}} = C_{-\underline{k}\downarrow} C_{\underline{k}\uparrow} \qquad \text{------(3-2)}$$

where we see that $b^{+}_{\underline{k}}$ creates a pair in the state $|\underline{k}\uparrow - \underline{k}\downarrow>$ and $b_{\underline{k}}$ annihilates a pair in that same state. By direct substitution we attain the relations;

$$\left[b_{\underline{k}}, b^{+}_{\underline{k}'} \right] = 0$$

$$\left[b_{\underline{k}}, b_{\underline{k}'} \right] = \left[b^{+}_{\underline{k}}, b^{+}_{\underline{k}'} \right] = 0$$

$$\left[b_{\underline{k}}, b^{+}_{\underline{k}} \right] = 1 - (n_{\underline{k}\uparrow} + n_{\underline{k}\downarrow}) \qquad \text{------(3-3)}$$

where $n_{\underline{k}\uparrow}$ and $n_{-\underline{k}\downarrow}$ are the number operators for the states $\underline{k}\uparrow$ and $-\underline{k}\downarrow$ respectively. It should be emphasized here that although at first glance one might suspect that these pairon operators are boson operators and obey Bose statistics, the factor $(n_{\underline{k}\uparrow} + n_{-\underline{k}\downarrow})$ represents the Pauli principle restriction, disallowing pairs to be created in states already occupied either by other pairs or single particles. Hence, we are not considering a Bose gas.

Having established the notation, we are now in a position to write down the Hamiltonian for the reduced problem as has been outlined, ignoring other interactions not altered by the transition into the superconducting phase. This Hamiltonian then has the form:

$$H_{red} = \sum_{k\sigma} \varepsilon_{\underline{k}} n_{\underline{k}\sigma} + \sum_{\underline{k}\underline{k}'} V_{\underline{k}\underline{k}'} b^{+}_{\underline{k}'} b_{\underline{k}} \qquad \text{------(3-4)}$$

It has already been stated that under certain circumstances, $V_{\underline{k}\underline{k}'}$ is attractive (negative) and in this case, for the most stable situation, it is clear that the ground state of H_{red} has no pair state occupied by a single electron. Hence the ground state reduced Hamiltonian can be written as:

$$H^{o}_{red} = \sum_{\underline{k}} 2\varepsilon_{\underline{k}} b_{k}^{+} b_{\underline{k}} + \sum_{\underline{k}\underline{k}'} V_{\underline{k}\underline{k}'} b^{+}_{\underline{k}'} b_{\underline{k}} \qquad \text{------(3-5)}$$

The wave function for the ground state of this system is given by:

$$\Psi_{o} = \prod_{\underline{k}} \left[u_{\underline{k}} + v_{\underline{k}} b^{+}_{\underline{k}} \right] \mid 0 > \qquad \text{------(3-6)}$$

where $\mid 0 >$ is the vacuum state and $u_{\underline{k}}$ and $v_{\underline{k}}$ describe the relative probability of occupation of each state. $v_{\underline{k}}$ is the amplitude probability that a pair state is filled, while $u_{\underline{k}}$ is the corresponding vacancy amplitude. Of necessity,

$$u_{\underline{k}}^{2} + v_{\underline{k}}^{2} = 1$$

Hence this ground state wave function is just a product of all constituent configurations with suitable occupational probability amplitudes.

Curiously enough, this wave function Ψ_{o} is not an eigenstate of the number operator N_{op}, the operator for the number of particles in the

system. To insist that this wave function be an eigenstate of N_{op} in changing the occupation of one pair state, we would be required to alter the occupation of others in order to conserve N_o. Since this wave function does not have a definite number of particles, we must minimize the energy, subject to the constraint that the expectation value of N_{op} is N_o, i.e.

$$< \Psi_o \mid N_{op} \mid \Psi_o > = N_o$$

Using a Lagrangian multiplier scheme and considering H^o_{red} of equation (3-5) it can be shown [21] that the quantity to be minimized is, in fact;

$$W = \sum_{\underline{k}} 2\epsilon_{\underline{k}} v_{\underline{k}}^2 + \sum_{\underline{kk'}} V_{\underline{kk'}}\, u_{\underline{k}}\, v_{\underline{k}}\, u_{\underline{k}'}\, v_{\underline{k}'} \qquad \text{------(3-7)}$$

Minimizing this term we obtain for the ground state the relationships;

$$u_{\underline{k}}^2 = \frac{1}{2}\left(1 + \frac{\epsilon_{\underline{k}}}{E_{\underline{k}}}\right) \qquad \text{------(3-8a)}$$

$$v_{\underline{k}}^2 = \frac{1}{2}\left(1 - \frac{\epsilon_{\underline{k}}}{E_{\underline{k}}}\right) \qquad \text{------(3-8b)}$$

as well as the product

$$u_{\underline{k}}\, v_{\underline{k}} = \frac{\Delta_{\underline{k}}}{2E_{\underline{k}}} \qquad \text{------(3-9)}$$

where $E_{\underline{k}}$ is defined by

$$E_{\underline{k}} = \left[\epsilon_{\underline{k}}^2 + \Delta_{\underline{k}}^2\right]^{\frac{1}{2}} \qquad \text{------(3-10)}$$

This is the energy required to create an excitation in the state $|\ \underline{k}\ >$ in the superconducting state. The other parameter $\Delta_{\underline{k}}$ is the "energy gap" parameter and it is seen to satisfy the integral equation

$$\Delta_{\underline{k}} = - \sum_{\underline{k}'} V_{\underline{k}\underline{k}'}\, u_{\underline{k}'}\, v_{\underline{k}'} \qquad \text{------(3-11)}$$

which thus takes the form (from (3-9))

$$\Delta_{\underline{k}} = - \sum_{\underline{k}'} V_{\underline{k}\underline{k}'}\, \frac{\Delta_{\underline{k}'}}{\left[\varepsilon_{\underline{k}'}^{\,2} + \Delta_{\underline{k}'}^{\,2}\right]^{\frac{1}{2}}} \qquad \text{------(3-12)}$$

From (3-10) we see that in the superconducting case the energy required to create a quasiparticle in the state $|\ \underline{k}\ >$ differs from that of the normal material by an energy $\Delta_{\underline{k}}$. This feature will be further discussed in the next Section.

This energy gap equation (3-12) is easily solved if certain simplifying assumptions are made. For example, if it is assumed that $V_{\underline{k}\underline{k}'}$ is a simple non-retarded, $\underline{k}$ independent potential of the form

$$V_{\underline{k}\underline{k}'} = -V_o \qquad \text{for } |\ \varepsilon_{\underline{k}}\ | < \omega_c, \text{ some cut off energy}$$

$$= 0 \qquad \text{outside this shell of } \omega_c$$

then one finds that the solution of (3-12) takes the form;

$$\Delta_{\underline{k}} = \Delta_o \qquad \text{for } |\ \varepsilon_{\underline{k}}\ | < \omega_c$$

$$= 0 \qquad \text{otherwise}$$

where
$$\Delta_o = \frac{\omega_c}{\sinh\left[\frac{1}{N(0)V_o}\right]}$$

$$\doteq 2\omega_c \exp\left[-\frac{1}{N(0)V_o}\right] \qquad \text{------(3-13)}$$

in the weak coupling limit.

Having now determined the ground state of a superconductor one can, by substituting this result into the ground state energy equation (3-7) and subtracting the ground state energy of the normal phase, determine the condensation energy of a superconductor:

$$W_n - W_s = \frac{1}{2} N(0) \Delta_o^2 = 2 N(0) \omega_c^2 \exp\left[\frac{-2}{N(0)V}\right]$$

3.3 EXCITATIONS FROM THE GROUND STATE:

Suppose now we consider the injection of an electron into the system in the state $|\ \underline{k}\uparrow\ >$ (its mate $|\ -\underline{k}\downarrow\ >$ being unoccupied). The existence of this single particle occupying $|\ \underline{k}\uparrow\ >$ serves to block the participation of the pair state $|\ \underline{k}\uparrow - \underline{k}\downarrow\ >$ in the pairing interaction and thus the energy of the interacting pairs is increased by (see equation (3-7));

$$-2\epsilon_{\underline{k}} v_{\underline{k}}^2 - 2\left[\sum_{\underline{k}'} V_{\underline{k}\underline{k}'} u_{\underline{k}'} v_{\underline{k}'}\right] u_{\underline{k}} v_{\underline{k}} \qquad \text{------(3-14)}$$

In blocking this state from interacting, recall, we have added a single particle of energy $\epsilon_{\underline{k}}$ to the system. We must add this term to the total

energy change, which is now given by:

$$\varepsilon_{\underline{k}} \left[1 - 2v_{\underline{k}}^{2} \right] + 2\Delta_{\underline{k}} u_{\underline{k}} v_{\underline{k}} \qquad \text{------(3-15)}$$

where we have used the relation (3-11),

$$\Delta_{\underline{k}} = - \sum_{\underline{k}'} V_{\underline{k}\underline{k}'} u_{\underline{k}'} v_{\underline{k}'}$$

Substituting our values for $u_{\underline{k}}$ and $v_{\underline{k}}$ from equations (3-8a) and (3-8b) into the above we obtain the energy difference between the ground state and a single excitation, namely,

$$\text{Excitation Energy} = \frac{\varepsilon_{\underline{k}}^{2}}{E_{\underline{k}}} + \frac{\Delta_{\underline{k}}^{2}}{E_{\underline{k}}} = E_{\underline{k}}$$

$$= (\varepsilon_{\underline{k}}^{2} + \Delta_{\underline{k}}^{2})^{\frac{1}{2}} \qquad \text{------(3-16)}$$

Thus we see that the minimum amount of energy required to add a single particle excitation to the system is $\Delta_{kF} \equiv \Delta_{o}$ in our approximation.

This requirement is graphically illustrated in Figure 3.2 where a plot of $E_{\underline{k}}$ vs k is illustrated for both a normal material and a superconducting material.

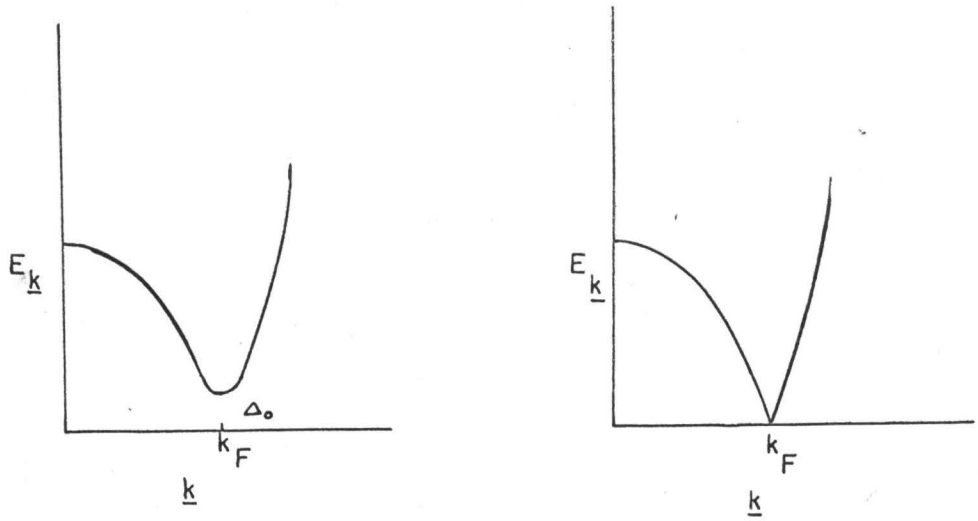

FIGURE 3.2

$E_{\underline{k}}$ vs $\underline{k}$ PLOTS FOR A SUPERCONDUCTING AND NORMAL MATERIAL

Here we can graphically see the difference between the superconducting and normal case. In the normal case, microscopic excitations above the Fermi surface are possible, while in the superconducting case, the minimum excitation as evidenced from Figure 3.2 is seen to be the energy gap parameter Δ_o.

It should be pointed out that it is important to consider this $E_{\underline{k}}$ vs $\underline{k}$ curve for k values less than k_F. We know that since the interaction has caused a smoothing out of the sharp jump in the single particle occupation number, there is a finite probability of finding a state $\underline{k} < \underline{k}_F$ empty where in the non-interacting case this probability would be zero. Consequently, it is meaningful to consider the possibility of injecting

a single particle into a state below the Fermi surface. In all cases, we find that the excitation energy $E_{\underline{k}}$ is positive.

If, on the other hand, we were to consider a closed system of particles (i.e. we can't introduce electrons from an external source), then from these considerations we see that the minimum energy required to create an excitation from the ground state is $2\Delta_o$; Δ_o to remove the electron from a bound pair state and another Δ_o to place it into a single particle state. Alternatively, one can look upon this process as the production of two single particle states and consequently the minimum energy required is $2\Delta_o$.

These considerations are important as we shall see in studying the process of single-particle tunneling across an insulating barrier between two superconductors. The process can be considered as the removal and injection of electrons in a superconductor.

These excited states can be treated in a neat shorthand notation if we judiciously choose new operators from the previously chosen $C_{\underline{k}\uparrow}C_{-\underline{k}\downarrow}$ and $C^{+}_{\underline{k}\uparrow}C^{+}_{-\underline{k}\downarrow}$ which annihilate and create pairs. As was pointed out by Bogoliubov[38] and Valatin[39], if new operators are formed as given by

$$\gamma_{\underline{k}\uparrow}^{+} = u_{\underline{k}} C^{+}_{\underline{k}\uparrow} - v_{\underline{k}} C_{-\underline{k}\downarrow} \qquad \text{------(3-17a)}$$

and

$$\gamma_{-k\downarrow} = u_{\underline{k}} C_{-\underline{k}\downarrow} + v_{\underline{k}} C_{\underline{k}\uparrow}^{+} \qquad \text{------(3-17b)}$$

and we consider the operation of this new operator $\gamma^{+}_{\underline{k}}$ on the ground state wave function:

$$\gamma^{+}_{\underline{k}\uparrow} \mid \Psi_o > = \mid \psi_{\underline{k}\uparrow} >$$

then this $\gamma^{+}_{\underline{k}\uparrow}$ acting on the ground state creates a quasiparticle in the state $|\underline{k}\uparrow>$. The components of $\gamma^{+}_{\underline{k}\uparrow}$ from equation (3-17a) ensure that the $|\ \underline{k}\uparrow>$ state is filled and the $|\ -\underline{k}\downarrow>$ is empty.

Similarily, we see that $\gamma_{\underline{k}\uparrow}$ destroys a quasiparticle in the state $|\underline{k}\uparrow>$. Thus one immediately has the results:

$$\gamma^{+}_{\underline{k}\uparrow} \mid \Psi_o > = \mid \Psi_{\underline{k}\uparrow} >$$

$$\gamma^{+}_{-\underline{k}\downarrow} \mid \Psi_o > = \mid \Psi_{-\underline{k}\downarrow} >$$

$$\gamma_{\underline{k}\uparrow} \mid \Psi_o > = 0$$

$$\gamma_{\underline{k}\uparrow} \mid \Psi_o > = 0 \qquad \text{------(3-18)}$$

The last two of these operations are equal to zero as $\mid \Psi_o>$ is the vacuum state for quasiparticles. These operators obey Fermi Dirac statistics;

$$\{\gamma_{\underline{k}\sigma}, \gamma^{+}_{\underline{k}'\sigma'}\} = \delta_{\underline{k}\underline{k}'}, \delta_{\sigma\sigma'}$$

$$\{\gamma_{\underline{k}\sigma}, \gamma_{\underline{k}'\sigma'}\} = \{\gamma^{+}_{\underline{k}\sigma}, \gamma^{+}_{\underline{k}'\sigma'}\} = 0$$

Again we can determine the quasiparticle excitation energy by evaluating

$$W_{\underline{k}} = < \Psi_{\underline{k}} \mid H \mid \Psi_{\underline{k}} >$$

to find

$$W_{\underline{k}} = W_s + E_{\underline{k}}$$

as previously shown.

The advantages of this transformation is that it is easier to see physically what happens to the system when a quasiparticle is created. Consider for example, the $\gamma^{+}_{\underline{k}\uparrow}$ operator of equation (3-17a). This is simply an ordinary creation operator $C^{+}_{\underline{k}\uparrow}$ of the state $|\ \underline{k}\uparrow>$ with amplitude corresponding to the probability of that state originally being empty, and a normal annihilation operator $C_{-\underline{k}\downarrow}$ of the state $|\ -\underline{k}\downarrow\ >$ with amplitude corresponding to the probability of that state originally being filled. The combination of these two operations makes the state $|\ \underline{k}\uparrow\ >$ certainly filled and the state $|\ -\underline{k}\downarrow\ >$ certainly empty. Hence we can say that the operator $\gamma^{+}_{\underline{k}\uparrow}$ certainly creates a quasiparticle in the state $|\underline{k}\uparrow\ >$.

CHAPTER IV

FIELD THEORETIC TREATMENT OF TIME RETARDED INTERACTIONS

We are now familiar with the basic interactions and concepts determining the phenomenon of superconductivity. However, in this BCS treatment of a superconductor, little is really known about the electron-phonon-electron interaction $V_{kk'}$, and in fact, the crudest solution possible $V_{kk'} = V_o$ was used originally. Even with this simple approach, however, surprisingly good agreement and accurate predictions resulted. In real metals, we cannot treat the superconducting state as resulting from unretarded interactions and undamped quasiparticles of the normal state. Retardation and damping, we shall see, play important roles in the description of a superconductor.

In this Chapter the techniques used to describe these effects are outlined and the application of these techniques to explain certain anomolous behaviour of lead is presented. We shall see, in fact, that because of these retardation effects, interesting results can be extracted concerning the phonon density of states.

4.1 TWO COMPONENT NAMBU FORMALISM:

In the Hartree Fock approximation, taking into account all the interaction terms so far discussed, we find that we can write a modified zero order Hamiltonian:

$$H_o' = H_o + H_{HF} + H_\phi \qquad \text{------(4-1)}$$

where

H_o = free electron Hamiltonian

H_{HF} = Hartree and Fock terms

H_ϕ = a pairing term

$$= \sum_k \{\phi^*_{\underline{k}} C^+_{\underline{k}\uparrow} C^+_{-\underline{k}\downarrow} + \text{hermitian conjugate}\}$$

We see now, however, that the Hamiltonian is no longer a one-particle Hamiltonian if this pairing term is added. This difficulty was overcome by Nambu[40], and independently with a similar treatment by Gor'kov[41], where a two component spinor field was introduced,

$$\psi_{\underline{k}} = \begin{pmatrix} C_{\underline{k}\uparrow} \\ C^+_{-\underline{k}\downarrow} \end{pmatrix}$$

and

$$\psi^+_{\underline{k}} == (C^+_{\underline{k}\uparrow} \; C_{-\underline{k}\downarrow}) \qquad \text{------(4-2)}$$

where $C^+_{\underline{k}\uparrow}$ and $C_{\underline{k}\uparrow}$ are the usual creation and annihilation operators. Then, from these definitions, and equations (2-15) we have the usual anticommutation relations in matrix form;

$$\{\Psi_{\underline{k}}, \Psi^+_{\underline{k}'}\} = \delta_{kk'} \, 1$$

$$\{\Psi_{\underline{k}}, \Psi_{\underline{k}'}\} = 0$$

where 1 is the 2 x 2 unity matrix.

Using this redefinition of terms, we can now more conveniently write the modified zero-order Hamiltonian H_o' as:

$$H_o' = \sum_{\underline{k}} \psi^+_{\underline{k}} \left[\bar{\epsilon}_{\underline{k}} \tau_3 + \phi_{\underline{k}} \tau_1 \right] \psi_{\underline{k}} + \sum_{\underline{k}} \bar{\epsilon}_{\underline{k}} \qquad \text{------(4-3)}$$

where $\bar{\epsilon}_{\underline{k}}$ = sum of free electron energy and Hartree Fock correction

$$\bar{\epsilon}_{\underline{k}} = \epsilon_{\underline{k}} + \epsilon_{HF}$$

and τ_i = Pauli spin matrices

$$\tau_1 = \begin{pmatrix} 0 & 1 \\ 1 & 0 \end{pmatrix} \quad , \quad \tau_3 = \begin{pmatrix} 1 & 0 \\ 0 & -1 \end{pmatrix} \qquad \text{------(4-4)}$$

The use of this convenient formalism enables one to express the system in terms of single, four-component Green's functions. More explicitly, we define this four-component Green's function matrix as:

$$G._{\alpha\beta}(\underline{k}\ t) = -i < 0 \mid T\{\psi_{\underline{k}\alpha}(t)\ \psi^+_{\underline{k}\beta}(0) \mid 0 > \qquad \text{------(4-5)}$$

where $\mid 0 >$ is the ground state for N_o electrons and $\psi_{\underline{k}}(t) = e^{iH_o't}\ \psi_{\underline{k}}(0)\ e^{-iH_o't}$. T is the Wick time ordering operator.

Parenthetically, a few words could perhaps be added at this point about the physical significance of the Green's function approach. From equation (4-5), we can see that we are simply taking the inner product of a state $\underline{k}$ at time t = 0 with that time evolved state at a later time t.

Hence, squaring this term simply gives us, (having injected a particle into a state $\underline{k}$ at time t = 0), the probability of the propagator being in that same state after a time t. Clearly, with no damping effects (as in the free electron model) this probability is always unity and we can consider the spectral energy distribution of such a Green's function as a δ function located at the energy of the state ω_o. If damping effects are included, however, this ideal situation is not the case and there is a finite probability that the propagator will scatter out of the original state $\underline{k}$ in a time t into another state. No longer is the spectral energy distribution a δ function, but a smeared out Lorentzian function with finite width owing to the finite lifetime of the particle in the $\underline{k}$ state.

Returning to equation (4-5), we can associate the diagonal elements of this Green's function matrix $G._{11}$ and $G._{22}$ with normal state propagators, while the off-diagonal elements (the Gor'kov functions[41]) are related to the amplitude of subtracting or adding a pair of particles to the system without creating excitations. In Green's function formalism, it is often convenient to Fourier transform these functions into ω space and work in terms of these energy propagators. For the non-interacting system, we can write the true free electron Green's function in ω space in the Nambu notation as a 2 x 2 matrix, namely;

$$G_o(\underline{k}\ \omega) = \frac{\omega\ 1 + \varepsilon_{\underline{k}}\ \tau_3}{\omega^2 - \varepsilon_{\underline{k}}^{\ 2} + i0^+} \qquad \text{------(4-6)}$$

where $i0^+$ is an incremental distance in the i direction.

If we now write the irreducible self-energy for a propagator as $\Sigma(\underline{k}, \omega)$, which is again a 2x2 matrix, the most general form that this self-energy can take is of the form

$$\Sigma(\underline{k}\ \omega) = \left[1 - Z(\underline{k}, \omega)\right] \quad \omega(1) + \varepsilon_{HF}(\underline{k}\ \omega)\ \tau_3 + \phi(\underline{k}\omega)\ \tau_1 \qquad \text{------(4-7)}$$

where $Z(\underline{k}\ \omega)$ is a renormalization function for the free electron with a real and imaginary part.

It should be noted that $\phi(\underline{k}\ \omega)$ in this general case need not be real. In fact, the imaginary part of this function contributes to the damping rate of the quasiparticles.

Using Dyson's equation[42];

$$G^{-1}(\underline{k}\ \omega) = G_o^{-1}(\underline{k}\ \omega) - \Sigma(\underline{k}\ \omega) \qquad \text{------(4-8)}$$

which relates the non-interacting Green's function to the interacting Green's function via this self-energy function, and our general expression for the self-energy from equation (4-7), we have the matrix solution for the general Green's function:

$$G(\underline{k}\ \omega) = \frac{\omega\ Z(\underline{k}\omega)\ (1) + \bar{\varepsilon}(\underline{k}\omega)\ \tau_3 + \phi(\underline{k}\omega)\ \tau_1}{Z^2(\underline{k}\ \omega)\ \omega^2 - \varepsilon^2(\underline{k}\ \omega) - \phi^2(\underline{k}\omega) + i0^+} \qquad \text{------(4-8a)}$$

4.2 THE GAP EQUATIONS:

Using this up to now general approach, one now uses a self-consistent perturbative approach to determine these functions ϕ and Z. i.e. one expands $\Sigma(\underline{k}\omega)$ to a given or prescribed order in terms of the propagators $G(\underline{k}\omega)$ which themselves include this self-energy $\Sigma(\underline{k}\omega)$ to be calculated.

It has been shown by Migdal[43] that expanding to lowest order in phonon and coulomb propagators will treat the electron-phonon interaction exactly to order $(m/M)^{\frac{1}{2}} \sim 10^{-2}$ where m = electron mass M = ion mass.

Within this approximation to first order, utilizing the familiar rules for interpreting diagrams, one obtains for this self-energy term

$$\Sigma(\underline{k}\omega) = i \int \tau_3 G(\underline{k}'\omega') \tau_3 \{ \sum_{\lambda} | g_{\underline{k}\underline{k}'\lambda} |^2 D_{\lambda} (\underline{k}-\underline{k}', \omega-\omega') + V_c(\underline{k}-\underline{k}', \omega-\omega') \} \frac{d^3\underline{k}'}{(2\pi)^3} \frac{d\omega'}{2\pi} \qquad \text{------(4-9)}$$

Where $V_c(\underline{k}-\underline{k}', \omega-\omega')$ is a screened coulomb potential between electrons, $| g_{\underline{k}\underline{k}'\lambda} |$ is the electron, phonon coupling term for the λ'^{th} phonon branch as defined in equation (2-26), and $D_{\lambda}(\underline{q}, \varepsilon)$ is the Green's function for the phonon propagator. Denoting the energy of the $q\lambda^{th}$ phonon by $\omega(\underline{q}\lambda)$ to zeroth order $D_{\lambda}(\underline{q}\varepsilon)$ is given by

$$D_{\lambda} (\underline{q}\ \varepsilon) = \frac{2\ \omega(\underline{q}\lambda)}{\varepsilon^2 - \omega^2(\underline{q}\lambda) + i0^+} \qquad \text{------(4-10)}$$

This set of integral equations now specifies the superconducting state in terms of the phonon spectrum. More explicitly, recalling from equation (4-1) that we originally associated the pairing energy term with the function $\phi(\underline{k}\omega)$, a gap function $\Delta(\underline{k}\omega)$ can now be defined such that:

$$\Delta(\underline{k}\ \omega) \quad = \quad \phi(\underline{k}\ \omega)/\ Z(\underline{k}\ \omega) \qquad \text{------(4-11)}$$

which, it turns out, is simply an energy dependent generalization of the BCS energy gap of equation (3-12). In particular, the energy gap in the quasi-particle excitation spectrum is obtained from the solution of this energy dependent gap at Δ_o. i.e. $\Delta(\Delta_o) = \Delta_o$

After very involved but not unknown manipulative techniques[24,44], and after comparison and equating of coefficients in equation (4-7), these four dimensional equations can be reduced to a pair of coupled, one dimensional integral equations involving an energy dependent gap function $\Delta(\omega)$ and the renormalization function $Z(\omega)$ of the form[23].

$$\Delta(\omega) \quad = \quad \frac{N(0)}{Z(\omega)} \int_{\Delta(\Delta_o)}^{\omega_c} d\omega' \ \mathrm{Re} \left\{ \frac{\Delta(\omega')}{(\omega'^2 - \Delta^2(\omega'))^{\frac{1}{2}}} \right\} \left[K_+ \ (\omega\omega') - N(0)u_c \right]$$

$$\text{------(4-12)}$$

$$|1 - Z(\omega)|\ \omega \quad = \quad N(0) \int_{\Delta(\Delta_o)}^{\omega_c} d\omega' \ \mathrm{Re} \left\{ \frac{\omega'}{(\omega'^2 - \Delta^2(\omega'))^{\frac{1}{2}}} \right\} \left[K_-(\omega\omega') \right]$$

where ω_c is a cut off in energy $\approx 10\omega_{DEBYE}$ where the phonon contribution to this pair of equations has converged and further limits would not result in a change in this portion of the contribution. Unfortunately, this rapid convergence is not the case for the electron-electron repulsion v_c, as this term does not decrease rapidly for $\omega > \omega_{DEBYE}$. In order to circumvent this problem, an effective "pseudopotential" u_c is defined to compensate for this region outside ω_c not considered. This corrected potential method is an approximate method and still open to improvement.

It has been shown[45] that this pseudopotential term can be given approximately by:

$$u_c = V_c \,/\, 1 + N(0)\, V_c \, \ell n \left(\frac{E_F}{\omega_c} \right) \qquad \text{------(4-13)}$$

where

E_F = Fermi energy

V_c = spherical average of v_c

$N(0)$ = density of electron states at the Fermi surface

The kernels $K_{\pm}(\omega, \omega')$ in equation (4-12) are related to the contribution from the phonons to these equations and are defined by;

$$K \pm (\omega, \omega') = \int_0^{\infty} dv\, \alpha_\lambda^2(v) F_\lambda(v) \left[\frac{1}{\omega' + \omega + v + i0^+} \pm \frac{1}{\omega' - \omega + v - i0^+} \right] \qquad \text{------(4-14)}$$

where the product function

$$\alpha_\lambda^2(v) F_\lambda(v) = \frac{N(0)}{8\pi k_F^{\,2}} \int_{<2k_F} \frac{d^3q}{q} \; | g_{\underline{kk'},\lambda} |^2 \; \delta (v - \omega(\underline{q}, \lambda) \qquad \text{------(4-15)}$$

In the above, the integral over momentum transfer $\underline{q} = \underline{k} - \underline{k}'$ is performed throughout a sphere of radius $2k_F$ (twice the Fermi momentum). This is determined by assuming a spherical Fermi surface (free electron model) and hence the maximum allowed q - transfer is the diameter of the Fermi sphere. It is also assumed that the electron-phonon coupling term $g_{\underline{k}\underline{k}',\lambda}$ depends only on $\underline{q}$ (local approximation). These approximations appear to be sufficiently accurate for the work reported here. It is, in fact, possible to write a more general form for $\alpha_\lambda^2(\nu)F_\lambda(\nu)$ independent of these assumptions, namely

$$\alpha_\lambda^2(\nu)F_\lambda(\nu) = \frac{\int_{S_F} d^2k \int_{S_F} d^2k' \frac{\left|g_{kk',\lambda}\right|^2}{(2\pi)^3 v_F} \delta(\nu - \omega(\underline{k}-\underline{k}', \lambda)}{\int_{S_F} d^2k} \qquad \text{------(4-16)}$$

where the two integrals in k and k' are taken over the Fermi surface S_F and v_F is the Fermi velocity. Equation (4-16) will reduce to (4-15) in the appropriate limit.

Clearly, a summation over all possible phonon branches yields:

$$\alpha^2(\nu)F(\nu) = \sum_\lambda \alpha_\lambda^2(\nu)F_\lambda(\nu) \qquad \text{------(4-17)}$$

which simply describes all possible scatterings due to phonons of energy ν of a particular electron on the Fermi surface, to an arbitrary state on S_F averaged over all electrons at the Fermi surface.

Another way of saying this is that given an interacting Fermi surface, this function describes all possible scatterings

This quantity $\alpha^2(v)F(v)$ is of central importance to the phenomenon of superconductivity, as may be deduced from reflections as to the significance of equation (4-12). This equation tells us that this term, along with the electron-electron pseudopotential u_c of equation (4-13) is the determining factor for the onset of superconductivity in a material.

4.3 NUMERICAL SOLUTIONS OF THE GAP EQUATIONS:

Numerical solutions of these gap equations as applied to lead were first obtained by Schrieffer et al[29] who chose a phonon density of states distribution to roughly fit deviations from the BCS predicted electron tunneling curves of Rowell et al[27]. The chosen $F(\omega)$ consisted of two Lorentzian functions, one centered at 4.4 meV with a half width of 0.75 meV and the other centered at 8.5 meV with a half width of 0.5 meV. As little was known about the electron-phonon coupling parameter $\alpha^2(\omega)$, it was assumed to be a constant in energy and was adjusted such that the solution to these gap equations yielded $\Delta(\Delta_o) = 1.35$ meV - the experimentally observed value of the lead energy gap. From previous considerations of Bogoliubov et al[45] and Morel and Anderson[46], $N(0)u_c$ was estimated to be:

$$N(0)u_c \approx 0.11$$

This identical calculation has been repeated by the author using an iterative technique, commencing with the very crude estimate $\Delta(\omega) = \Delta_o = 1.35$ meV. Convergence to a stable solution occured in

FIGURE 4.1

Real (solid line) and imaginary (dotted line) parts of $\Delta(\omega)$ from the solution of the Eliashberg gap equations for the model $\alpha^2(\omega)F(\omega)$ of Schrieffer et al[29] $N(0)u_c = 0.11$

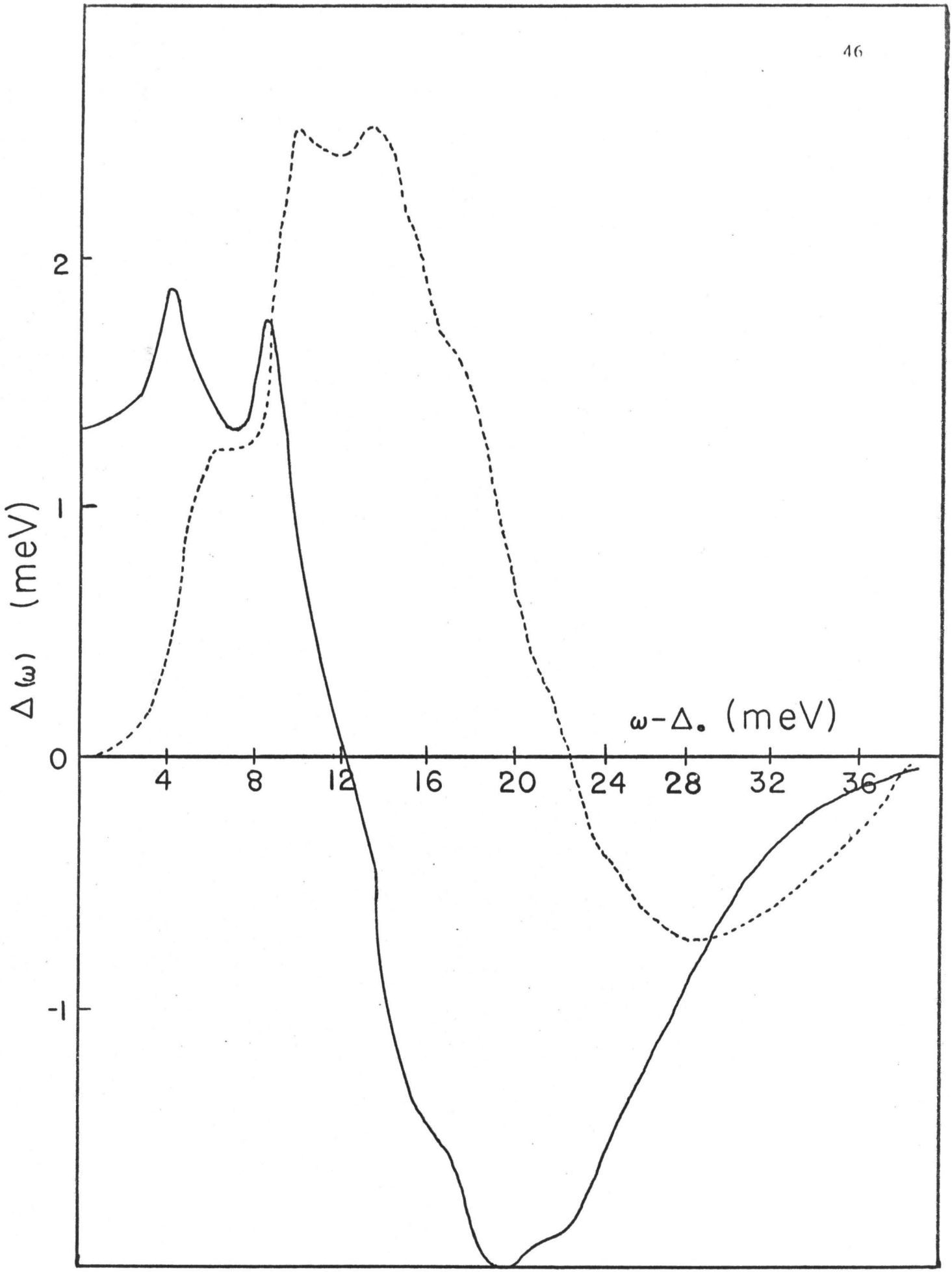
2
1
0
-1
Δ(ω) (meV)
ω-Δ. (meV)
4
8
12
16
20
24
28
32
36

approximately eight iterations. This solution, identical to that as originally solved by Schrieffer et al[29] is illustrated in Figure 4.1. The real part of $\Delta(\omega) \equiv \Delta_1(\omega)$ is the solid line curve while the imaginary part $\equiv \Delta_2(\omega)$ is represented by the dotted-line curve.

It is interesting to note a peak in the real part $\Delta_1(\omega)$ at the points $\omega = \Delta_o + \omega_t$ and $\omega = \Delta_o + \omega_\ell$ where ω_t and ω_ℓ are the chosen transverse and longitudinal peak points in the phonon density of states $F(\omega)$. This peaking in $\Delta(\omega)$ at these points indicates some sort of resonance phenomenom in the phonon contribution to these gap equations. It should also be noted that the imaginary part $\Delta_2(\omega)$ is small until ω approaches a certain critical threshold for the emission of transverse phonons at which point $(\Delta_o + \omega_t)$ there is a sharp rise in $\Delta_2(\omega)$. There is a similar sharp rise in the region $\Delta_o + \omega_\ell$, indicating a higher probability of longitudinal phonon emission. This finite imaginary part $\Delta_2(\omega)$, being of the same order as the real part $\Delta_1(\omega)$ indicates clearly that there is a strong coupling of the electrons to the phonons in lead. This means that for given electron energies there is a high probability for phonon emission and hence a short lifetime for certain states. The fact that this imaginary part is comparable to the real part suggests that at least in lead, the effect of the short lifetime is of major importance.

CHAPTER V

ELECTRON TUNNELING IN SUPERCONDUCTORS

Electron penetration through a region that is classically not allowed is now well documented by experimental evidence. This non-classical phenomenon was first applied to a theory describing α particle decay[47] of radioactive nuclides below the expected threshold level. Later, Fowler and Nordheim[48] applied the tunneling phenomenon to a theory of field emission of electrons from metallic surfaces and developed the fundamental field emission equation named after them.

The application of this phenomenon to describe current flow through an oxide between two metals (more explicitly, superconductors) will be described in this Chapter. In addition, it will be shown that, using this technique certain information about the superconductors used can be extracted.

5.1 TUNNELING PROBABILITY:

To be specific, we are interested in the tunneling of electrons from one thin metal film to another through an insulating barrier whose thickness is of the order of ≈ 20 A^{o}. It should be emphasized that the quotation of 20 A^{o} is quite an arbitrary figure as this thickness gives reasonable agreement when inserted into the tunneling equations. No conclusive evidence as to the thickness of these oxides used in these

FIGURE 5.1

Model of a tunnel junction as a finite potential barrier between two metals.

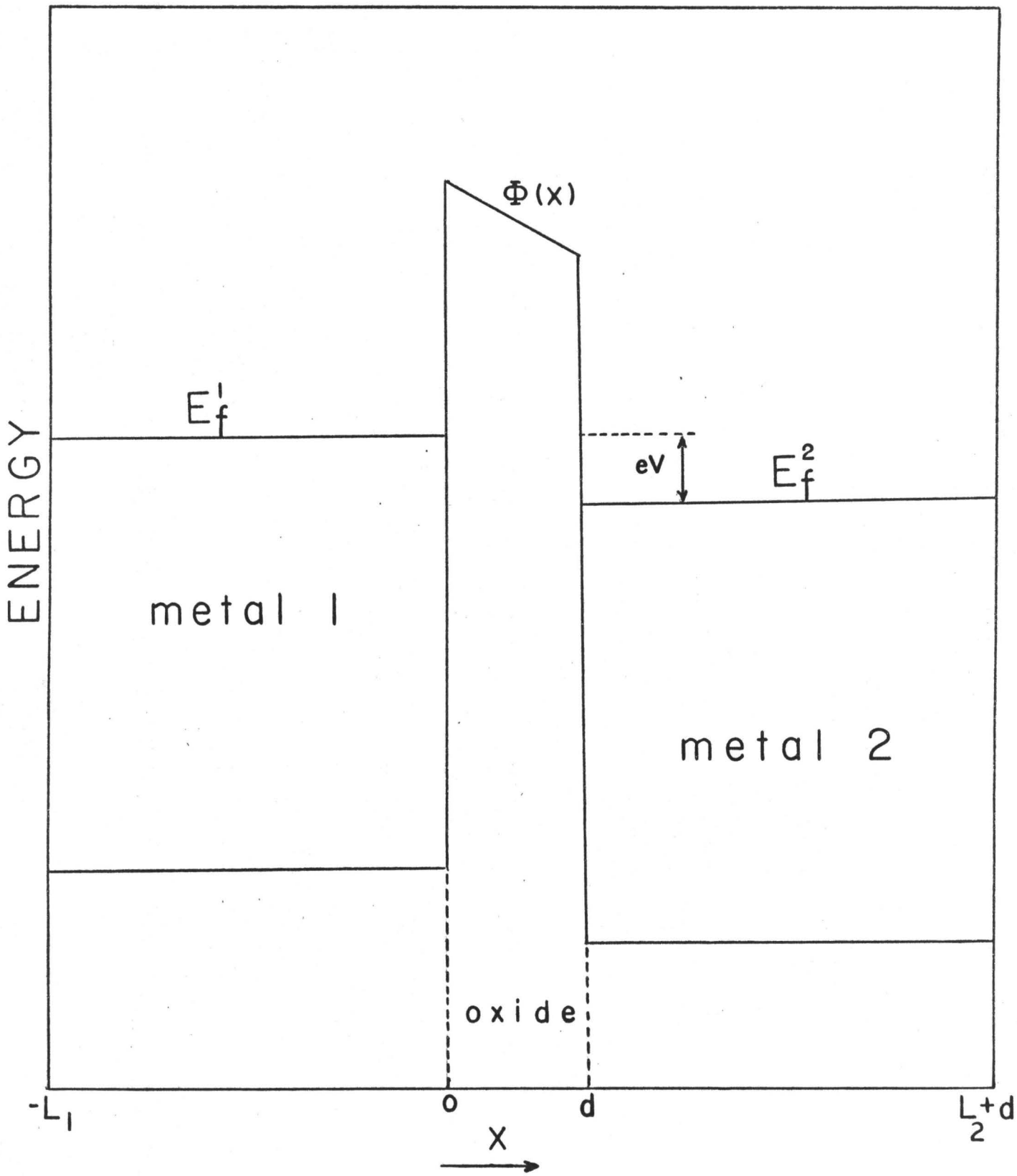
Φ(x)
E_f^1
eV
E_f^2
ENERGY
metal 1
metal 2
oxide
$-L_1$
0
d
L_2+d
X

investigations has been reported.

This type of system, a metal-insulator-metal sandwich, can be schematically represented by a well of electrons on either side of a high potential barrier, as illustrated in Figure 5.1. In this Figure:

V = applied voltage across the barrier

e = electron charge

E_F^1 and E_F^2 = the Fermi energies associated with metals 1 and 2

$\phi(x)$ = the barrier height as a function of x

The standard text book solution[31] of this tunneling problem, assuming that the tunneling probability is small, tells us that the transmission probability is given by:

$$T = \frac{16E_x\,(\phi(x) - E_x)}{\phi(x)^2} \exp\left[-\frac{2}{\hbar}\int_o^d 2m\left[\phi(x) - E_x\right]^{\frac{1}{2}} dx\right] \qquad \text{------(5-1)}$$

where E_x = kinetic energy associated with the x component of velocity $= \frac{\hbar^2 k_x^2}{2m}$,

d = barrier thickness

m = electron mass

A W.K.B. treatment is used to obtain this result. For low applied bias, the height of the barrier is approximately a constant $\phi(x) \doteq \phi_o$ and this approximation allows us to simplify the transmission probability T to:

$$T = \frac{16E_x(\phi_o - E_x)}{\phi_o} \exp\left[-\frac{2}{\hbar}\left[2m(\phi_o - E_x)\right]^{\frac{1}{2}} d\right] \qquad \text{------(5-2)}$$

It should be noted that in this treatment the barrier penetration is an exponentially decaying function of the barrier thickness, and consequently from a practical point of view, this limits the thickness to a small range for usable devices which operate on this principle.

5.2 THE TUNNELING EQUATIONS:

The Hamiltonian for the tunneling system was first set up by Bardeen[49] and later revised by Cohen, Falicov and Phillips[50]. Using this formalism, one can describe the complete tunneling system by an effective Hamiltonian:

$$H_{eff} = H_1 + H_2 + H_T \qquad \text{------(5-3)}$$

where H_1 and H_2 are the full Hamiltonians for metals 1 and 2 in the absence of tunneling between them, and H_T is a kind of interaction operator which transfers electrons between the two metals.

$$H_T = \sum_{\underline{kp}} T_{\underline{pk}} C^{+}_{\underline{k}} C_{\underline{p}} + \text{Hermitian conjugate} \qquad \text{---(5-4)}$$

where $C^{+}_{\underline{k}}$ and $C_{\underline{k}}$ are the usual particle creation and annihilation operators for metal 1 and $C^{+}_{\underline{p}}$ and $C_{\underline{p}}$ are similar operators for metal 2. $T_{\underline{pk}}$ is the matrix element between state $\underline{k}$ in metal 1 and $\underline{p}$ in metal 2. By a straight forward analysis[51], it can be shown that this matrix element reduces approximately to:

$$\left| T_{\underline{pk}} \right|^2 = \frac{h}{4m} \frac{v_F^2}{L_1 L_2} \left| \text{Transmission} \right| \qquad \text{------(5-5)}$$

where v_F is the Fermi velocity.

This includes electrons with kinetic energies near the Fermi energy $E_F = \frac{h^2 k_F^2}{2m}$ for which these tunneling matrix elements are peaked sharply for electrons moving in the x direction.

We are now in a position to consider the tunneling current across the barrier with a given applied voltage V. Assuming that there is no coulomb interaction between electrons of the different metals, and assuming no interaction of the tunneling electron with the barrier, one can calculate the rate of transfer of electrons from metal 1 to metal 2 as:

$$W_{1\to 2} = \frac{2\pi}{\hbar} \sum_{ab} | < a_1 | < b_2 | H_T | 0_1 > | 0_2 > |^2 \delta(\varepsilon_{a1} + \varepsilon_{b1} - eV) \qquad \text{------(5-6)}$$

where $| a_1 >$ and $| b_2 >$ are the exact eigen states of the full Hamiltonians of the individual metals, H_1 and H_2 respectively, with eigenvalues ε_{a1} and ε_{b2}.

i.e. $H_1 | a_1 > = \varepsilon_{a1} | a_1 >$

and $H_2 | b_2 > = \varepsilon_{b2} | b_2 >$

where ε_{a1} and ε_{b2} are measured relative to the ground state energies in 1 and 2 respectively. Substituting for H_T from equation (5-4) into equation (5-6) yields:

$$W_{1\to 2} = \frac{2\pi}{\hbar} \sum_{a_1 b_2} \Big| \sum_{\underline{pk}} T_{\underline{pk}} \langle a_1 | C_{\underline{k}} | 0 \rangle \langle b_2 | C_{\underline{p}}^{+} | 0 \rangle \Big|^2 \delta(\varepsilon_{a1} + \varepsilon_{b2} - eV)$$

------(5-7)

At $0^{o}K$ electrons cannot tunnel in the reverse direction as no states are available.

Using the identity

$$\int d\omega \;\; \delta(\varepsilon_{a1} - \omega) \;\; \delta(\varepsilon_{b2} + \omega - eV) = \delta(\varepsilon_{a1} + \varepsilon_{b2} - eV)$$

we can rearrange equation (5-7) and it can be readily seen that the current density is proportional to

$$\int_0^{eV} d\omega \sum_{\underline{kp}} |T_{\underline{kp}}|^2 \sum_{a_1} |\langle a_1 | C_{\underline{k}} | 0_1 \rangle|^2 \sum_{b2} |\langle b_2 | C_{\underline{p}}^{+} | 0_2 \rangle|^2$$

$$\times \;\; \delta(\varepsilon_{a1} - \omega) \;\; \delta(\varepsilon_{b2} + \omega - eV)$$

-------(5-8)

$$= \int_0^{eV} N_{T+}^{(2)}(E)\, N_{T-}^{(1)}(eV - E)\, dE \qquad \text{-------(5-9)}$$

where $N_{T+}^{(2)}(E)$ is an effective tunneling density of states for metal 2 given by

$$N_{T+}^{(2)}(E) = \sum_{\underline{p}b2} |\langle b_2 | C_{\underline{p}}^{+} | 0_2 \rangle|^2 \delta(\varepsilon_{b2} - E) \qquad \text{----(5-10)}$$

and

$$N_{T-}^{1}(E) = \sum_{\underline{k}a_1} |< a_1 \mid C_{\underline{k}} \mid 0_1 >|^2 \ \delta(\varepsilon_{a1} - E)$$

Physically this $N_{T+}^{(2)}(E)$ is the density of available states at energy E in metal 2, while $N_{T-}^{(1)}(E)$ is the density of occupied states in metal 1 with energy E.

Clearly, this result tells us that we take an electron from metal 1 of energy (eV - E) measured relative to that metal, and inject it into metal 2 with energy E. This transition is proportional to the product of the density of filled states in metal 1 and the density of empty states in metal 2.

One can conveniently picture this single particle tunneling process by invoking the dispersion curve for excitations presented in Chapter III, where the excitation energy is given by:

$$E_{\underline{k}} = [\varepsilon_{\underline{k}}^{2} + \Delta_{\underline{k}}^{2}]^{\frac{1}{2}}$$

(see Figure 3.2)

Using this model for excitations (single particle states) one can first consider a junction of the type metal-insulator-superconductor as is illustrated in Figure 5.2a.

In this tunneling process, an electron of state $\mid \underline{k}\uparrow >$ is extracted from below the Fermi surface of the normal metal leaving behind a hole in this state, and thereby creating an excitation energy $\varepsilon_{a1} = \mid \varepsilon_{\underline{k}} \mid$.

FIGURE 5.2

E vs. k plots for (a) metal-insulator-superconductor (b) superconductor-insulator-superconductor and the possible tunneling paths.

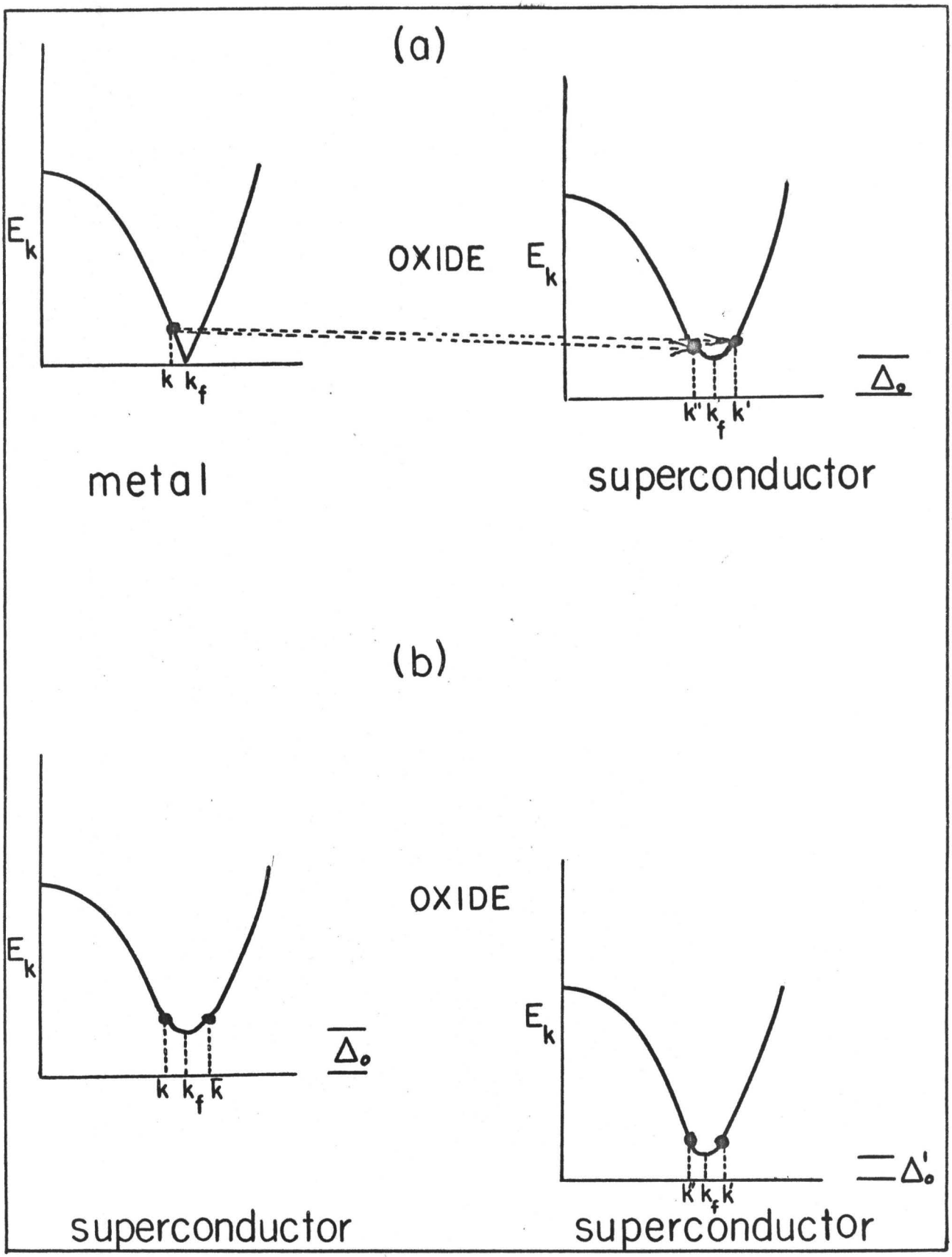
(a)
E_k
k k_f
OXIDE
E_k
k'' k_f k'
$\overline{\Delta_o}$
metal
superconductor
(b)
E_k
k k_f $\bar{k}$
$\overline{\Delta_o}$
OXIDE
E_k
k'' k_f k'
$=\Delta'_o$
superconductor
superconductor

This electron can now be inserted into the state $|\underline{k}'\rangle$ or $|\underline{k}''\rangle$ as is illustrated in the Figure. For example, if the particle is deposited in $|\underline{k}\uparrow\rangle$ an excitation energy of $\varepsilon_{b2} = (\varepsilon_{\underline{k}'}^2 + \Delta_{\underline{k}'}^2)^{\frac{1}{2}}$ will be imparted to the superconductor. Of course, this event will occur only if the pair state $|\underline{k}'\uparrow - \underline{k}'\downarrow\rangle$ is initially empty (the probability being $u_{k'}^2$). Energy is conserved when $|\varepsilon_k| + \varepsilon_{b2} = eV$. As was mentioned previously, however, we see that energy will also be conserved when the quasiparticle is inserted into the state $|\underline{k}''\uparrow\rangle$. Consider for the moment that $\Delta_{\underline{k}}$ = a constant Δ_o. Since we know that $\varepsilon_{\underline{k}'} = -\varepsilon_{\underline{k}''}$, a substitution of this equality into the equations defining $u_{\underline{k}}^2$ and $v_{\underline{k}}^2$ (equation (3-8)), yields the probability of state $|\underline{k}''\uparrow - \underline{k}''\downarrow\rangle$ being initially empty as $u_{\underline{k}''}^2 = v_{\underline{k}'}^2$. From these occupation considerations, therefore, the probability that the tunneling process will occur, is given by:

$$u_{\underline{k}'}^2 + v_{\underline{k}'}^2 = 1$$

Consequently, the tunneling process is not dependent on these coherence terms u and v. Returning to Figure 5.2a, and invoking conservation of energy considerations, we see that a tunneling event is not allowed until a threshold bias defined by

$$V = \frac{\Delta_o}{e}$$

is applied. Of course, this analysis is at an assumed temperature of 0^oK. At finite temperatures, thermally excited quasi particles can tunnel below this threshold bias due to the fact that their thermal energy

satisfies this requirement.

In a similar fashion, one can consider the superconductor-insulator-superconductor case as illustrated in Figure 5.2b. In this case, as before, the particle in state $|\underline{k}\uparrow\rangle$ can tunnel into either the state $|\underline{k}'\uparrow\rangle$ or the state $|\underline{k}''\uparrow\rangle$. In addition, however, one should note that the particle in state $|\overline{\underline{k}}\uparrow\rangle$ can also tunnel to the same two states. Employing this fact, and an identical argument as before, one finds that again the coherence factors drop out and the probability of tunneling (with respect to the Pauli principle) is $u_{\underline{k}}^2 + v_{\underline{k}}^2 = 1$.

At $0^{o}K$, there will be no current flow until the threshold bias

$$V = \frac{\Delta_o + \Delta_o'}{e}$$

is applied. Again, finite temperature excitations will smear out this expected sharp rise in the tunneling current at $\frac{\Delta_o + \Delta_o'}{e}$, and in the case of two dissimilar superconductors, a cusp in the current-voltage characteristic will result at the bias

$$V = \frac{\Delta_o - \Delta_o'}{e}$$

5.3 TUNNELING DENSITY OF STATES:

It has been shown[44,51], using the sophistication of the Green's function techniques in order to take into account lifetime effects, that this effective tunneling density of states defined by equation (5-10) is

given by:

$$N_{T\pm}(\omega) = N(0)\ \mathrm{Re}\left(\frac{\omega}{(\omega^2 - \Delta^2(\omega))^{\frac{1}{2}}}\right) \qquad \text{------(5-11)}$$

where Re refers to the real part component, N(0) = normal density of states at the Fermi surface. $\Delta(\omega) = \Delta_1(\omega) + i\Delta_2(\omega)$ = complex energy dependent gap function. In the case of a simple BCS superconductor where $\Delta(\omega) = \Delta_o$, we see that this solution to the tunneling density of states reduces to

$$N_{T\pm}(\omega) = N(0)\left(\frac{\omega}{\sqrt{\omega^2 - \Delta_o^2}}\right) \quad \text{for } \omega > \Delta_o$$

$$= 0 \quad \text{for } \omega < \Delta_o \qquad \text{------(5-12)}$$

as is expected. This function, the so called semiconductor model of a superconductor, is illustrated in Figure 5.3. Although in some respects this model is useful in interpreting tunneling data, care must be taken in the analysis of results. In this respect, one must always bear in mind that in this picture the states illustrated as being above the gap, and hence above the Fermi level, are really linear combinations of quasiparticles existing above and below the Fermi surface (i.e. the particles in $|k'>$ and $|k''>$ in our discussion of tunneling in this Section.

We have previously seen that in considering retardation and life-time effects, a complex energy dependent gap function $\Delta(\omega)$ results. Consequently the detailed structure must be considered in equation (5-11) and we find that this density of states is no longer a simple function,

FIGURE 5.3

B.C.S. tunneling density of states $N_T(\omega)$. ω is measured from the Fermi surface.

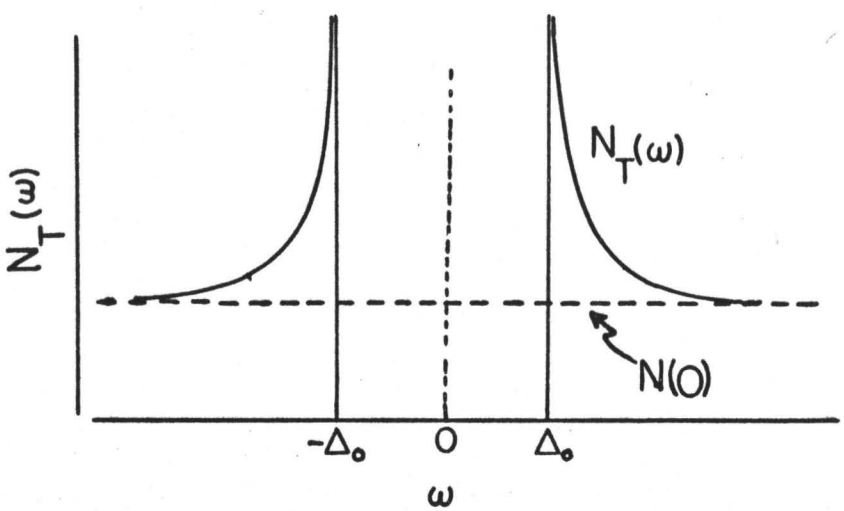
$N_T(\omega)$
$N_T(\omega)$
N(0)
$-\Delta_o$
0
Δ_o
ω

but it displays deviations from the simple BCS form of equation (5-12). A solution to the gap equations (4-12) for a particular choice of $\alpha^2(\omega)F(\omega)$ and $N(0)u_c$ will give us the form of this tunneling density of states $N_T(\omega)$.

Returning to our expression for the tunneling current flow, we can extract an expression for this term $N_T(\omega)$ in terms of our measurable variables I and V. In the simplest case of metal 1 in the normal state and metal 2 in the superconducting state, with recourse to equations (5-9) and (5-11), we obtain the result that:

$$\frac{\left(\frac{dI}{dV}\right)_S}{\left(\frac{dI}{dV}\right)_N} = \frac{N_{T\pm}(eV)}{N(0)} = Re\left(\frac{eV}{\sqrt{(eV)^2 - \Delta^2(eV)}}\right) \qquad \text{-----(5-13)}$$

where $\left(\frac{dI}{dV}\right)_S$ and $\left(\frac{dI}{dV}\right)_N$ are the derivatives of the I-V characteristic curves when the superconductor is in the superconducting and normal state respectively. Therefore a tunneling experiment (at 0^oK) for a metal-insulator-superconductor system will give us a direct measure of this tunneling density of states $N_T(\omega)$, and hence information about the energy dependence of the energy gap parameter $\Delta(\omega)$-- which in turn yields information about the phonon density of states, or more explicitly about $\alpha^2(\omega)F(\omega)$.

Alternatively, if one assumes a particular form of $\alpha^2(\omega)F(\omega)$ and $N(0)u_c$, the gap equations (4-12), when solved for $\Delta(\omega)$, will give us a particular form for $N_{T\pm}(\omega)$ and consequently predict the characteristics of a tunneling experiment.

FIGURE 5.4

Experimental tunneling density of states $N_T(\omega)$ for lead (solid line) compared with that predicted by the model $\alpha^2(\omega)F(\omega)$ of Schrieffer et al[29] (dotted line).

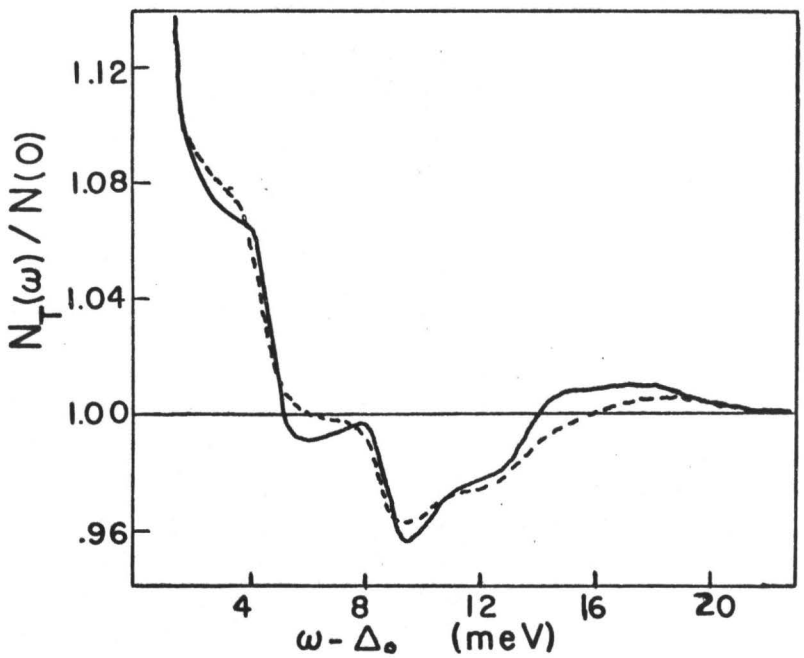
1.12
1.08
1.04
1.00
.96
$N_T(\omega) / N(0)$
4
8
12
16
20
$\omega - \Delta_o$ (meV)

5.4 GAP SOLUTIONS FOR $N_T(\omega)$:

As was outlined in Section 4.2, these gap equations were solved[29,44] for a model $F(\omega)$ closely resembling the phonon density of states of Pb as determined from neutron scattering experiments[52], and an adjustable parameter $\alpha^2(\omega) = \alpha_o$ = a constant. It was found that there was striking agreement in the predicted and experimental $N_{T\pm}(\omega)$ values in view of the crude choice of $F(\omega)$. The results of this comparison is shown in Figure 5.4 using the solution to the gap equations illustrated in Figure 4.1.

The physical reason for these deviations from the simple BCS predicted value is as follows. Upon scrutiny, one observes that there is a sharp deviation (drop) from the BCS expression at that point in energy $\Delta_o + \omega_{transverse}$. It has already been implied that at this point of high density of phonon states available for scattering, attenuation is very high. This attenuation is enhanced by the fact that there is a high density of quasiparticle states available for the electron to fall into at the edge of the gap (the singularity at the point $\Delta(\Delta_o)$). Consequently, a particle injected into a material at this prescribed energy has a high probability of emitting a phonon ω_t and dropping to the state $\Delta(\Delta_o)$. Therefore, the lifetime of such particles is greatly reduced and this lifetime effect manifests itself as a decrease in the density of single particle states at these prescribed energies. For a similar reason, there is a large drop in this density of states at $\Delta(\Delta_o) + \omega_{longitudinal}$.

To accurately determine the positions of maximum attenuation and consequent sharp deviations from BCS predictions, and even more important,

to discern any singularities in the phonon density of states[53], it is convenient to again differentiate the current-voltage characteristics[54], which gives one the derivative of $N_T(\omega)$. The sharp deviations from BCS now show up as peaks (maxima and minima) and van Hove singularities in $F(\omega)$, recognizable from neutron scattering experiments, have been identified[55] in these second derivative plots.

From Figure 5.4 and this discussion, it becomes apparent that if one were sufficiently knowledgeable about the product function $\alpha^2(\omega)F(\omega)$, one could reproduce the experimental results to a much better accuracy. Alternatively, with enough insight and intuition, one could, from careful inspection of the results of a tunneling experiment, extract the product function $\alpha^2(\omega)F(\omega)$ to a better accuracy than was achieved by Schrieffer et al[29].

A calculation of this inversion from experimental data to $\alpha^2(\omega)F(\omega)$ has been performed for lead[30], tin, indium, mercury[51] and lead-indium alloys[56]. An iterative procedure was employed commencing with an experienced guess of $\alpha^2(\omega)F(\omega)$, solving the gap equations and then comparing with experiment. $\alpha^2(\omega)F(\omega)$ was adjusted accordingly, and the procedure repeated. Using this type of an iterative method, an extremely good fit to $\alpha^2(\omega)F(\omega)$ was calculated reproducing very well the tunneling experiments. This function $\alpha^2(\omega)F(\omega)$ for lead, superimposed on a plot of $\frac{d^2I}{dV^2}$ vs V for an Pb-I-Pb junction, is illustrated in Figure 5.5. One can see explicitly how $\frac{d^2I}{dV^2}$ varies with respect to a critical point or maximum in the product function $\alpha^2(\omega)F(\omega)$.

FIGURE 5.5

$\alpha^2(\omega)F(\omega)$ for lead[30] with a plot of $\frac{d^2I}{dV^2}$ vs. V for a Pb-I-Pb junction. ω is measured from $2\Delta_o$.

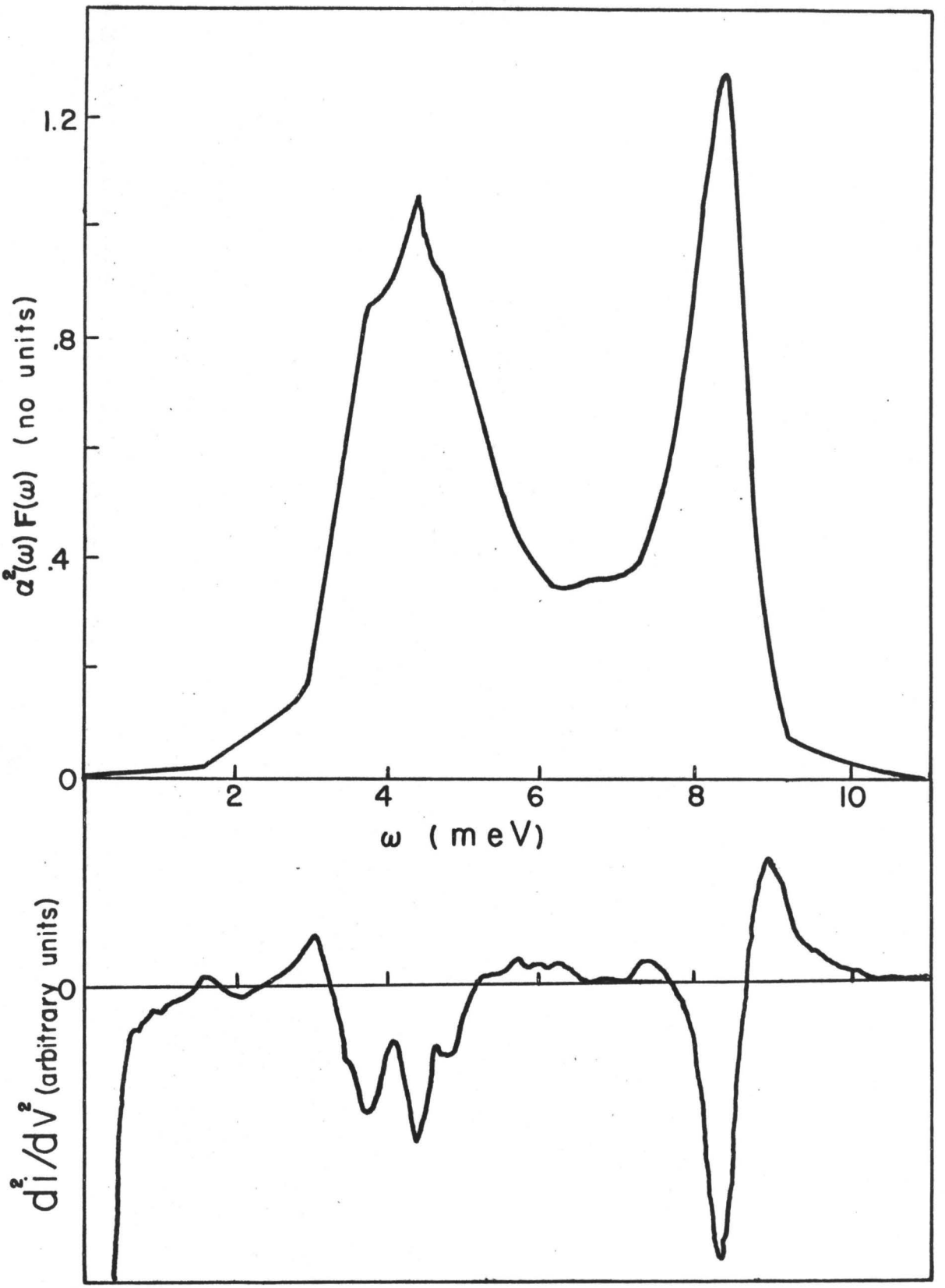
1.2
.8
.4
0
$\alpha^2(\omega)F(\omega)$ (no units)
2
4
6
8
10
ω (meV)
0
d^2i/dV^2 (arbitrary units)

CHAPTER VI

SAMPLE PREPARATION AND EQUIPMENT

One of the major problems facing the experimenter in the production of a tunnel junction suitable for the analysis of these effects in a superconductor, is the fabrication of an insulating barrier some tens of angstroms thick. Any small filaments or "shorts" of conductor through this insulator will be the preferred path for current transfer due to the relatively low probability for tunneling and hence any effects associated with the tunneling phenomenon will be masked by conventional conduction mechanisms.

The various methods used by investigators to fabricate these tunnel junctions are outlined in this Chapter. In addition, the techniques used to study the characteristics of the devices are described and the advantages and disadvantages of these techniques over others discussed.

6.1 JUNCTION CONSTRUCTION:

6.1-1 General Remarks -

There are two major requirements to be satisfied in order that a reasonably uniform barrier be constructed. Firstly, the host metal onto which the barrier is constructed should be reasonably smooth and free from contamination.

Secondly, the barrier material must be well bonded to the host metal in order to prevent cracking and breaking of the barrier during thermal cycling.

Vacuum deposited films satisfy the first criterion very well[57] and the naturally grown oxide of the host material appears to be the best candidate to fulfill the second requirement. When tunneling experiments have been required on bulk materials, several investigators have polished single crystal samples sufficiently smooth to thermally grow a uniform oxide adequate for tunneling. Dietrich[58] has reported successful tunneling experiments on tantalum prepared by electropolishing the tantalum, subsequently followed by careful cleaning, thermally growing of a thin oxide, and vacuum deposition of a metal over the oxide. Zavaritskii[59], on the other hand, has produced clean, smooth surfaces of single crystal tin by pouring molten tin onto optically flat glass in a vacuum, and cooling slowly. Subsequent oxidation of these smooth surfaces and vacuum deposition of a metallic film has produced a junction of suitable thickness for a tunneling investigation of energy gap dependence on crystallographic direction. Various attempts[60] following these and other methods have been attempted for single crystal lead but as yet have not met with success.

One of the more promising methods of preparing a tunnel junction into bulk material is that of the point contact method[61]. With this method an anodized point contact of Nb (or Ta, Al etc.) is brought into contact with the bulk material under study. This material has been previously oxidized so that on the surface there is an oxide much thicker

than is conducive for good tunnel junctions. Upon cooling of the system, the tip is pressed into the oxide until the penetration is sufficient to allow a reasonable probability for tunneling. Surprisingly enough, this method appears to produce useful tunnel junctions into bulk materials but there is some question as to surface damage due to the pressure of the tip causing results not indicative of the bulk material.

Another method, attempted successfully by this author was that of vacuum evaporating a thin film of an insulating oxide onto an already existing vacuum evaporated metallic film. Having deposited a 1000 Å film of lead, a layer of aluminum oxide was deposited by the slow evaporation of aluminium in a 5×10^{-4} torr atmosphere of oxygen. Using a thickness calibration described in a subsequent section, it was estimated the thickness of this film $\sim$ 20 Å . The evaporation was carefully controlled over $\sim$ 10 minutes to produce this film. This method displayed a limited amount of success in that most of the samples prepared displayed filaments or "shorts" behaviour. Approximately 20% of the samples attempted displayed tunneling as the dominant conduction mechanism. From the low probability of success it was concluded that, wherever possible, the naturally grown oxide was the best candidate.

Aluminum is a very likely material to serve as the base metal onto which the oxide is grown for two reasons. Firstly, even for extremely thin films, aluminum deposits in a uniform and electrically conducting manner. Conducting films, 75 Å thick on the average are easily produced. Secondly, aluminum oxidizes in atmospheric conditions very rapidly to a thickness suitable for a tunneling barrier. A widely accepted theory of oxidation[62] of aluminum assumes that the tunneling of

electrons through the oxide is necessary to further oxide growth. Consequently, if this process is arrested before completion of the formation of the barrier, by the addition on the surface of the oxide of a second metallic film, the tunneling probability is still finite and a usable tunnel junction will result.

6.1-2 Fabrication Procedure -

A soda-glass microscope slide was used as a substrate onto which the device was constructed. The slide previously was outgassed at about 200°C, under a vacuum of about 1 mm of mercury, for several hours. It was then washed using a commercial cleanser and carefully rinsed with distilled water. If the distilled water formed a smooth film over the entire surface of the slide with no grease spots appearing, it was considered clean enough and the preparation procedure proceeded. Although these steps were by no means considered elaborate cleaning procedures, it was observed that there was no serious dependence of the device characteristics on the degree of care taken beyond a certain minimum value in the cleansing operation[63].

After cleaning, the substrate was placed in a vacuum-coating unit and the base metallic film, in the form of a long strip was deposited in a vacuum of less than 1×10^{-5} torr. If the basis film was aluminum, the vacuum was broken to air for 1-2 minutes, the substrate was masked in such a fashion that cross strips could be deposited, and the evaporation procedure for the material under study was carried out. The final device was constructed to give a pattern of the form illustrated in Figure 6.1.

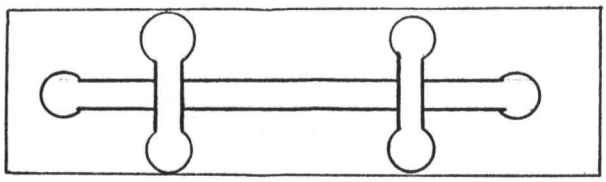

FIGURE 6.1

CONFIGURATION OF METAL-INSULATOR-METAL SANDWICHES

The larger pads at the ends of the strips were included to facilitate the fastening of electrical leads to the films. To achieve this end, indium was used as the solder to join the copper leads from the sample holder to these pads. Indium was used as it gives good electrical contacts and stands up well under thermal shocks. In addition indium has a low melting point (156.2^{o}C) and because of the fragility of the tunnel junction, high temperatures applied in the region of the barrier are not advisable. Using this procedure, tunneling junctions of the type Aℓ-I-X have been manufactured where I refers to the insulating barriers, and X refers to the superconductor under test.

In the literature, in discussing the characteristics of junctions, investigators have referred to the "resistance" of the device. This is purely an operational term in analogy with Ohm's law where the current voltage characteristic is linear and a resistance can be defined. For a tunnel junction, the I-V characteristic is approximately linear when the constituents are in the normal state. Under these circumstances one could refer to the "resistance" of the junction but it should be pointed

out that there is no power dissipation in the tunneling barrier and no resistance as it is usually defined. Nevertheless, it is sometimes convenient to catagorize junctions by their "resistances".

For the experiments described here it was convenient to produce junctions with resistances of 10 - 1000 ohms. Higher resistance junctions reduced tunneling currents unnecessarily and other conduction mechanisms began to dominate these characteristics thus masking out tunneling effects. Josephson tunnel junctions[64,65] on the other hand, require lower resistances, typically in the order of 10^{-1} or 10^{-2} ohms.

Generally the base, or aluminum film deposited was $\sim$ 100Å . The thickness of these films was monitored by a method described in a subsequent section. It has been noted[66,68] that for very thin films of aluminum, the superconducting transition temperature was enhanced, and since the transition temperature of bulk aluminum is 1.2°K, which was approximately the ultimate temperature of the cryostat used in this Thesis, these enhanced transition temperatures were imperative for our study of a superconductor-insulator-superconductor system. Utilizing this phenomenon, some investigators[67] have observed transition temperatures of thin Aℓ films as high as 4.5°K.

6.2 THE VACUUM COATING UNIT AND EVAPORATION TECHNIQUES:

6.2-1 Coating Unit -

An Edwards model 12E3 vacuum-coating unit was employed in the production of the thin films studied in this Thesis. With a liquid nitrogen trap in the form of a spirally wound length of $\frac{3}{8}$ " copper tubing

at the throat of the diffusion pump, (to reduce backstreaming of diffusion pump oil and to condense water and other vapours present), a vacuum of $\sim 1 \times 10^{-6}$ torr was obtainable although most evaporations were made in a vacuum $\lesssim 1 \times 10^{-5}$ torr. This coating unit had a 12-inch bell jar with a four position rotary filament holder to allow successive evaporations without breaking vacuum. Further, the substrate was masked in such a fashion that the mask could be changed with the aid of a mechanical access without breaking vacuum. This mechanical access also served both as a filament shutter, and as a device to successively feed materials to a hot filament.

6.2-2 Film Thickness Measurements -

Inside the coating unit very near the substrate, (and the same distance from the source filament as the substrate), was mounted a 6Mc/s A-T cut quartz crystal with gold electrodes on either face. It is well known[57] that for small changes in frequency of a quartz crystal oscillator, the frequency shift is a linear function of the change in mass on the surface. Hence an oscillator circuit external to the bell jar was connected to this crystal and the frequency of oscillation was monitored on a Hewlett Packard model 3734A digital counter so that the mass of material evaporated could be determined. Using a microbalance, slides were weighed before and after evaporation of various materials and, (utilizing figures for the bulk densities of these materials), a calibration curve of mass deposited on the substrate (and hence thickness, assuming the density) versus frequency shift of the oscillator was obtained.

FIGURE 6.2

Thickness vs. frequency shift calibration curve for 6 Mc quartz crystal used to determine deposited film thickness.

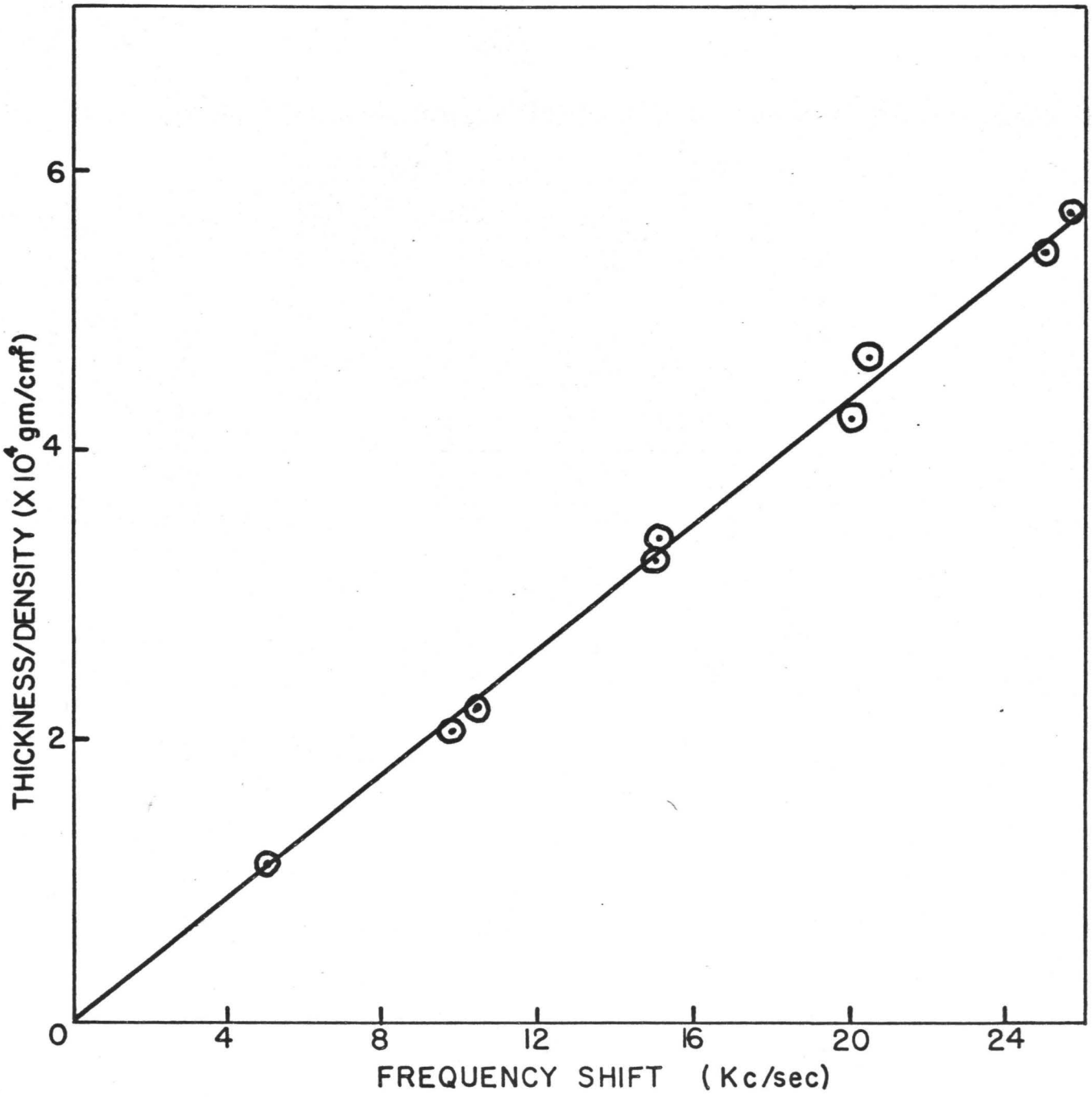
THICKNESS/DENSITY (X 10⁴ gm/cm²)
0
2
4
6
4
8
12
16
20
24
FREQUENCY SHIFT (Kc/sec)

FIGURE 6.3

Electron micrograph of (a) 500 Å lead film (b) 120 Å aluminum film. Magnification = 30,000 X.

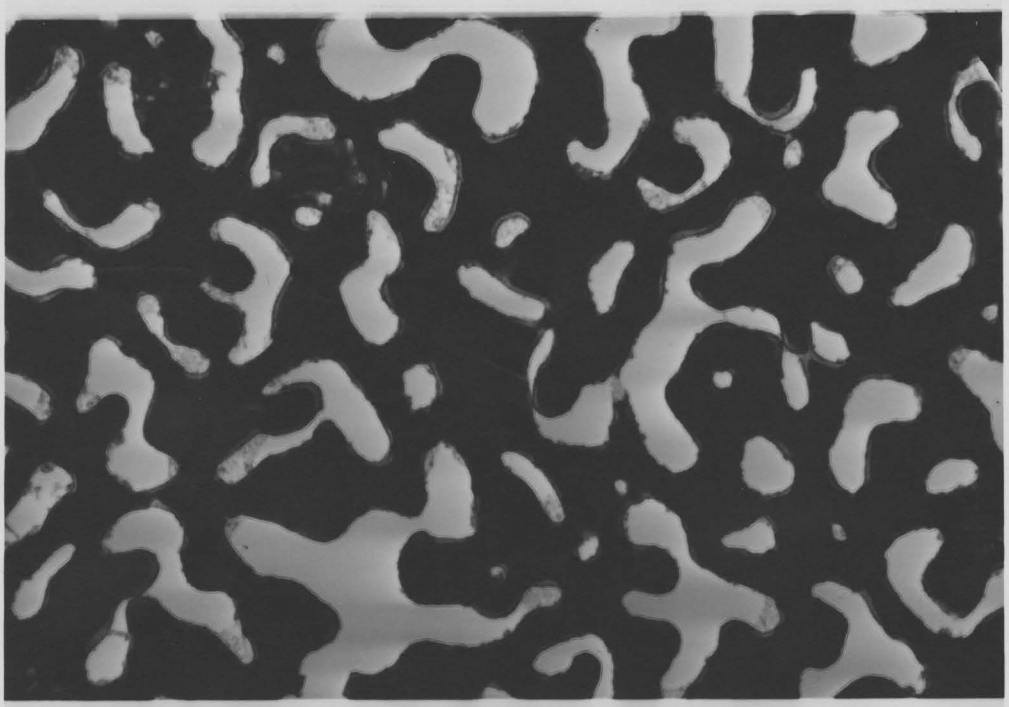

(a)

(b)

Such a calibration is shown in Figure 6.2 where reasonable linearity is observed. It should be emphasized that this calibration is strictly for this experimental arrangement and a different piece of apparatus would require a separate calibration.

It should also be pointed out that this is a measure of the average thickness over a macroscopic area and in certain materials is not a particularly good measure of the actual thickness. Figure 6.3 illustrates this point quite clearly in which an electron micrograph of a lead film evaporated onto a room temperature substrate, and measured as 500 Å thick, may be compared to a micrograph of a 120 Å aluminum film prepared in the same fashion at approximately the same rate of evaporation. Clearly, on this scale (magnification 30,000 x) there are large holes and islands on the lead film and in no way could it be considered uniform. In fact, it is quite surprising that an oxide can be grown on such a rugged surface uniformly enough to produce a tunnel junction[69]. On the other hand, the aluminum film of 120 Å displays many small crystallites spread in a much more uniform fashion throughout the film and hence thickness quotations are perhaps more meaningful. Thickness quotations in the literature should be carefully examined as to the method of measurement and the material used.

6.2-3 Film Fabrication Techniques -

Tungsten helical coils were used as filaments for the evaporation of aluminum. It has been pointed out[70] that even though alloying of the tungsten occurs at high temperatures, the tungsten is reprecipitated from

the melt as the aluminum evaporates and there is no significant contamination in the aluminum film deposited.

Although the vapour pressures of lead, bismuth and thallium, the three constituents of the alloy system investigated in this Thesis are approximately equal, it was found that a simple evaporation of the previously prepared bulk alloy from a molybdenum boat produced ambiguous results in the tunneling characteristics which could most easily be described as multigap behaviour--due to inhomogeneities or concentration gradients through the thickness of the film. This demand for a more reliable method for preparation of the films resulted in the utilization of a flash evaporation technique-evaporating tiny pellets of the alloy in such a fashion that no concentration gradient could appear through the film. Tiny pellets of the alloy were placed in a stainless steel tube approximately 1" above a molybdenum boat, and a stainless steel ramrod was inserted in the other end of the tube. The filament was heated far above that temperature required to evaporate either constituent of the alloy and the pellets, one by one, were pushed onto the filament by the ramrod such that they evaporated very rapidly. Although there was considerable difference in the size of these pellets, each pellet produced, on the average, approximately 20 $\mathring{A}$ of film. Hence throughout the film it was hoped that only small local fluctuations of concentration would result. This appeared to be the case as for all alloy concentrations considered, unambiguous current-voltage characteristics indicated good gap behaviour utilizing this method. The concentration of constituents of the film, averaged throughout the film thickness, was measured by an electron microprobe[71] and it was found that the concentrations of the

FIGURE 6.4

Flash evaporation arrangement.

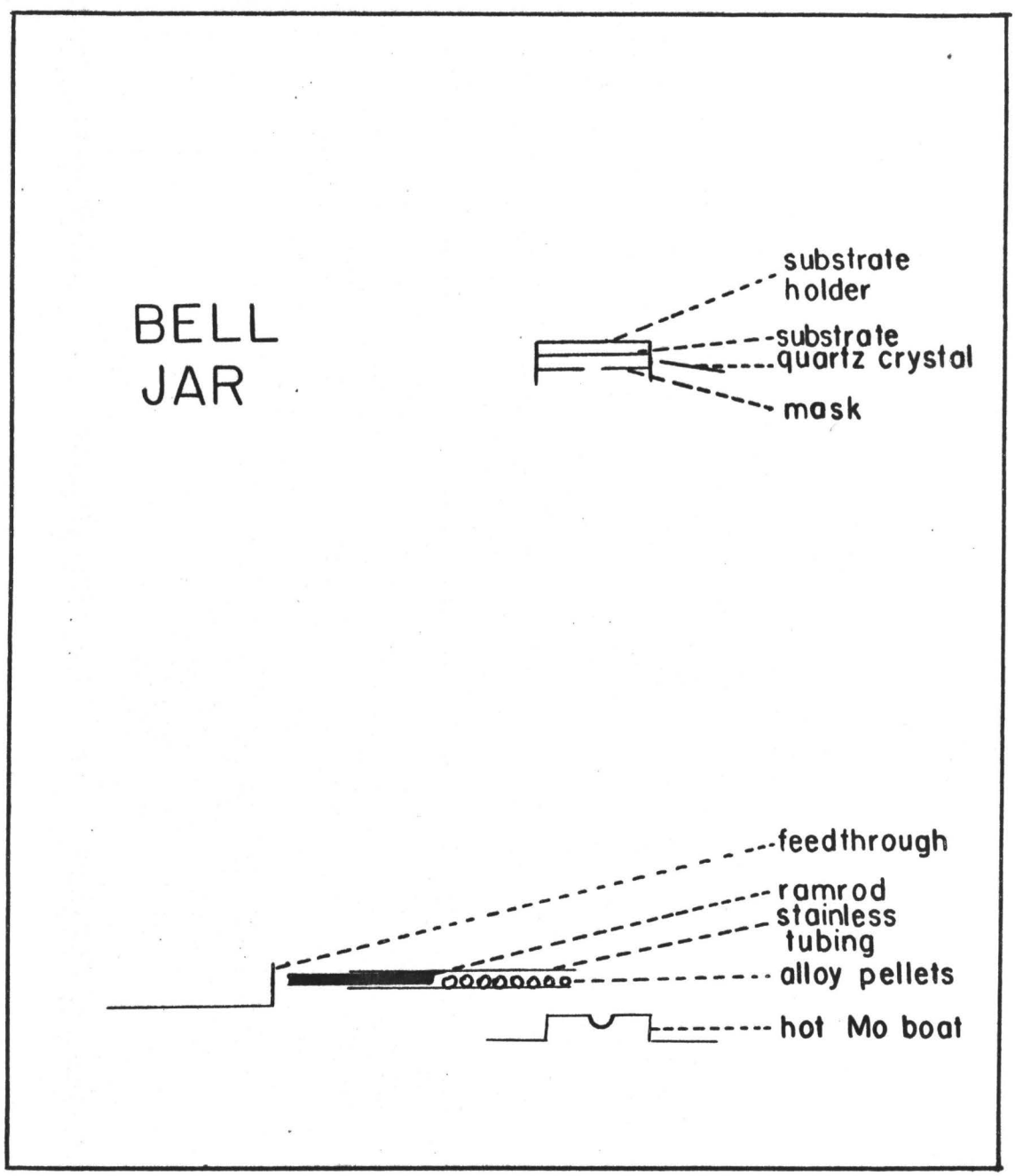
BELL
JAR
substrate
holder
substrate
quartz crystal
mask
feedthrough
ramrod
stainless
tubing
alloy pellets
hot Mo boat

constituents was within 5% of that of the bulk material. Since thallium was extremely toxic, rubber gloves were used at all times in the handling of this material.

A schematic representation of this method is illustrated in Figure 6.4.

6.3 ELECTRICAL CIRCUITRY:

6.3-1 Current-Voltage Characteristics-

For energy gap measurements, a dc voltage sweep circuit has been used. The circuit used to study these I-V characteristics is shown in Figure 6.5a. The variable dc bias for the junctions was obtained from a Harrison type 6200A programmable power supply which was resistance programmed by a variable external resistor included in the reference feedback circuit of the supply. For these experiments, a suitable voltage time sweep was obtained with the aid of a reversible dc variable speed-motor and a 10-turn, 10K ohm helipot resistor. A typical sweep speed used in the experiments for I-V plots was $\sim$.1 millivolt per minute. Current through the sample was monitored on the Y axis of a Moseley type 7001AX-Y recorder and the potential developed across it was monitored on the X-axis.

6.3-2 Harmonic Detection Circuit -

As was pointed out in Chapter V, for studies of the tunneling density of states function, it is extremely advantageous to investigate in much more detail the fine structure of the current-voltage characteristics. This closer scrutiny is achieved by differentiating the

FIGURE 6.5

(a) Circuitry used to measure I-V characteristics

(b) Circuitry used to measure derivatives of I-V characteristics.

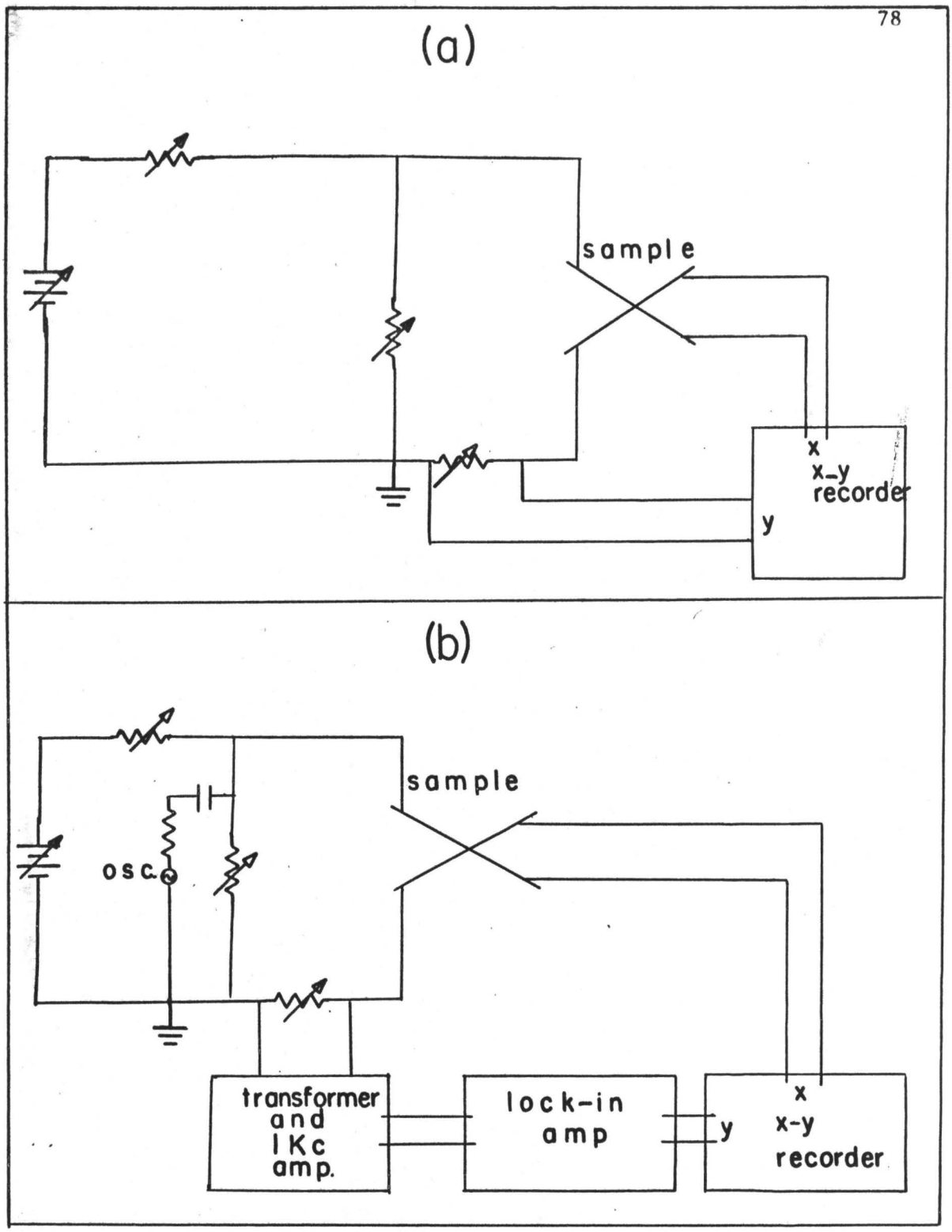
(a)
sample
x
x-y
recorder
y
(b)
sample
osc.
transformer
and
1Kc
amp.
lock-in
amp
y
x
x-y
recorder

original plot with respect to voltage i.e. by obtaining $\frac{dI}{dV}$ and $\frac{d^2I}{dV^2}$ versus V. A standard and very convenient method of obtaining these functions is by means of the a-c modulation or harmonic detection technique.

If one applies a small amplitude sinusoidal signal $V_1 \sin \omega t$ to the sample at angular frequency ω, and detects the resulting current through the sample at ω or the first harmonic 2ω, one obtained functions that are proportional to the derivatives $\frac{dI}{dV}$ and $\frac{d^2I}{dV^2}$ respectively.

To see this, suppose that the potential developed across the sample is:

$$V = V_o + V_1 \sin \omega t = V_o + \delta V$$

where V_o is the dc bias and V_1 is the amplitude of the modulation. Further suppose that one can consider the Taylor expansion of current as a function of voltage about the dc bias point. One consequently obtains

$$I(V) = I(V_o) + \left.\frac{dI}{dV}\right|_{V_o} \delta V + \frac{1}{2!} \left.\frac{d^2I}{dV^2}\right|_{V_o} (\delta V)^2$$

$$+ \frac{1}{3!} \left.\frac{d^3I}{dV^3}\right|_{V_o} (\delta V)^3 + \frac{1}{4!} \frac{d^4I}{dV^4} (\delta V)^4 + \text{-----}$$

$$+ \text{higher order terms}$$

Applying a sinusoidal function for $\delta V = V_1 \sin \omega t$ we obtain, after regrouping and suitable trigonometric substitutions.

$$I(V) - I(V_o) = I_{ac} = \left[\left.\frac{d^2I}{dV^2}\right|_{V_o} \frac{V_1^2}{4} + \left.\frac{d^4I}{dV^4}\right|_{V_o} \frac{V_1^4}{64} + \text{------} \right]$$

$$+ \sin \omega t \left[\left.\frac{dI}{dV}\right|_{V_o} V_1 + \frac{1}{8} \left.\frac{d^3I}{dV^3}\right|_{V_o} V_1^3 + \frac{1}{192} \left.\frac{d^5I}{dV^5}\right|_{V_o} V_1^3 + \text{---} \right]$$

$$+ \cos 2\omega t \left(- \frac{1}{4} \left.\frac{d^2I}{dV^2}\right|_{V_o} V_1^2 - \frac{1}{48} \left.\frac{d^4I}{dV^4}\right|_{V_o} V_1^4 - \text{---------} \right)$$

$$+ \sin 3\omega t \left(- \frac{1}{24} \left.\frac{d^3I}{dV^3}\right|_{V_o} V_1^3 - \frac{1}{384} \left.\frac{d^5I}{dV^5}\right|_{V_o} V_1^5 - \text{-------} \right)$$

$$+ \cos 4\omega t \left(\text{----------} \right)$$

+ higher order terms.

To first order in this expansion, we see that the fundamental frequency detected will be proportional to the first derivative $\left(\frac{dI}{dV}\right)$ of the I-V characteristic evaluated at the dc bias point V_o. In addition the first harmonic (2ω) is proportional to the second derivative $\left(\frac{d^2I}{dV^2}\right)$ of the characteristic. Experimentally, in the region of the characteristic that is almost linear, it is observed by tuning to various harmonics of the fundamental, that to the accuracy of the measuring instrument it is valid

to truncate each coefficient after its first term.

The circuitry used to measure these derivatives is illustrated in Figure 6.5b. The oscillator (General Radio model 1311A) supplies a 1000 c/s or 500 c/s (depending upon whether $\frac{dI}{dV}$ or $\frac{d^2I}{dV^2}$ is desired) on top of the dc applied bias across a dropping resistor. The amplitude of this signal must be small as compared to the sharpness of the detail on the curve to be investigated. If this ac modulation is too high, any sharp structure (in this case the sharp edge of the energy gap or van Hove singularities) will be smeared out. The signal to be detected across a measuring resistor is coupled to a Model 1034 Keithley transformer, followed by a twin-T narrow band 1000 c/s amplifier[72] subsequent to which it is fed to a PAR lock in amplifier. The dc signal from this final stage is then inserted into the Y axis of the X-Y recorder.

For accurate recording of $\frac{dI}{dV}$ measurements, an ac probe of amplitude no greater than 50 μ volts peak-to-peak was employed with no appreciable smearing of the fine structure resulting. In the more subtle non-linear regions above the energy gap, due to the fact that the non-linearities were not very pronounced, it was found that in order to detect any harmonics of the fundamental signal it was necessary to increase the amplitude of the fundamental at the possible expense of loss of the recorded fine structure. Increasing the signal to approximately 250μ V peak-to-peak seemed to give the best balance between these two conflicting problems, with no appreciable amount of smearing resulting.

Sensitivity was not the only problem confronting this method of measurement as drift in the oscillator or amplifiers gave a slowly varying time dependent signal not inherent in the device. Since low recorder

sweep speeds were employed in these experiments (1 - 2 hours per single trace), then such drift signals were, of necessity, required to be very much smaller than those changes being detected from the device, if accurate recordings were to be effected.

This simple detection system is adequate for purposes of comparison of predicted and experimental values (as will be discussed in the next Chapter). If quantitative work (i.e. inversion of the gap equations using experimental results) is to be carried out, however, a more elaborate bridge network[73] is required to balance out the large constant background signal.

6.4 CRYOSTAT AND SAMPLE HOLDER:

6.4-1 Cryostat -

Most of this work was carried out in an Andonian type 3-litre liquid helium dewar. Temperatures down to 1.10°K were obtained with the aid of an Edwards ISC 3000, 3000 litres/min rotary pump connected to a 6-inch pumping line system. For such temperature measurements the helium vapour pressure was measured[60] and conversion from vapour pressure to temperature was achieved through the T_{58} scale[74].

6.4-2 Sample Holder -

It was found that the simplest type of sample holder afforded the most flexibility. Total immersion of the sample in liquid He^4 at the end of a long thin-walled stainless steel tube allowed the samples to be introduced and removed from the cryostat while liquid was present. This allowed rapid shock cooling of the sample and permitted the examination

of several samples with one dewar-full of He^4. By this method, one could very quickly decide whether a particular sample would yield useful results or not thus permitting a subsequent rapid change of samples to be studied. In addition, electrical contacts were sometimes known to come loose during the cooling down of the sample, (probably due to differential contraction), and this quick change arrangement made immediate repairs possible. Also, it was found that Pb-I-Pb and Sn-I-Sn samples gave better tunneling characteristics if they were quickly immersed after preparation. If slowly cooled, the same device would develop filaments or shorts through the oxide during the cool down.

To minimize heat leaks, the leads to the sample were 0.003 inch diameter copper wire with enamel insulation, wound around the stainless steel support tube which served as support for the sample holder.

6.4-3 Magnet -

Since this sample holder was of the immersion type, and temperatures above $4.2^{o}K$ were not obtainable, it was sometimes necessary, in order to measure $\left(\frac{dI}{dV}\right)_S / \left(\frac{dI}{dV}\right)_N$ parameters, (see equation (5-13)) to apply a magnetic field to the device to drive it into the normal state. This was achieved by the insertion of a superconducting solenoid of niobium suspended on the sample holder in such a fashion that the device would be in the position of maximum field. The magnet itself was powered by a Harrison Lab model 520A power supply. Although normal-state studies were principally achieved in this manner it was convenient on occasion, however, to raise the temperature of the liquid helium bath to this end.

CHAPTER VII

RESULTS AND DISCUSSION

7.1 $F(\omega)$ and $\alpha^2(\omega)F(\omega)$:

Having determined the influence that the phonon density of states has on the superconducting properties of a particular material, we are now in a position to calculate $F(\omega)$, the phonon density of state, and $\alpha^2(\omega)F(\omega)$ the product function determining superconductivity, utilizing the techniques outlined in Appendix A. In this Thesis such calculations have been applied in particular to the following materials, namely, Na, K, Aℓ, Pb, $Pb_{.8}Tℓ_{.2}$, $Pb_{.6}Tℓ_{.4}$, $Pb_{.4}Tℓ_{.6}$, $Tℓ_{.8}Bi_{.2}$ and $Tℓ_{.1}$, $Bi_{.9}$. The results of these calculations for the various materials studied are outlined in Figures 7-1 and 7-9. As will be outlined in the next Section, the detailed shape of some of these functions is suspect due to the non-convergence of the force constant model used to calculate them. Although the general shape of some of these functions may be incorrect (most probably in pure lead and high lead-concentration alloys), for bulk thermodynamic properties and for the determination of superconductivity, it appears to be adequate.

In each of these figures, the product function $\alpha^2(\omega)F(\omega)$ is superimposed on the phonon density of states $F(\omega)$. Since the units of $F(\omega)$ are given to be $(meV)^{-1}$ while those of $\alpha^2(\omega)F(\omega)$ are dimensionless, the electron-phonon coupling function $\alpha^2(\omega)$ has units of energy (meV).

FIGURE 7.1

Calculated $\alpha^2(\omega)F(\omega)$ (dotted line) as a function of phonon energy ω compared with density of phonon states $F(\omega)$ (solid line) for sodium.

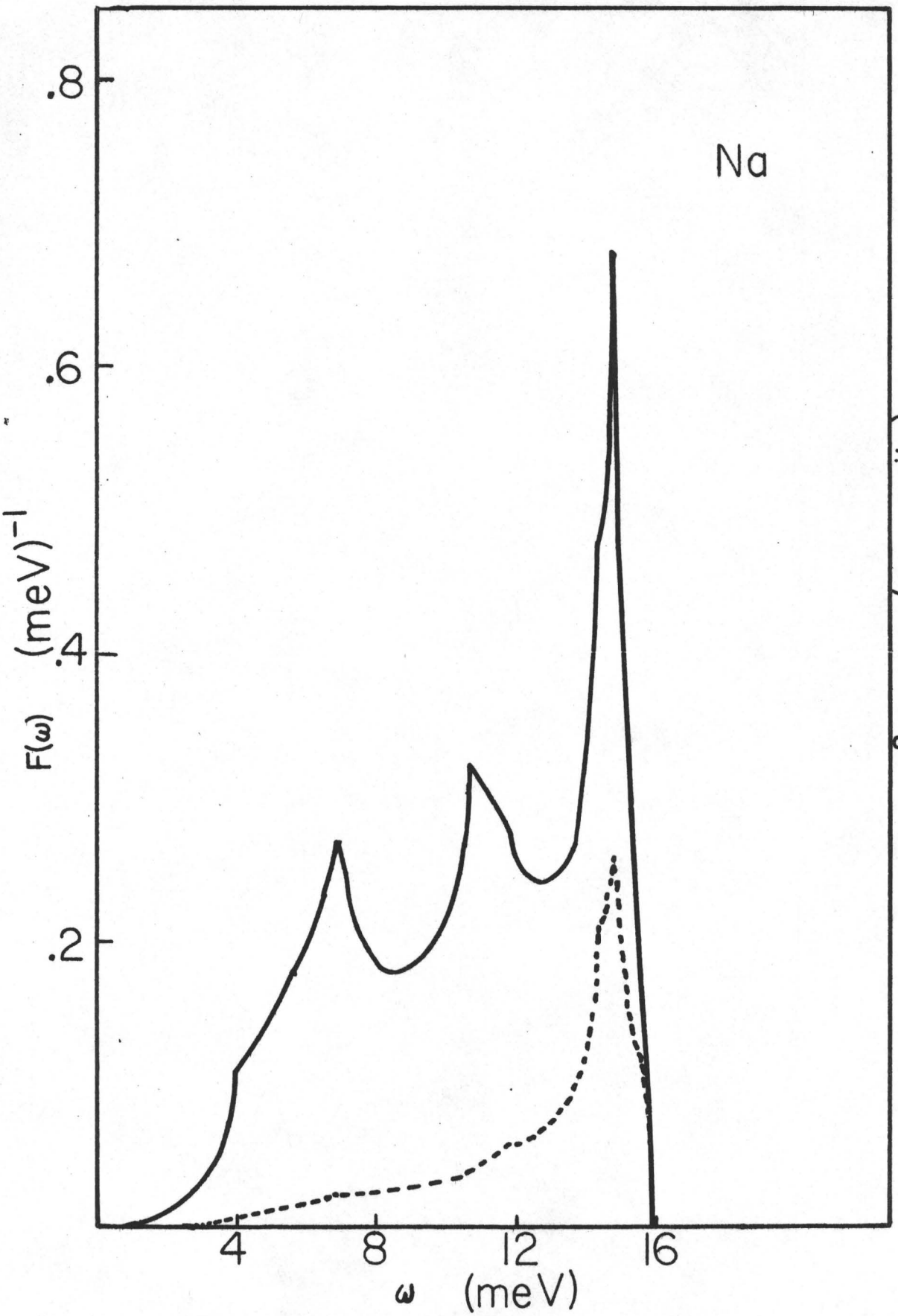
Na
.8
.6
.4
.2
F(ω) (meV)⁻¹
α²(ω) F(ω) (no units)
4
8
12
16
ω (meV)

FIGURE 7.2

Calculated $\alpha^2(\omega)F(\omega)$ (dotted line) as a function of phonon energy ω compared with the phonon density of states $F(\omega)$ (solid line) for potassium.

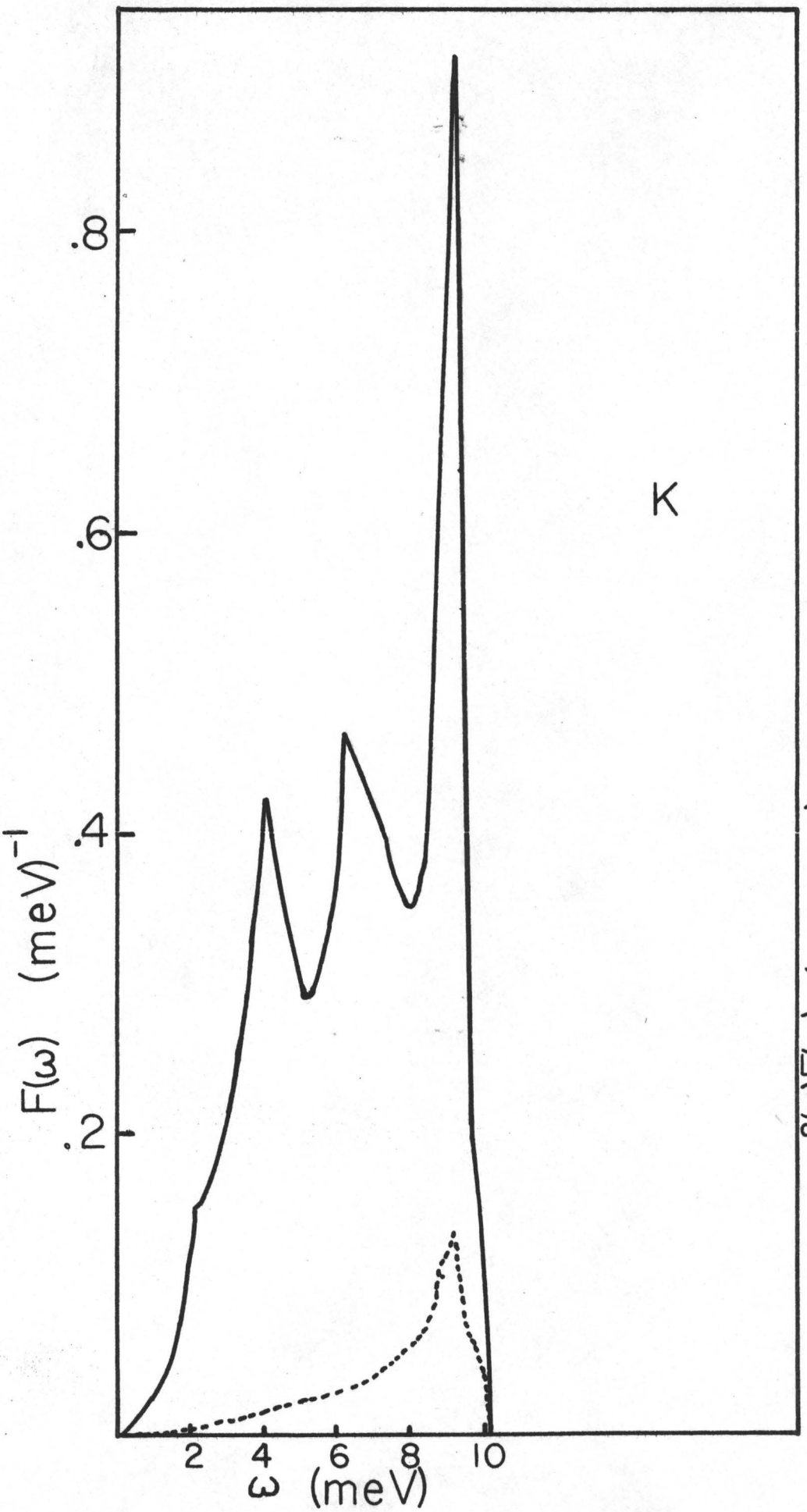
.8
.6
.4
.2
F(ω) (meV)⁻¹
K
α²(ω)F(ω) (no units)
2
4
6
8
10
ω (meV)

FIGURE 7.3

Calculated $\alpha^2(\omega)F(\omega)$ (dotted line) as a function of phonon energy ω compared with the density of phonon states $F(\omega)$ (solid line) for aluminum.

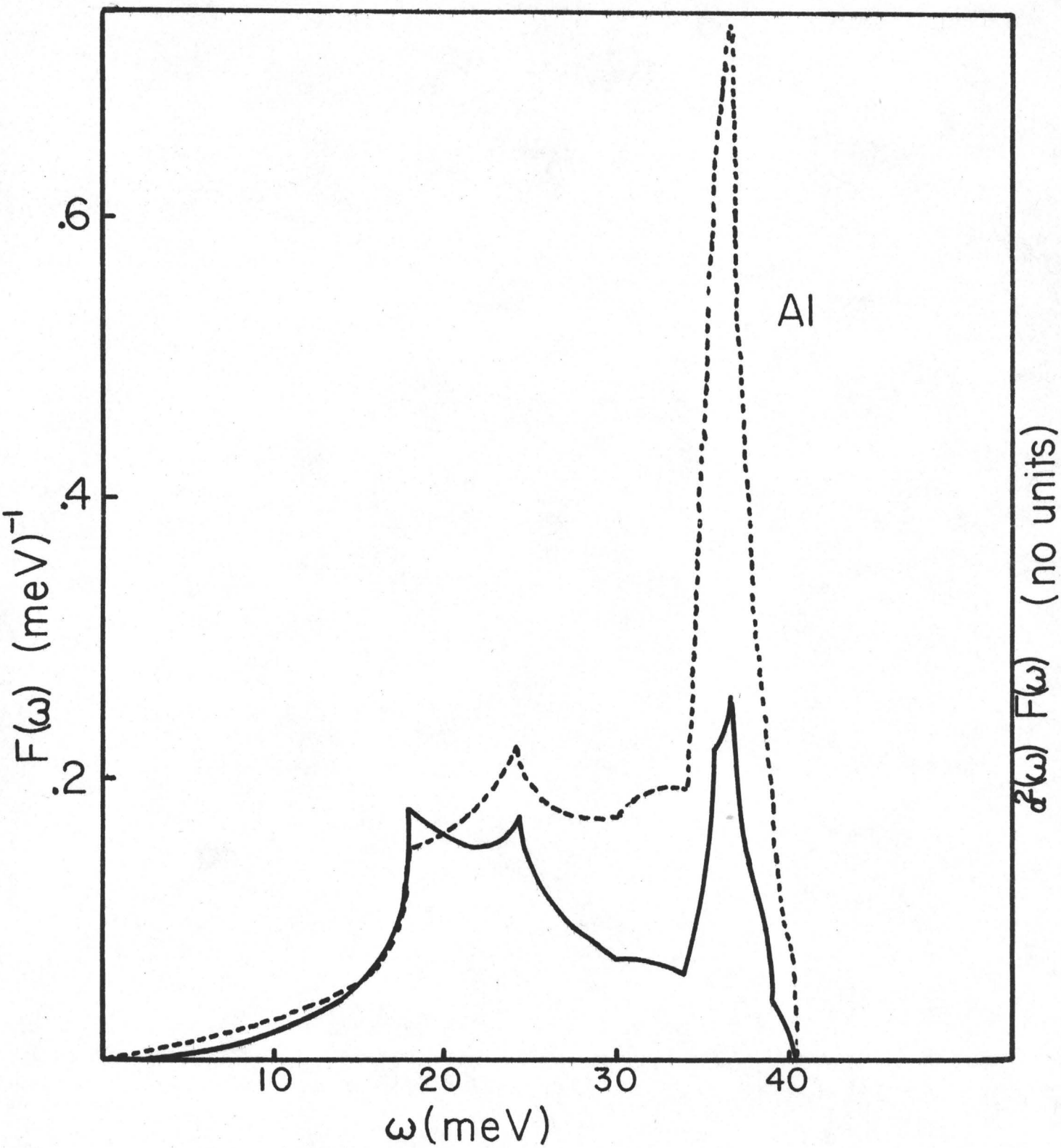
.6
.4
.2
F(ω) (meV)⁻¹
Al
α²(ω) F(ω) (no units)
10
20
30
40
ω(meV)

FIGURE 7.4

Calculated $\alpha^2(\omega)F(\omega)$ (dotted line) as a function of phonon energy ω compared with the phonon density of states $F(\omega)$ for $Tl_{.9}Bi_{.1}$.

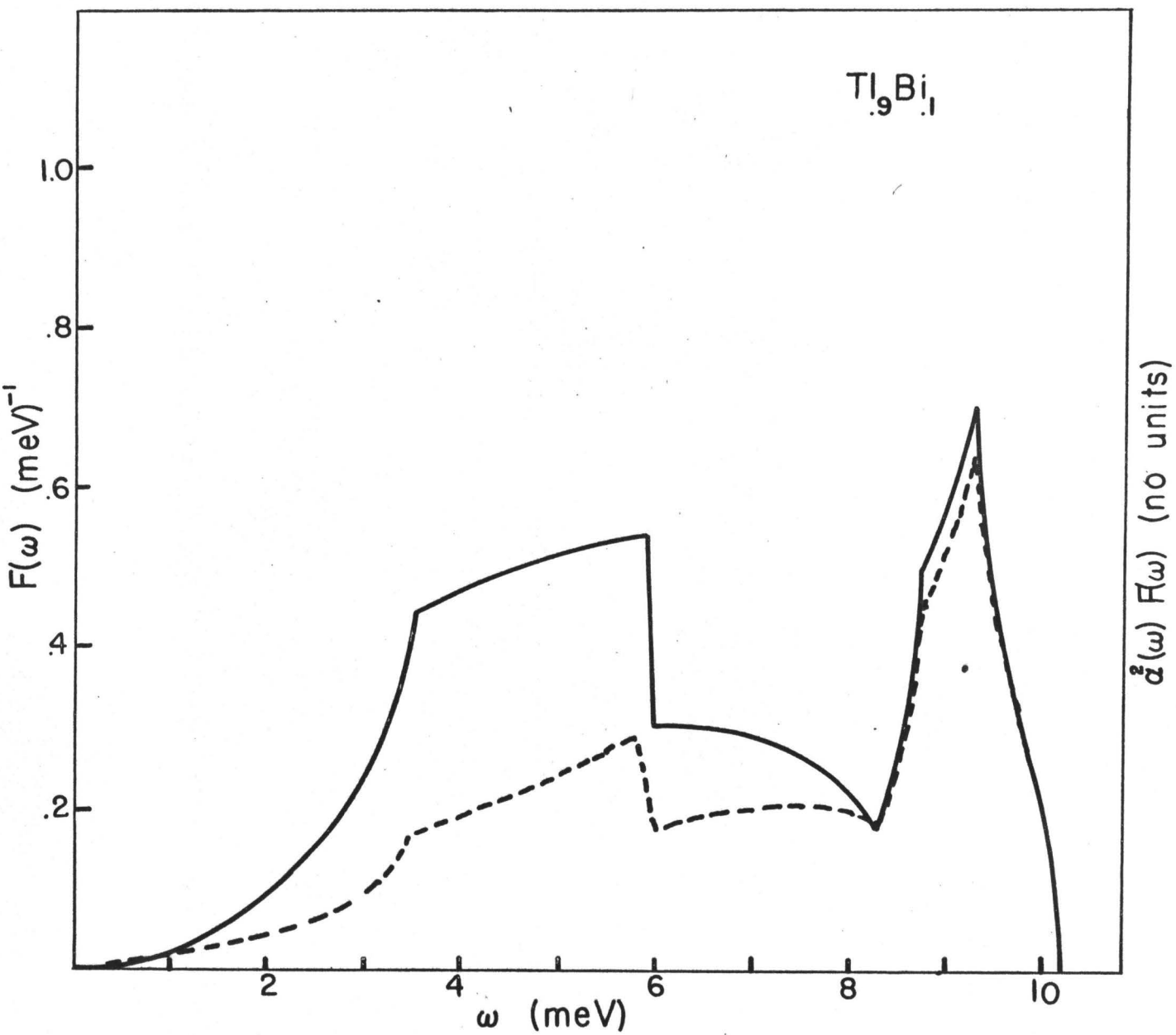
$Tl_{.9}Bi_{.1}$
1.0
.8
.6
.4
.2
$F(\omega)$ $(meV)^{-1}$
2
4
6
8
10
ω (meV)
$\alpha^2(\omega)$ $F(\omega)$ (no units)

FIGURE 7.5

Calculated $\alpha^2(\omega)F(\omega)$ (dotted line) as a function of phonon energy ω compared to the density of phonon states $F(\omega)$ (solid line) of $Tl_{.8}Bi_{.2}$.

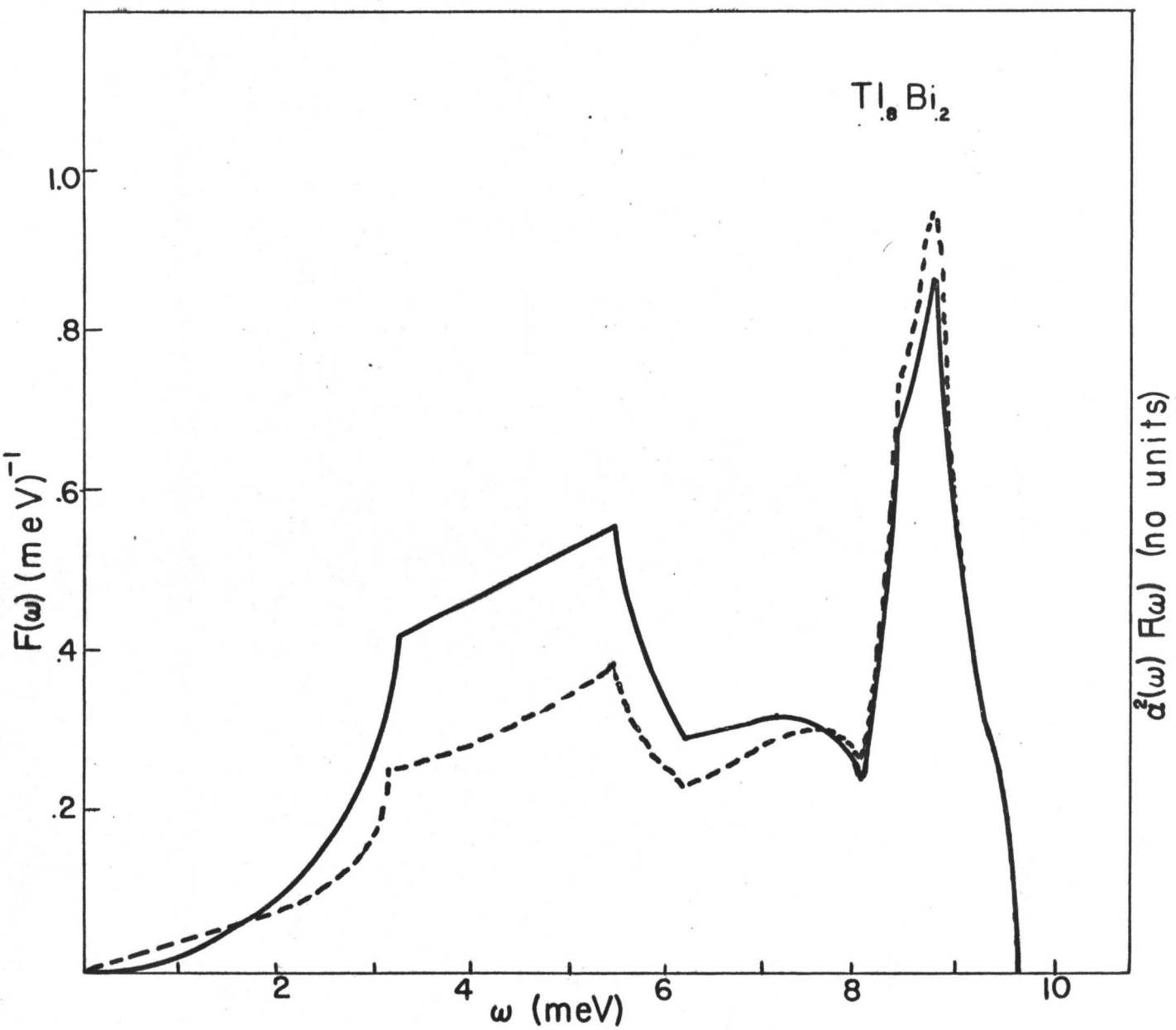
$Tl_{.8}Bi_{.2}$
1.0
.8
.6
.4
.2
$F(\omega)$ (meV)$^{-1}$
2
4
6
8
10
ω (meV)
$\alpha^2(\omega)$ $F(\omega)$ (no units)

FIGURE 7.6

Calculated $\alpha^2(\omega)F(\omega)$ (dotted line) as a function of phonon energy ω compared to the density of phonon states $F(\omega)$ (solid line) in $Pb_{.4}Tl_{.6}$.

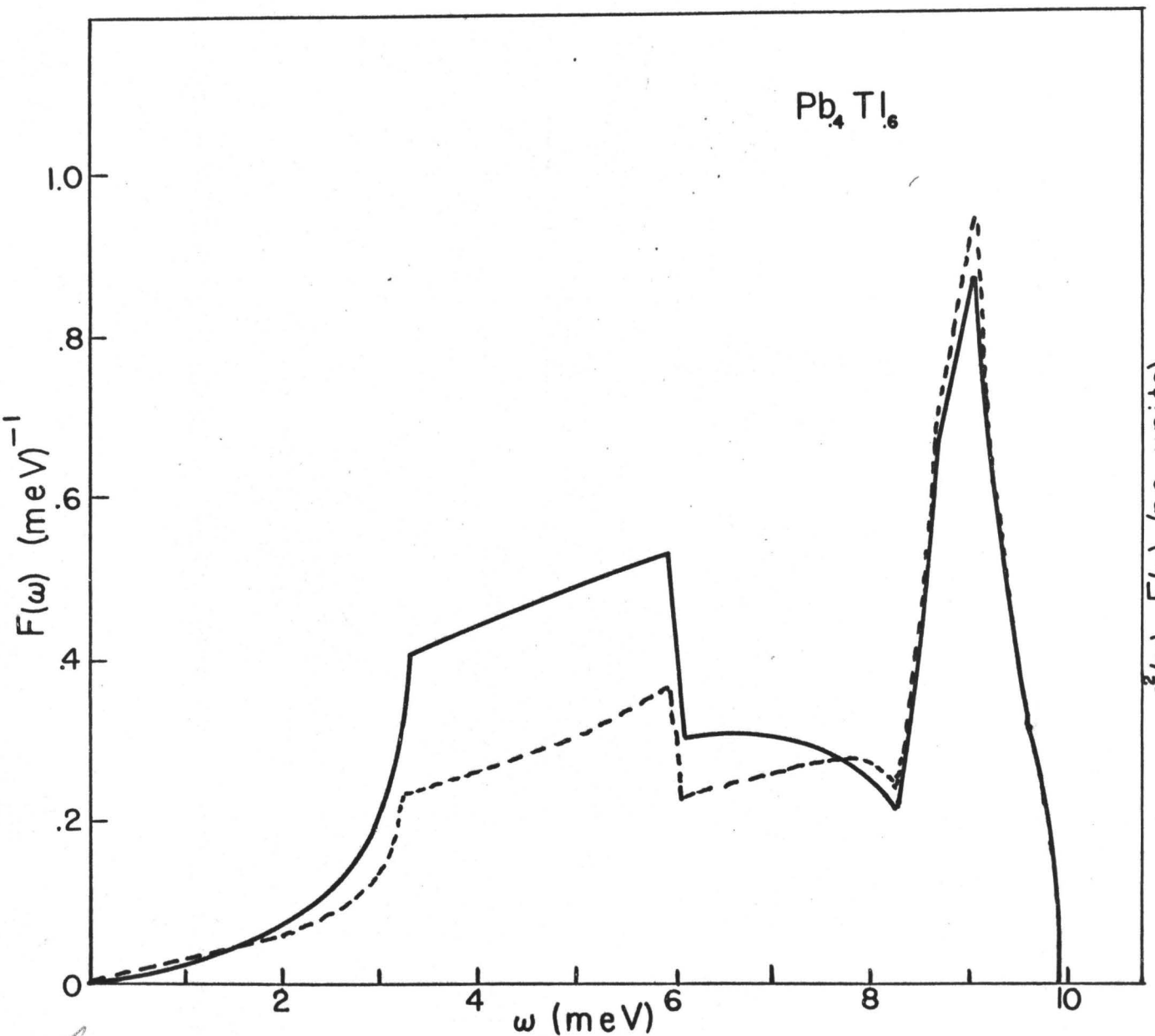
Pb.4 Tl.6
1.0
.8
.6
.4
.2
0
F(ω) (meV)⁻¹
2
4
6
8
10
ω (meV)
α²(ω) F(ω) (no units)

FIGURE 7.7

Calculated $\alpha^2(\omega)F(\omega)$ (dotted line) as a function of phonon energy ω compared with the phonon density of states $F(\omega)$ (solid line) in $Pb_{.6}Tl_{.4}$.

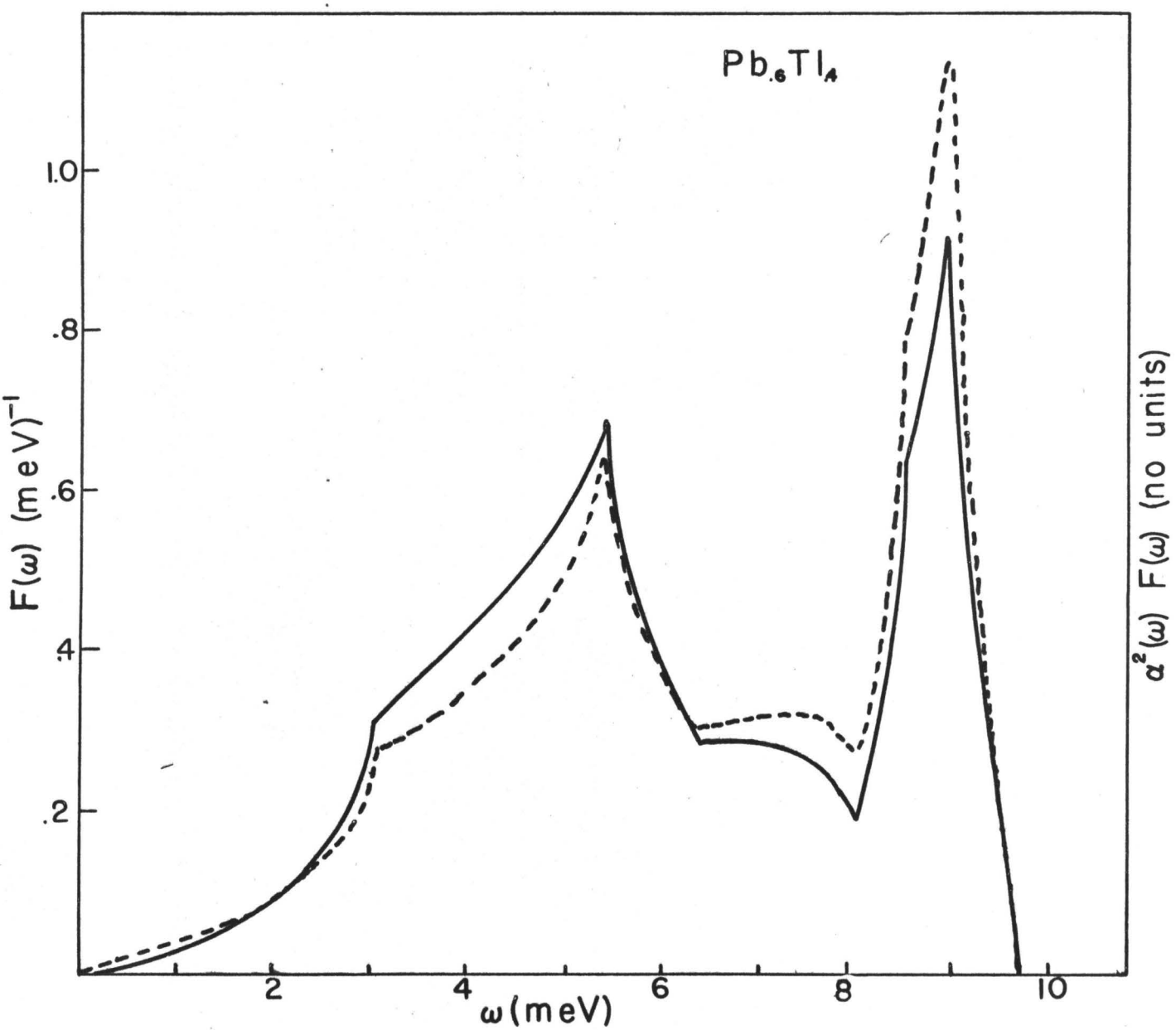
Pb.6Tl.4
1.0
.8
.6
.4
.2
F(ω) (meV)⁻¹
2
4
6
8
10
ω (meV)
α²(ω) F(ω) (no units)

FIGURE 7.8

Calculated $\alpha^2(\omega)F(\omega)$ (dotted line) as a function of phonon energy ω compared with the density of phonon states $F(\omega)$ (solid line) in $Pb_{.8}Tl_{.2}$.

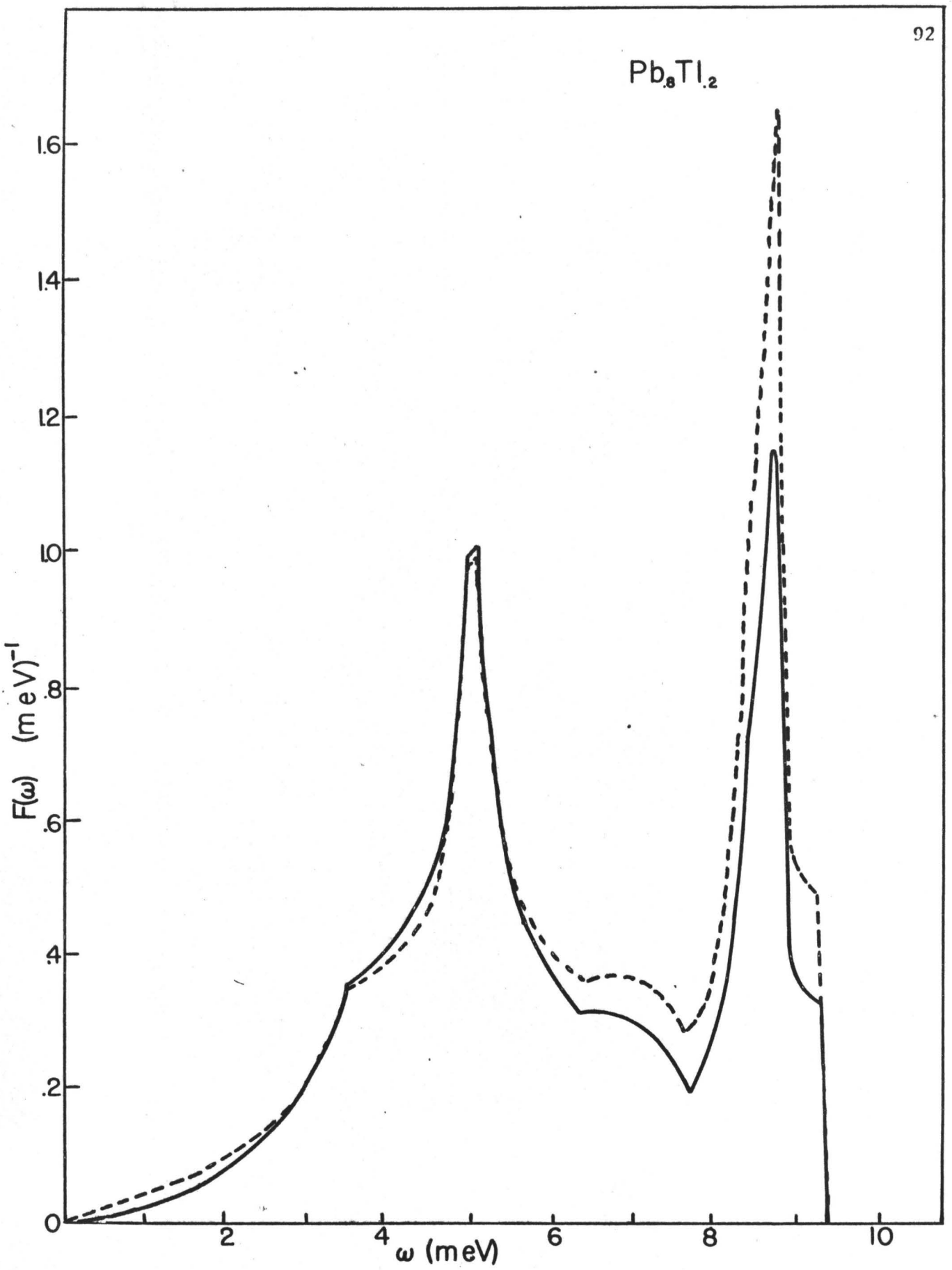
$Pb_{.8}Tl_{.2}$
1.6
1.4
1.2
1.0
.8
.6
.4
.2
0
F(ω) (meV)$^{-1}$
2
4
6
8
10
ω (meV)
$\alpha^2(\omega)$ F(ω) (no units)

FIGURE 7.9

Calculated $\alpha^2(\omega)F(\omega)$ (dotted line) as a function of phonon energy ω compared with the calculated density of phonon states $F(\omega)$ (dotted line) in lead.

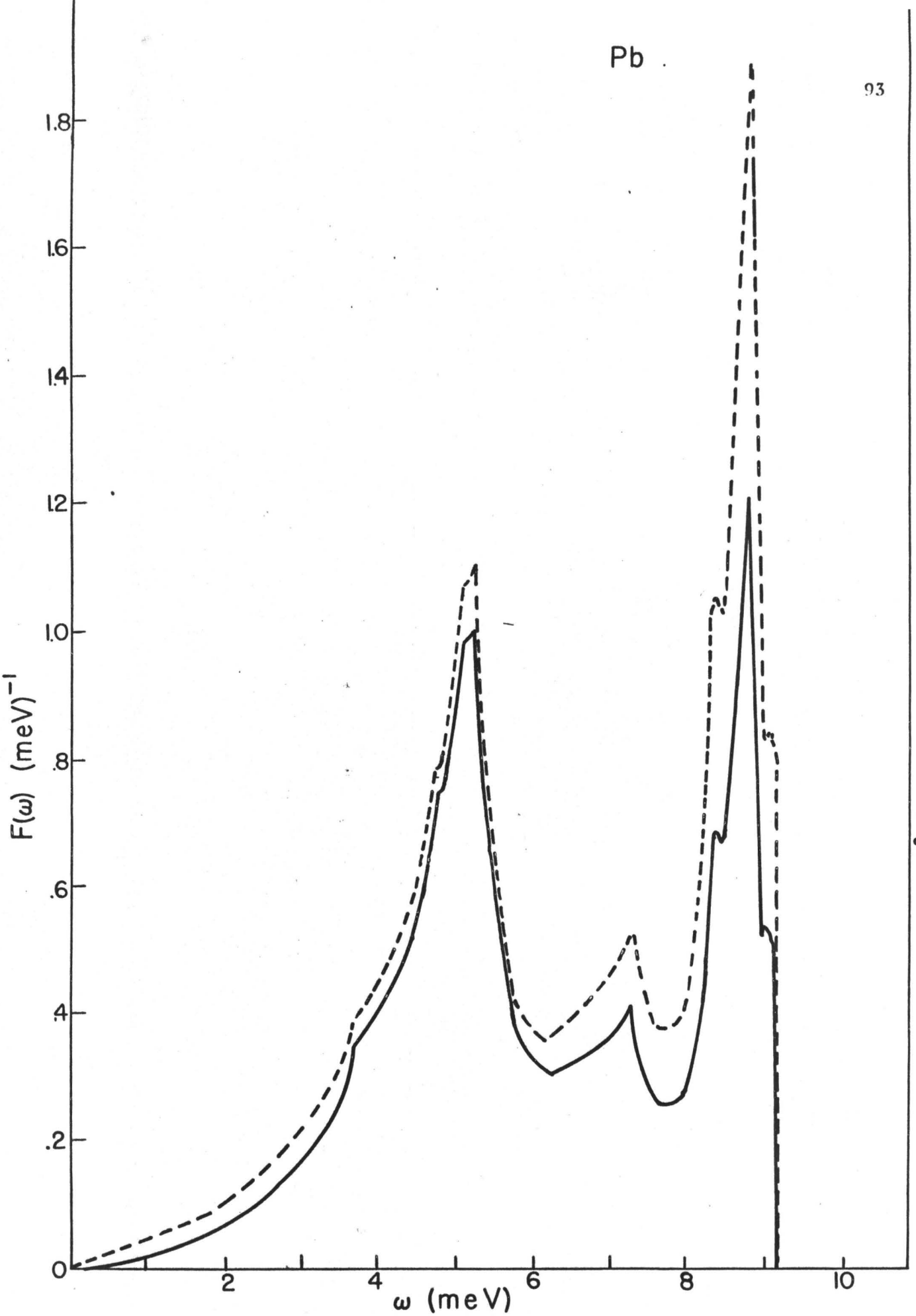
Pb
1.8
1.6
1.4
1.2
1.0
.8
.6
.4
.2
0
F(ω) (meV)⁻¹
2
4
6
8
10
ω (meV)
α²(ω) F(ω) (no units)

FIGURE 7.10

The coupling function $\alpha^2(\omega)$ as a function of phonon energy ω for lead.

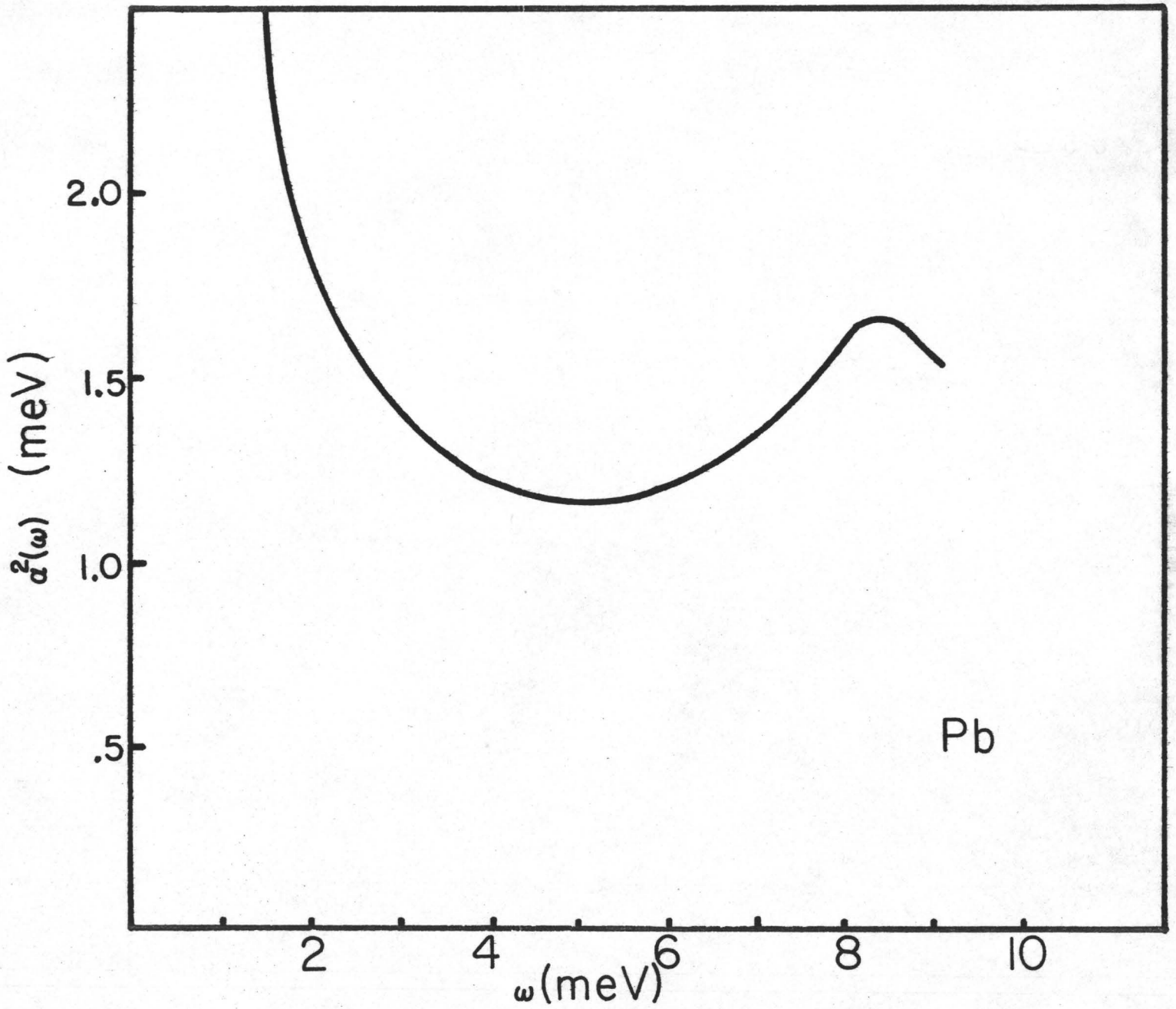
2.0
1.5
1.0
.5
$\alpha^2(\omega)$ (meV)
Pb
2
4
6
8
10
ω(meV)

It should be readily observed that this product function, so important in the determination of superconductivity, has no more critical points than the original density of states $F(\omega)$. Also, it should be noted that the original critical points in $F(\omega)$ appear in exactly the same position in energy in $\alpha^2(\omega)F(\omega)$. Hence, neglecting band structure, no new critical points are generated in $\alpha^2(\omega)F(\omega)$. Therefore, in performing a tunneling experiment, the critical points that one associates with the product function $\alpha^2(\omega)F(\omega)$ are, in fact the critical points of the true phonon density of states $F(\omega)$.

In the region of low energy, in each of the cases discussed, there appears to be a linear relationship between $\alpha^2(\omega)F(\omega)$ and ω. This can be understood, with recourse to equation (2-26), by noting that the electron-phonon coupling term $|g_{\underline{k}\underline{k}'\lambda}|^2$ varies as $\frac{1}{\omega}$, thereby altering the ω^2 dependence of $F(\omega)$ to ω dependence of $\alpha^2(\omega)F(\omega)$. In order to perhaps more clearly illustrate this point, the function $\alpha^2(\omega)$ for lead, obtained simply by dividing $\alpha^2(\omega)F(\omega)$ by $F(\omega)$ is plotted in Figure 7-10.

Here we see that $\alpha^2(\omega)$ is a smoothly varying function, divergent as $\frac{1}{\omega}$ in the region of low ω and slightly peaked in the region of the longitudinal peak of $F(\omega)$.

This peaking, which appears in all these materials to a greater or lesser extent in the longitudinal or high energy region, is due to the following reason. In the transfer of momentum $\underline{q}$ from an electron to a phonon, there are two distinct types of processes. Firstly, there is the simple or normal process where the total $\underline{q}$ given up by the electron is taken up in the phonon. This process can simply be written:

$$\underline{k} - \underline{k}' = \underline{q}$$

where $\underline{k}$ and $\underline{k}'$ are the initial and final momentum states of the electron. There is, however, another type of process, the so-called Umklapp process[75] in which some of the momentum transfer is taken up by the complete crystal, and the interaction can be written:

$$\underline{k} - \underline{k}' = \underline{q} + \underline{K}_n$$

where $\underline{K}_n$ is a reciprocal lattice vector. In a simplified reciprocal lattice, these two processes can be illustrated. See Figure 7-11.

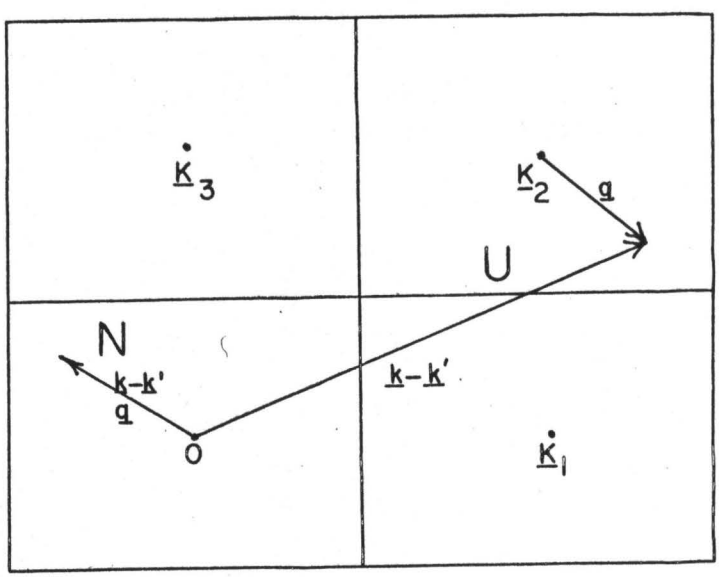

FIGURE 7-11

MOMENTUM TRANSFER PROCESSES

(The normal process is labeled as N and the Umklapp process as U.)

For normal processes (in the first Brillouin zone) we see that in calculating the probability of transition from a $\underline{k}$ state to a $\underline{k}'$ state (equation (2-26)), there is a dependence on the scalar product $|\underline{\varepsilon} \cdot \underline{q}|^2$

where $\underline{\varepsilon}$ is the polarization vector of the phonon $\underline{q}$. For a normal process, clearly $|\underline{\varepsilon} \cdot \underline{q}|^2$ is zero for pure transverse modes, and consequently, inside the first Brillouin zone where we have normal processes, and where phonons are approximately longitudinal or transverse, there is a very high weighting of the longitudinal modes. For the contrasting case of Umklapp processes, we see, with recourse to Figure 7-11, that $|\underline{K} + \underline{q} \cdot \underline{\varepsilon}|^2$ can, under certain circumstances, be greater for transverse modes than longitudinal modes. On the average, for Umklapp processes, the longitudinal and transverse modes will be approximately equally weighted.

Hence, in this calculation of $\alpha^2(\omega)F(\omega)$, where we integrate over a sphere of radius $2k_F$ to include all possible scatterings, the longitudinal peak will have a greater weighting than the transverse, the degree of which will depend upon what fraction of the sphere $2k_F$ is in the first Brillouin zone.

This perhaps can be seen more clearly if one compares $\alpha^2(\omega)F(\omega)$ for materials where $2k_F$ just reaches outside the first zone (Na) and materials where the first zone is not the major volume of this sphere (Pb). In the former case, the peaking of the $\alpha^2(\omega)$ coupling term is very pronounced in the longitudinal peak region, indicating that normal processes are the dominant scattering processes, while in the latter case, there is a slight peaking in the longitudinal region, indicating an almost equal weighting of the transverse with longitudinal modes. This indicates that the major portion of the scattering involves Umklapp processes.

Clearly then, the electron phonon coupling is much weaker with transverse phonons when the Fermi surface is small, than in materials

whose Fermi surface extends substantially beyond the first Brillouin zone.

7.2 VALIDITY OF BORN VON KARMAN ANALYSIS FOR PHONONS IN LEAD:

As was mentioned earlier, the calculation of the $\alpha^2(\omega)F(\omega)$ and $F(\omega)$ functions for Pb may be viewed with some suspicion. This calculation, as outlined in Appendix A is performed utilizing a Born Von Karman [76], 8 nearest neighbour force constant analysis. It is found, however, that these force constants are still fluctuating rather severely from those of say a 7 nearest neighbour fit. Fortunately, $\alpha^2(\omega)F(\omega)$ has been studied rather extensively using the tunneling technique and a very carefully determined $\alpha^2(\omega)F(\omega)$ has been extracted. For purposes of comparison, this $\alpha^2(\omega)F(\omega)$ relationship and the calculated $F(\omega)$ are superimposed in Figure 7-12. The differences between these two functions, our first comparison with experiment, are very large[80] and the validity of both methods of determining these functions must be questioned.

The reproducibility of the tunneling results for Pb as obtained by many investigators is convincing enough evidence for the likely validity of the experimentally determined $\alpha^2(\omega)F(\omega)$ -- at least for thin film observations. An electron diffraction investigation of the orientation of the crystallites of Pb on a thin film indicates that there is a random orientation of such crystallites in such films which have thicknesses $\lesssim$ 1500 Å. Hence a tunneling experiment samples equally all crystallographic directions. Due to the non-convergent force constant model for lead, one then turns to this as a source of error.

FIGURE 7.12

A comparison of critical points of $\alpha^2(\omega)F(\omega)$ obtained from tunneling[30] (dotted line) and $F(\omega)$ calculated from a Born von Karman force constant analysis (solid line).

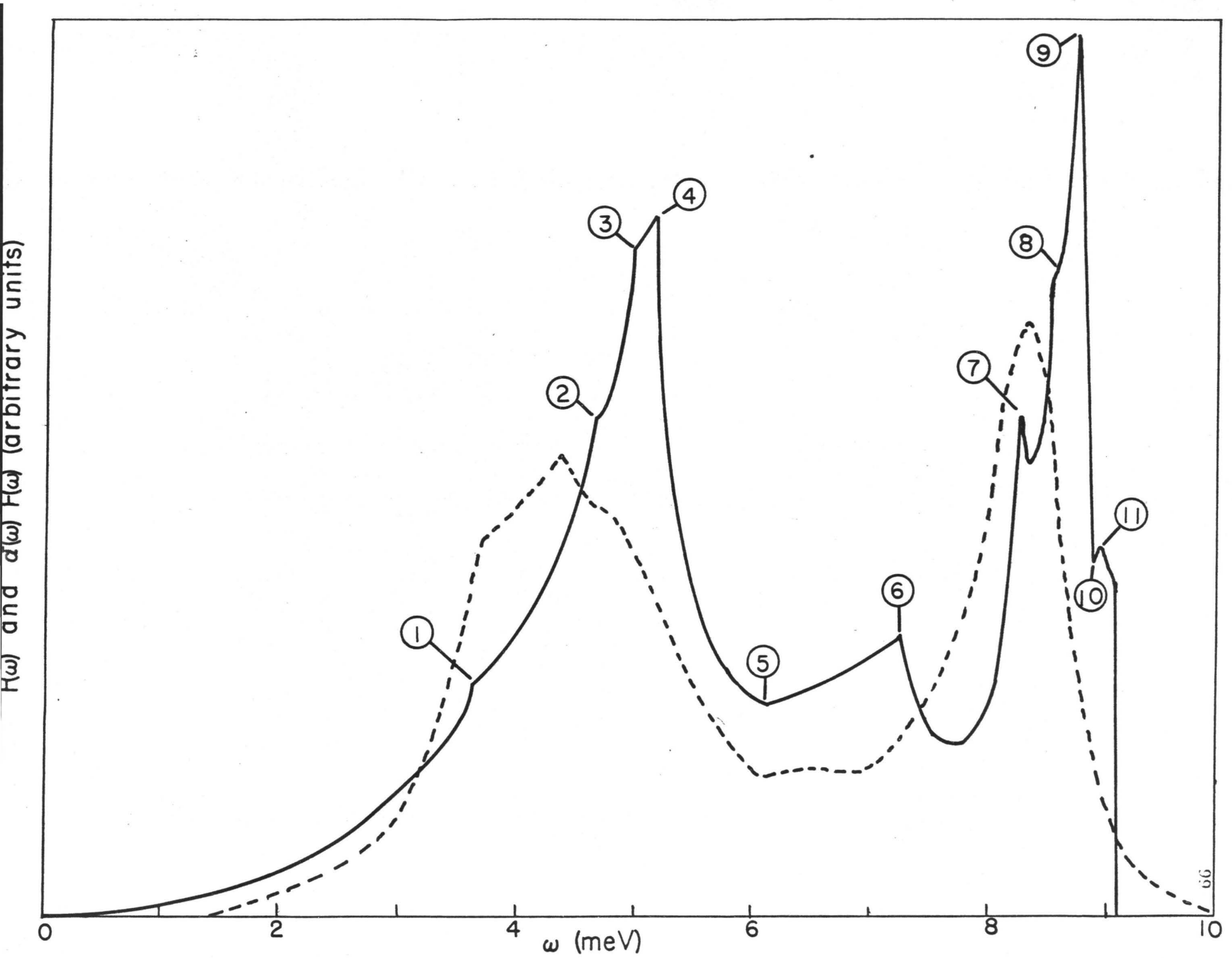
H(ω) and α²(ω) F(ω) (arbitrary units)
ω (meV)
0
2
4
6
8
10
1
2
3
4
5
6
7
8
9
10
11

The detailed nature of the discrepancies is worth considering. In particular, a number of critical points are identifiable in the tunneling curve which occur at the same frequencies in the calculated curve. The identifiable critical points are numbered in Figure 7-12. The points 1, 2, 3, 5, and 7 can be seen reasonably clearly in the tunneling curve at the same energies at which they occur in the calculated curve. The points 8, 10, and 11 cannot be seen in the tunneling curve but would probably require more resolution to be visible. On the other hand, the points 4, 6, and 9 are in definite conflict; no trace of these points appears in the tunneling curve.

All these critical point determinations by this calculation were located by finding the frequencies and their gradients for approximately 170,000 points in the Brillouin zone. The co-ordinates of these critical points are listed in Table 7-1. One immediately sees that the critical points which agree in the two curves are those which occur for $\underline{q}$ in high symmetry directions. These are directly observed as extremes in the high symmetry dispersion curves[52]. On the other hand, the peaks of the calculated curve which are not in the tunneling curve occur for $\underline{q}$ in off symmetry directions and are therefore derived from the force constant model. The positions of these off symmetry critical points are illustrated in Figures 7-13, 7-14 and 7-15. Here energy contour maps for selected symmetry planes on which these saddle points occur are drawn, locating the turnovers.

In order to illustrate more fully the sensitivity of the force constant model, $F(\omega)$ has been calculated for a much cruder model based on 5 nearest neighbours. The comparison of this and the 8 nearest neighbour

TABLE 7-1

The Position of the 11 Critical Points Observable in $F(\omega)$ of Figure 7-12. The Momentum Values are in Units of $\frac{2\pi}{a}$ Where a is the Interionic Distance.

CRITICAL POINT	WAVE VECTOR COMPONENTS (in units of $2\pi/a$)		
	q_x	q_y	q_z
1	.500	.500	.000
2	.660	.000	.000
3	.750	.750	.000
4	.766	.234	.234
5	1.000	.500	.000
6	.797	.484	.109
7	.750	.750	.000
8	.578	.578	.000
9	.734	.185	.185
10	.734	.000	.000
11	.500	.500	.500

FIGURE 7.13

Equi-energy contours locating critical point 9 on y = z plane of Brillouin zone.

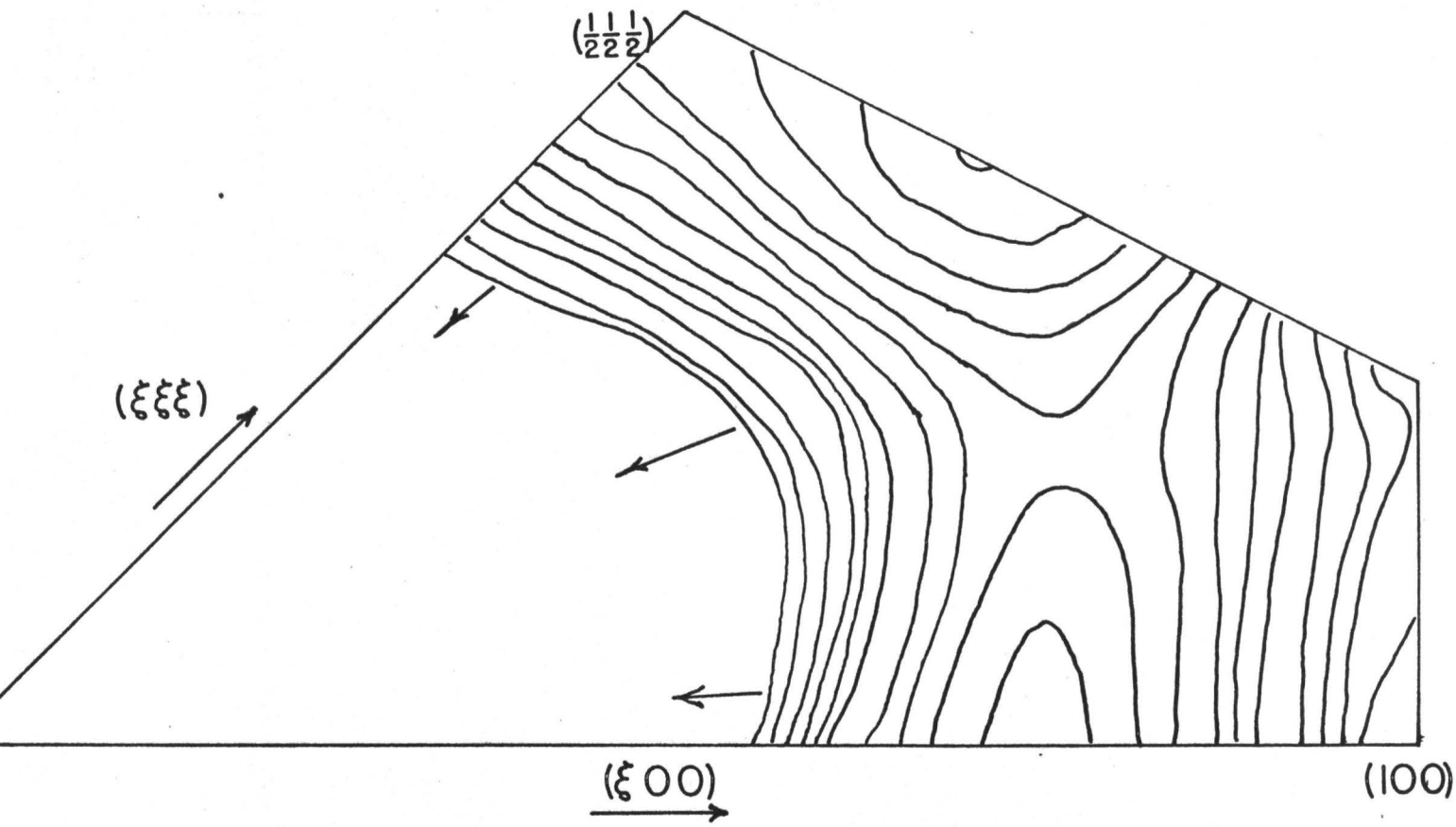
$(\frac{1}{2}\frac{1}{2}\frac{1}{2})$
$(\xi\xi\xi)$
$(\xi 00)$
(100)

FIGURE 7.14

Equi-energy contours locating critical point 6 on $x + y + z = \frac{3}{2}$ plane of Brillouin zone.

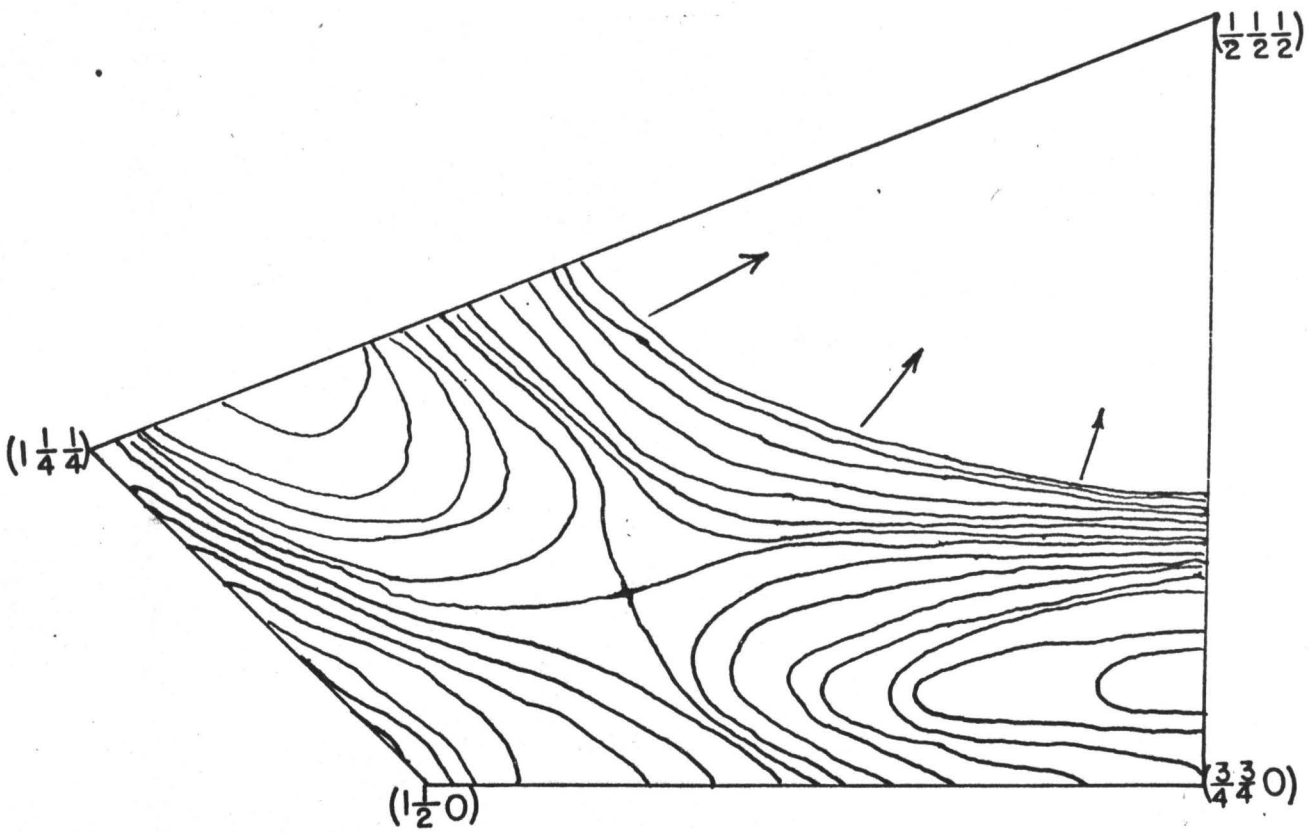
(1 1/4 1/4)
(1/2 1/2 1/2)
(1 1/2 0)
(3/4 3/4 0)

FIGURE 7.15

Equi-energy contour map locating critical point 4 on y = z plane of Brillouin zone.

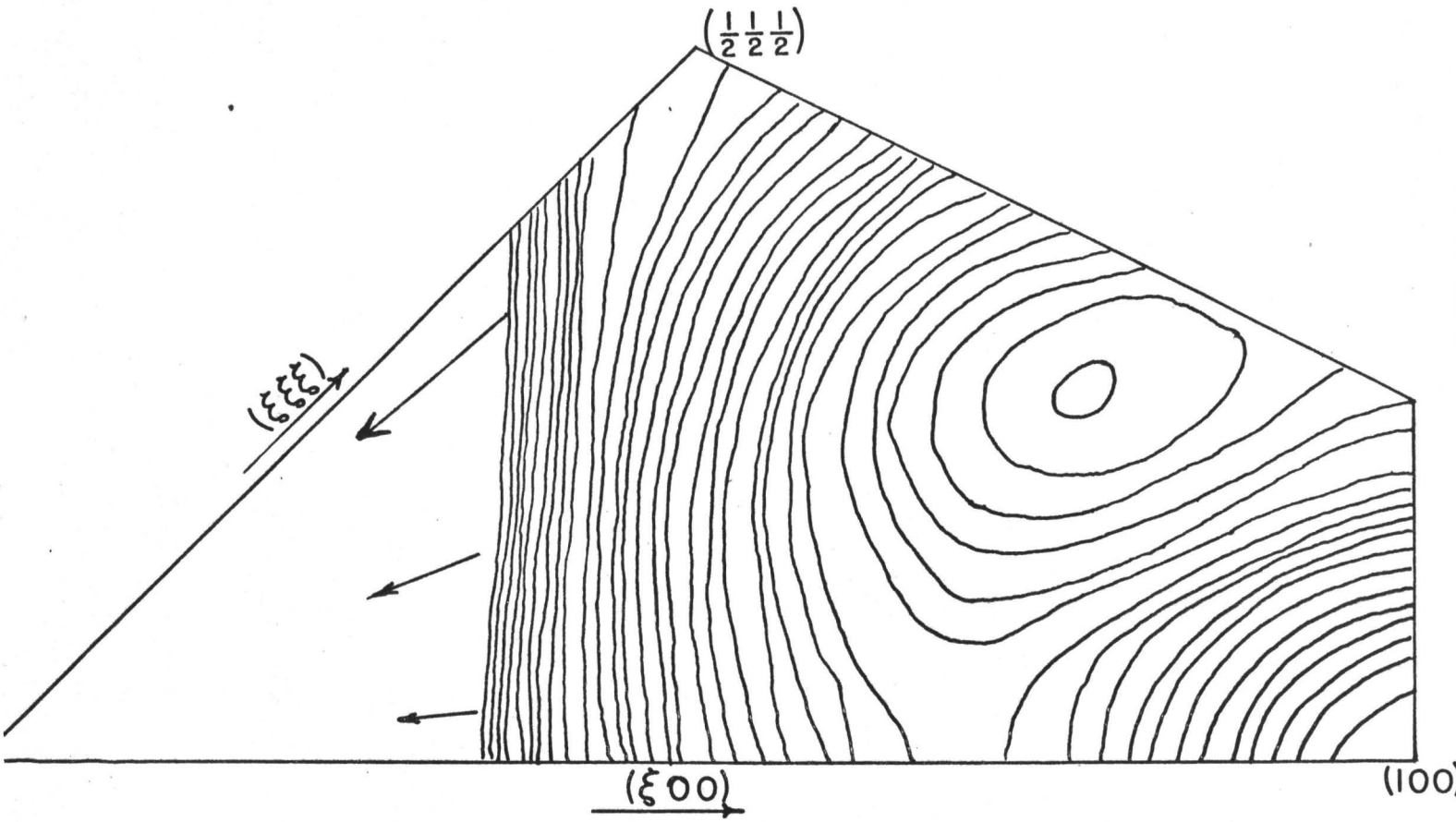
$(\frac{1}{2}\frac{1}{2}\frac{1}{2})$
$(\xi\xi\xi)$
$(\xi 00)$
(100)

calculation is illustrated in Figure 7-16. The cruder model, of course, represents a less successful fit to the highly structured lead dispersion curves in the symmetry directions. The difference between the two calculations is, however, apparent. The on-symmetry critical points have shifted slightly while the peaks generated from the off-symmetry critical points are comparatively much more affected. In addition, the position of these critical points in the Brillouin zone shift about as the model is slightly changed.

It should also be noted that the cruder fit represents improved agreement with the tunneling results. A similar effect is noted in the work of Bennett[77] who achieves better qualitative agreement with the tunneling results by fitting Kubic harmonics to interpolate dispersion curves to off-symmetry directions. In the case of materials with less highly structured dispersion curves (for example the alloy $Pb_{.4}Tl_{.6}$)[28] we shall see that much better agreement between tunneling experiments and the Born von Karman calculation is achieved.

The conclusion thus appears to be that for highly structured dispersion curves in symmetry directions, the interpolated off-symmetry points are in error and the fitting of a more realistic model to lead dispersion curves is necessary to give a more reliable density of states $F(\omega)$ and thus better agreement with tunneling curves.

Neutron scattering experiments in off-symmetry directions could also be performed in order to locate these off-symmetry critical points. One can conclude from this analysis that in the case that there are long range forces (i.e. when the force constants do not converge over many neighbours) the details of the resultant phonon density of states function

FIGURE 7.16

Phonon density of states $F(\omega)$ for lead calculated from an 8 nearest neighbours model (solid line) and a 5 nearest neighbours model (dotted line).

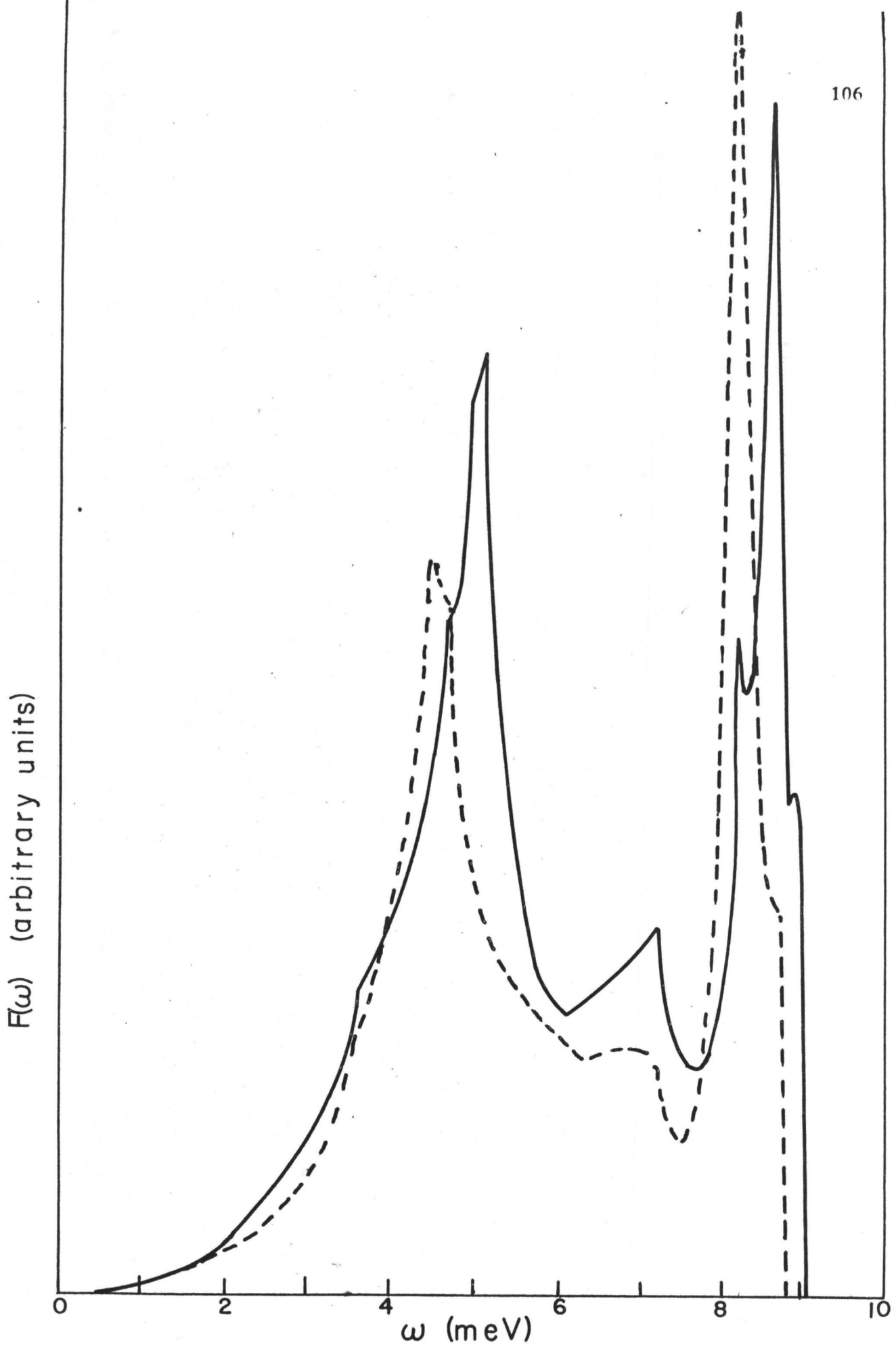
F(ω) (arbitrary units)
0
2
4
6
8
10
ω (meV)

should not be strongly trusted although it is probably adequate for calculating bulk thermodynamic properties.

Another method of determining the phonon density of states is utilized by Stedman et al[78], where a mesh over the entire Brillouin zone is determined and neutron scattering experiments are performed for q-vectors both in on and off symmetry directions. Employing this data, a judicious interpolation of energy contours between the measured points is performed and the density of phonon states $F(\omega)$ calculated accordingly. The results of such an investigation, along with the $\alpha^2(\omega)F(\omega)$ relationship from a tunneling experiment, is illustrated in Figure 7-17. The general features of the two curves are encouragingly similar, but this method of determining $F(\omega)$ represents a large amount of work in order to cover the Brillouin zone with a sufficiently fine mesh. It may be noted that this method presents one with a formidable task, although it would ideally yield the correct result, and a simpler approach to the solution would perhaps lie in determining a more physically realistic model amenable to the calculation of off-symmetry dispersion characteristics. The pseudopotential method[79], capable of reproduction of measured dispersion curves of the simpler materials shows promise to this end, but extensive refinements and concentrated effort must still be applied to reproduce the more complicated detail in lead.

7.3 SOLUTION OF GAP EQUATION:

7.3-1 The Energy Gap Δ_o-

Having now determined the function $\alpha^2(\omega)F(\omega)$ we are now in a position to make some realistic comparisons with experiment. Given

FIGURE 7.17

A comparison of $\alpha^2(\omega)F(\omega)$ obtained from tunneling[30] (solid line) and $F(\omega)$ obtained by the method of Stedman et al[78] (dotted line) for lead.

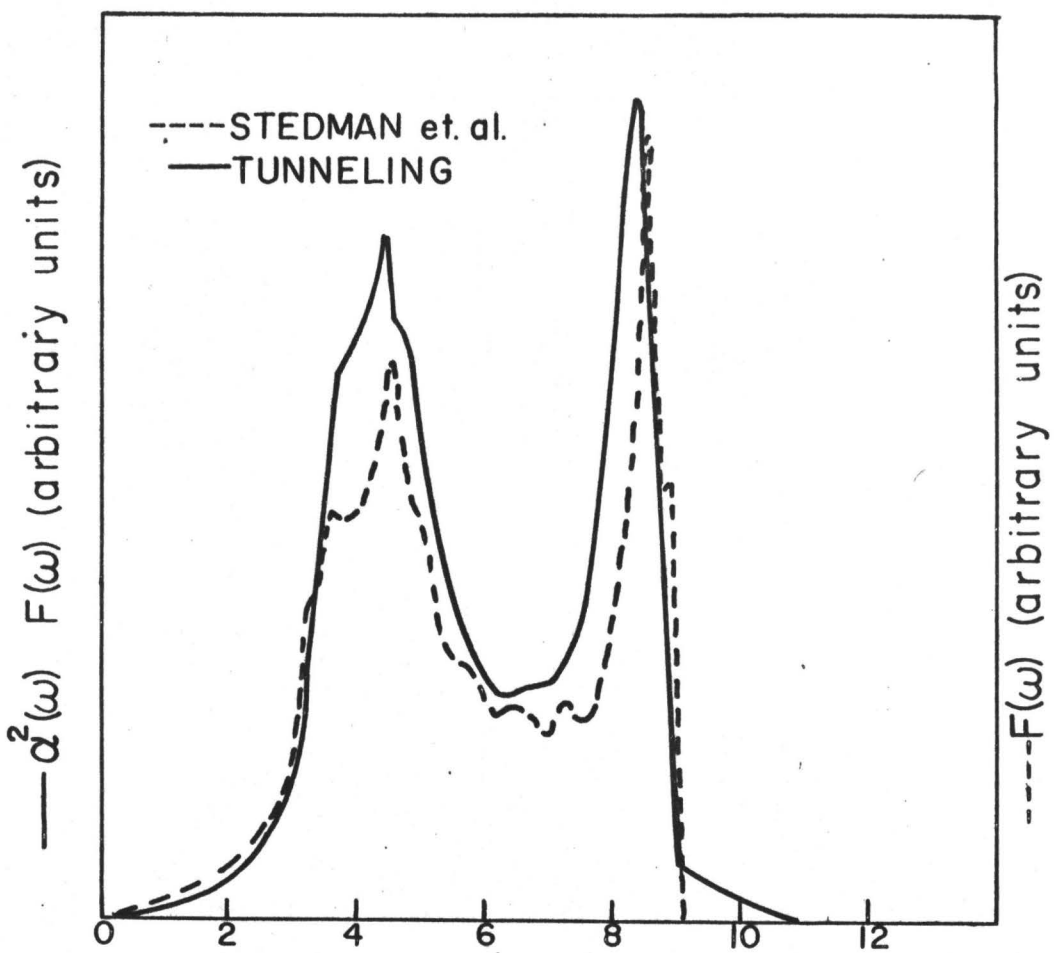
----STEDMAN et. al.
—TUNNELING
—α²(ω) F(ω) (arbitrary units)
----F(ω) (arbitrary units)
0
2
4
6
8
10
12

$\alpha^2(\omega)F(\omega)$ we can solve directly the Eliashberg gap equations (equation (4-12)) for an energy dependent energy gap $\Delta(\omega)$. To relate this to a more physically meaningful quantity, we can determine this solution for $\Delta(\Delta_o)$ (i.e. the value of the energy gap parameter at the edge of the energy gap Δ_o). This Δ_o term is what is experimentally measured in the course of a tunneling experiment.

The solution to these equations is obtained in an iterative fashion as follows. The value of $\Delta(\Delta_o)$ (or Δ_o) is guessed at[†] and inserted into the equations. The set of equations is then solved from this estimate, thus yielding new values for Δ_o and $\Delta(\omega)$. This new solution is in turn reinserted into these equations and the iteration proceeds. Depending upon the strength of the electron-phonon coupling, error in an initial guess, and the degree of convergence required, the number of iterations needed for convergence may vary from about 4 to 12. In solving these equations care must be taken that the contribution due to the phonons has converged, thus including all enhancement due to the phonons. To achieve this end, it was found that a cut-off ω_c = 5 x (cut-off of longitudinal peak) was an acceptable cut-off point to choose, with all contributions beyond this point being negligible. The only parameter remaining is that determining the electron-electron repulsion $N(0)u_c$. The present knowledge of this term appears to be quite limited as other investigators[30] have used this as a variable parameter to fit experimental results. This

---

[†] In most cases where the experiments had been performed before the calculations, this first guess consisted of the experimentally determined value of Δ_o, although it was found that any bad guess would converge to the same answer.

repulsion term, as was explained earlier, has not really converged at the cut-off ω_c and an electron-electron pseudopotential must be introduced to compensate for that part outside ω_c not considered in the integration. This was first discussed by Bogoliubov, Tolmalov and Shirkov[45] and given approximately by;

$$u_c = \frac{V_c}{1 + N(0)\, V_c \ln (E_F/\omega_c)} \qquad \text{------(7-1)}$$

where E_F = Fermi energy

$N(0)$ = normal density of states at Fermi surface

V_c = true screened Coulomb potential at the Fermi surface.

This term was further discussed and calculated for several materials by Morel and Anderson[46] but again these were approximate solutions and some doubt as to the exact values still exists.

(i) Solution for Aluminum -

Using this approximate solution for u_c and the $\alpha^2(\omega)F(\omega)$ relationship for aluminum calculated in Section 7.1, the gap equations for aluminum were solved in the manner previously outlined. It was found that the converged solution for these equations yielded as an energy gap[83].

$$\Delta_o = .190 \text{ meV}$$

Assuming the weak coupling limit for superconductivity[21], namely,

FIGURE 7.18

Comparison of the resulting $\alpha^2(\omega)F(\omega)$ for a choice of form factor in the range 0 to 2 p_F . The solid line is the Heine-Abarenkov pseudopotential form factor-- the dotted line a more or less arbitrary distortion to this.

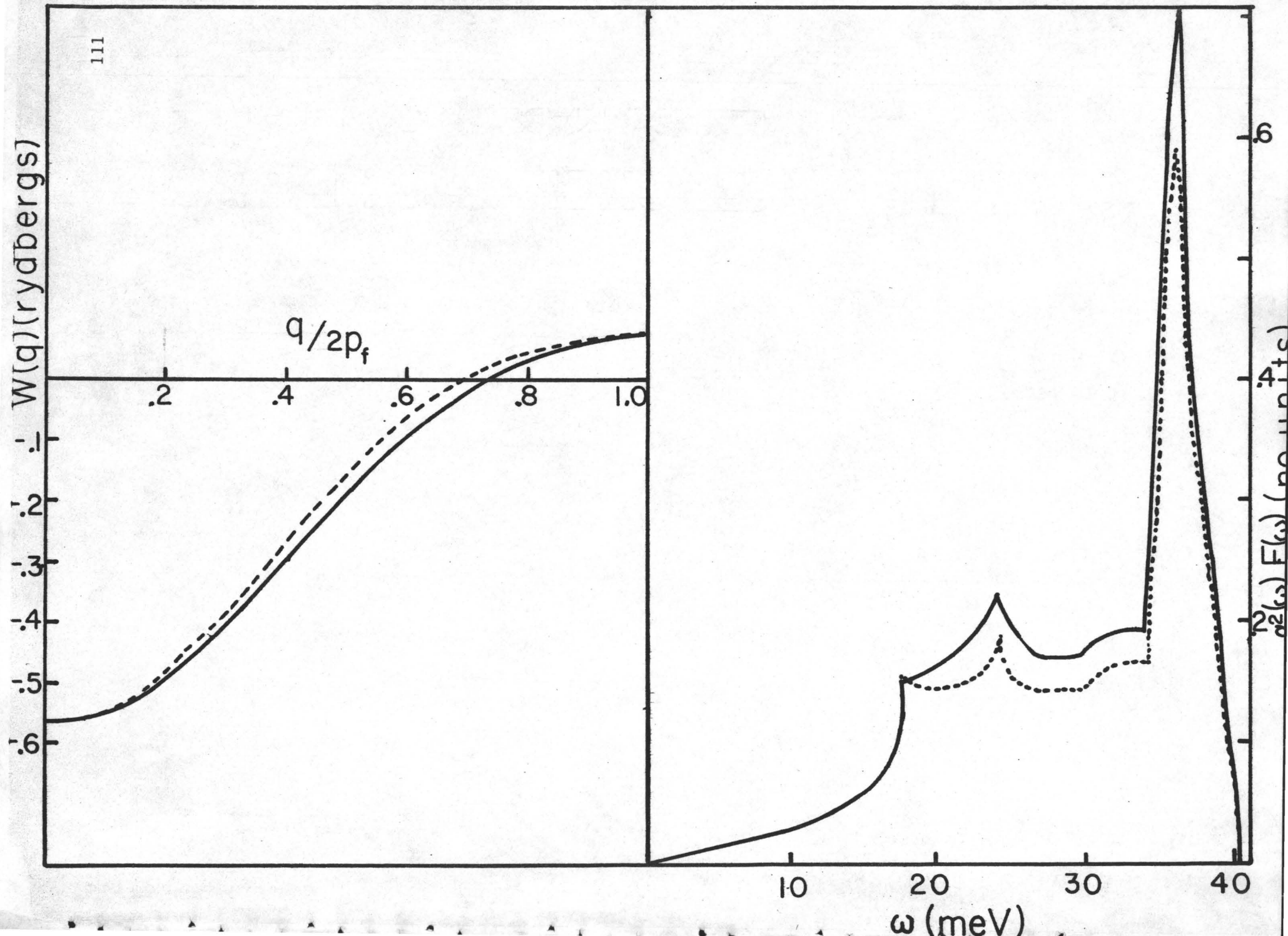
W(q)(rydbergs)
q/2p_f
.2
.4
.6
.8
1.0
.1
.2
.3
.4
.5
.6
10
20
30
40
ω (meV)
.2
.4
.6

$$\frac{2\Delta_o}{kT_c} = 3.52,$$

this calculated energy gap corresponds to a transition temperature,

$$T_c = 1.25^oK$$

which is in excellent agreement with the experimentally determined bulk value of 1.18^oK.

The effect of different pseudopotential form factors on the calculation of the transition temperature is best illustrated by solving the gap equations from the alternative pseudopotential illustrated in Figure 7-18. This gives an estimated gap

$$\Delta(\Delta_o) = .12 \text{ meV}$$

which corresponds to a critical temperature

$$T_c = .8^oK$$

which is not in very good agreement with experimentally measured values. The choice of pseudopotential form factor is therefore quite important and in the cases where it is available the Heine-Abarenkov form[34], as tabulated by Harrison[79], is used.

The real and imaginary part of the energy gap function $\Delta(\omega)$ obtained in the solution of these equations for aluminum is illustrated in Figure 7-19. As in previous discussions, the real part $\Delta(\omega)$ has peaks suggestive of resonances at the points of peaks in $\alpha^2(\omega)F(\omega)$ with the

FIGURE 7.19

Real (solid line) and imaginary (dotted line) solutions of $\Delta(\omega)$ for aluminum using $\alpha^2(\omega)F(\omega)$ of Figure 7.3.

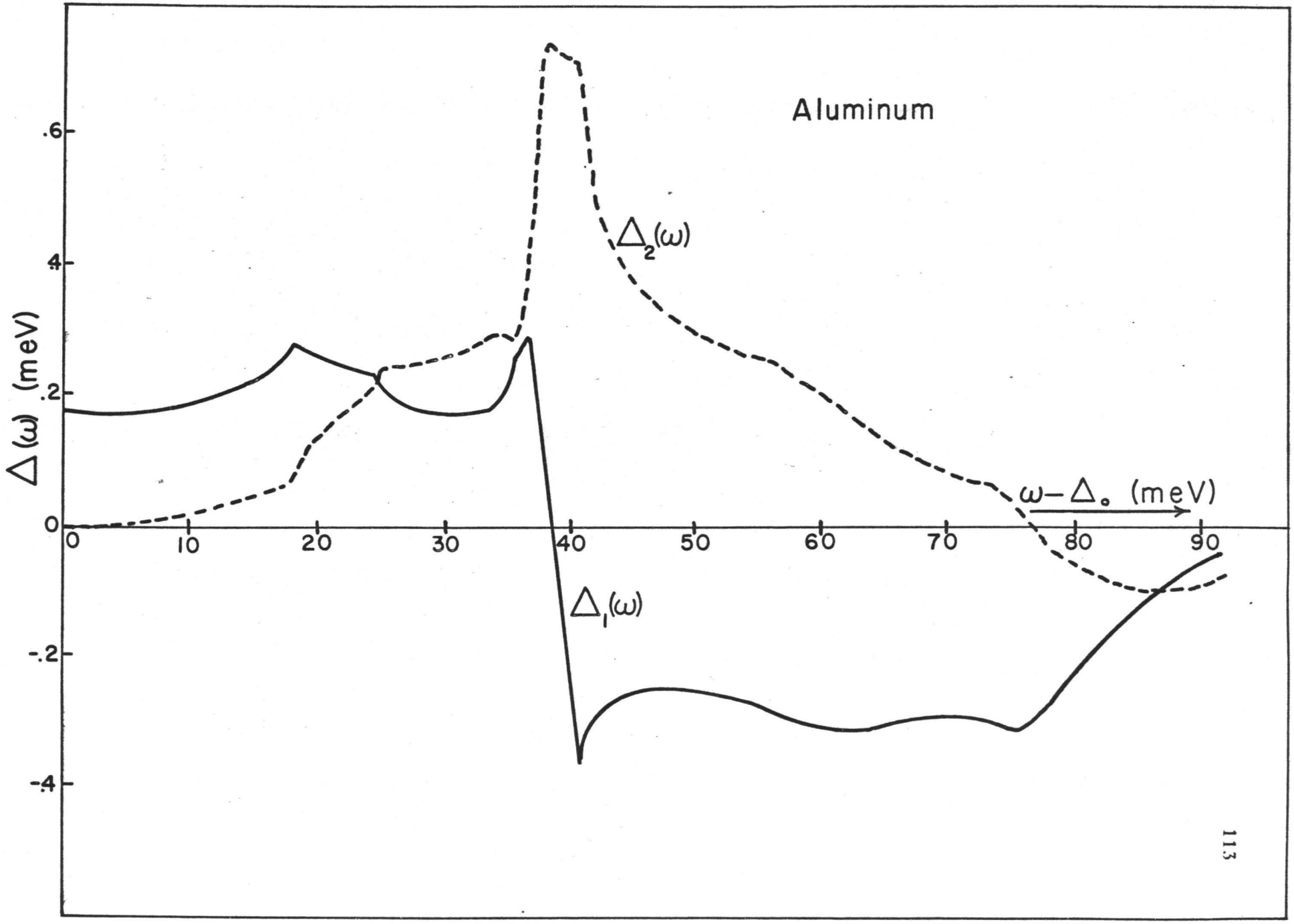
Aluminum
$\Delta_2(\omega)$
$\Delta_1(\omega)$
$\Delta(\omega)$ (meV)
$\omega - \Delta_0$ (meV)
.6
4
.2
0
-.2
-.4
0
10
20
30
40
50
60
70
80
90

imaginary part $\Delta_2(\omega)$ increasing rapidly at these points, illustrating the strong behaviour of the fundamental frequencies. It should be noted that these solutions extend up to a much higher energy than the phonon energy cut-off, due to the strength of multiphonon processes.

(ii) Solution for Alloys -

This procedure was repeated for the selected alloys for which the $\alpha^2(\omega)F(\omega)$ parameters were calculated, and related energy gaps were determined accordingly. Experimental values for the energy gaps of such alloys were also obtained from tunneling measurements. The results of those calculations, and of the experiments for these alloys are given in Table 7-2.

TABLE 7-2

MATERIAL	No. OF ELECTRONS/ ATOM	$N(0)u_c$	Δ_o CALC. (meV)	Δ_o EXPT (meV)
Pb	4	.13	1.49	1.38 ± .05
$Pb_{.8}Tl_{.2}$	3.8	.12	1.37	1.27 ± .10
$Pb_{.6}Tl_{.4}$	3.6	.12	1.08	1.02 ± .10
$Pb_{.4}Tl_{.6}$	3.4	.10	.67	.68 ± .10
$Tl_{.8}Bi_{.2}$	3.4	.10	.67	.66 ± .10
$Tl_{.9}Bi_{.1}$	3.2	.10	.38	.35 ± .05

The errors quoted for the experimentally determined values include both the instrumental measuring errors and such errors, arising from

preparation problems, as might be associated with uncertainties in the constituents of the alloys. Each experimentally measured value quoted represents at least two different samples prepared in order to ascertain consistency.

The values of $N(0)u_c$ have been determined from a range of sources; calculated from the expression equation (7-1), from the work of McMillan and Rowell[51], and from the estimates of Wu[82].

From this comparison, we see that for most of the materials listed, including aluminum reported earlier, the two values obtained are within the somewhat uncertain estimate of the error. It should be noted that the two materials $Pb_{.4}Tl_{.6}$ and $Tl_{.8}Bi_{.2}$, possessing the same number of electrons per atom and hence very similar sized Fermi surfaces also display very similar superconducting properties. This similarity will be seen even more clearly in the next Section when the tunneling results are presented.

From this sort of analysis, one can clearly see what sort of an effect electron concentration has on the superconducting properties. Indeed, it is quite clear that the electron concentration has quite a pronounced effect on the coupling of electrons to phonons and consequently on the onset of superconductivity.

(iii) Solution for Sodium and Potassium -

In order to understand more easily why some materials superconduct at higher temperatures[84], it is perhaps instructive to look at the separate parameters which control $\alpha^2(\omega)F(\omega)$ and try to estimate their relative importance. Clearly a most important term which was just illustrated is the size of the Fermi surface. The more the Fermi surface

reaches out into the second and higher Brillouin zones, the more Umklapp processes are possible and consequently the stronger will be the electron-phonon coupling. This is illustrated in equation (4-15) where the integration over momentum transfer $\underline{q}$ extends over a sphere of radium $2k_F$. The greater the value of k_F, the greater will be the amount of phase space available for the integration, so that superconductivity should be greatly enhanced as a result.

To consider other variables controlling the superconducting nature of materials, we shall contrast two different metals whose properties are fairly well known and whose differences and similarities are, in some ways, understood. Sodium and potassium are two such metals. They have identical crystal structure and a valence of unity. Their Fermi surfaces are nearly spherical and their phonon dispersion curves are very similar except for a scaling factor. It is seen in Figures 7-1 and 7-2 that their energy distributions $F(\omega)$ have much the same shape except that the ratio of the average phonon energies of the two materials is

$$\frac{\omega(Na)}{\omega(K)} = 1.635$$

The appearance of the energy factor in the denominator of equation (2-26) would favour K over Na as a more likely superconductor but this effect is nearly cancelled out by the ion mass factor M. The ratio of the ion masses in these two materials is

$$\frac{M(Na)}{M(K)} = .59$$

Next, in normalized units of $\frac{2\pi}{a_o}$ where a_o = lattice parameter, these two materials have identical Fermi surfaces. Hence, the phase space integration is identical over the two materials and this does not affect the result as to which will be the more likely superconductor. The remaining term, which finally determines as to which material is more likely to superconduct, is thus the pseudopotential form factor squared. This quantity is substantially larger in sodium than in potassium, as can be seen in Figure 7-20. In the end, it appears, from this analysis, that sodium is more likely to superconduct than potassium. In fact, the results for the gap calculation $\Delta(\Delta_o)$ in these two systems as a function of different values of the electron-electron term are presented in Table 7-3. Corresponding critical temperatures are also quoted using the BCS relation between Δ_o and T_c.

TABLE 7-3

CRITICAL TEMPERATURE FOR SODIUM AND POTASSIUM AS A FUNCTION OF THE COULOMB PART $N(0)u_c$

$N(0)u_c$	Na Δ_o(meV)	Na T_c(^oK)	K Δ_o(meV)	K T_c(^oK)
0.00	2.8×10^{-3}	18.5×10^{-3}	$.43 \times 10^{-3}$	3.0×10^{-3}
0.01	1.1×10^{-3}	7.0×10^{-3}	$.12 \times 10^{-3}$	$.8 \times 10^{-3}$
0.02	$.40 \times 10^{-3}$	3.0×10^{-3}	$.02 \times 10^{-3}$	$.13 \times 10^{-3}$
0.03	$.11 \times 10^{-3}$	$.7 \times 10^{-3}$	$<.005 \times 10^{-3}$	$<33.0 \times 10^{-6}$
0.04	$.02 \times 10^{-3}$	$.13 \times 10^{-3}$	$<<.005 \times 10^{-3}$	$<<33.0 \times 10^{-6}$
0.05	$<.005 \times 10^{-3}$	$<33 \times 10^{-6}$		

FIGURE 7.20

Comparison of the square of the pseudopotential form factor in sodium and potassium.

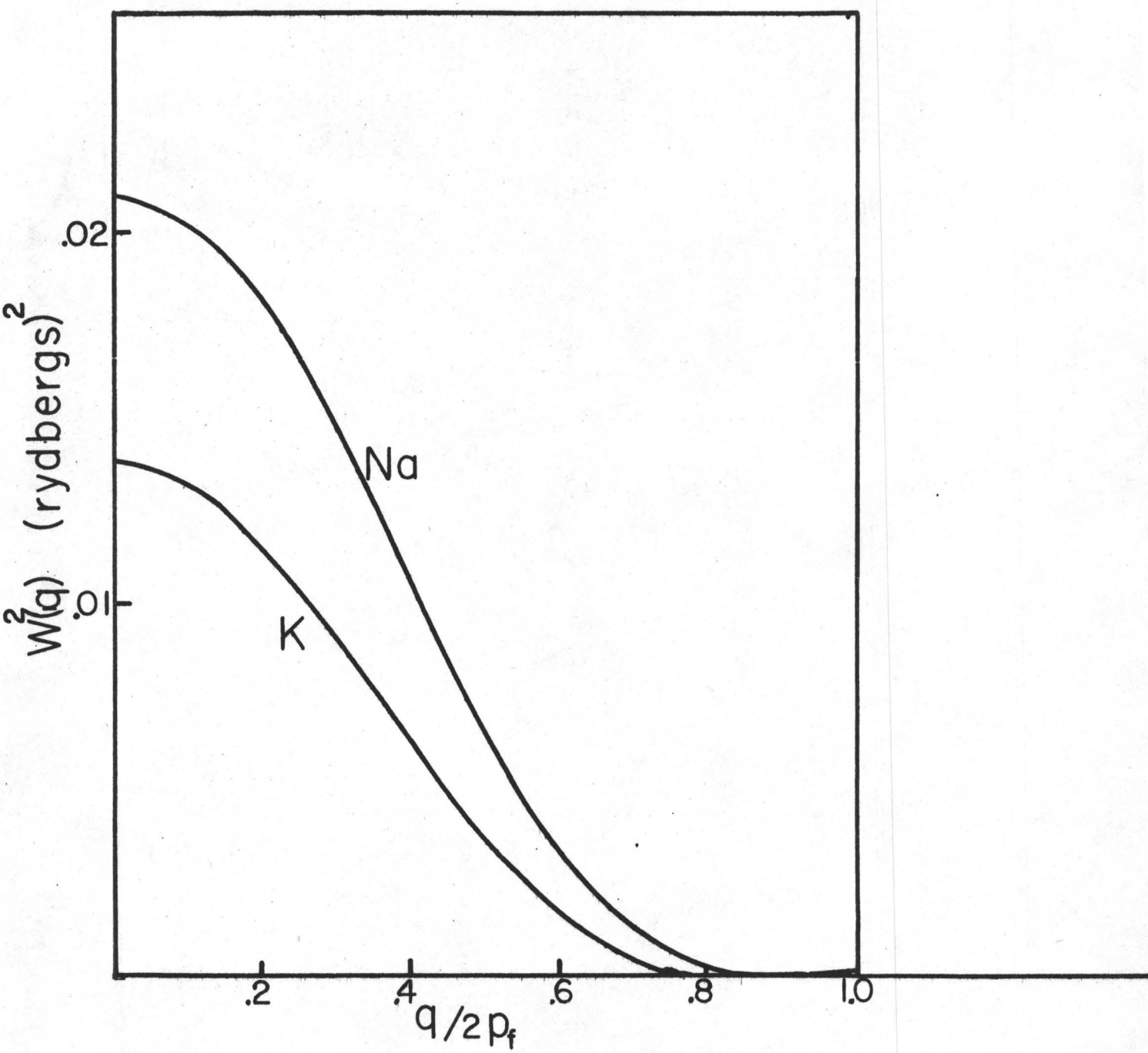
.02
.01
$W^2(q)$ (rydbergs)^2
Na
K
.2
.4
.6
.8
1.0
$q/2p_f$

If there were no Coulomb repulsion at all ($u_c = 0$) it is seen that sodium would have a critical temperature of 18.5 millidegrees, while in potassium it would only be 3 millidegrees. As the Coulomb repulsion term $N(0)u_c$ is slowly switched on, these estimates are drastically reduced. The Table ends at a $N(0)u_c$ value much less than what a realistic value would be[46]. Since those critical temperatures as calculated, however, are exceedingly small, it was felt that no significant purpose would be achieved by extending the calculations in question.

7.3-2 Tunneling Density of States-

In comparing calculated and experimentally obtained values for the energy gap $\Delta(\Delta_o)$, we are, in some ways, comparing the bulk properties of these materials. There is, however, an even more critical comparison available when a tunneling experiment is performed on such a material. As was outlined in Chapter V, we recall that the tunneling density of states for electrons is given by the expression:

$$N_T(\omega) = N(0)\mathrm{Re}\left\{ \frac{\omega}{(\omega^2 - \Delta^2(\omega))^{\frac{1}{2}}} \right\}$$

where $\Delta(\omega)$ = energy gap parameter

$N(0)$ = density of electron states at the Fermi surface in the normal state.

If we consider the case where one of the materials of a tunnel junction is in the normal state, and one is in the superconducting state, we can obtain, from equation (5-13), the expression:

$$\frac{\left(\frac{dI}{dV}\right)_S}{\left(\frac{dI}{dV}\right)_N} = \frac{N_T(eV)}{N(0)}$$

at $T = 0^{\circ}K$.

In addition, it was also noted that, the application of a reasonable functional form to $\alpha^2(\omega)F(\omega)$ to the solution of the gap equations resulted in the appearance of detailed structure in the energy gap parameter $\Delta(\omega)$, and consequent structure in the tunneling density of states which, from the above equation, is reflected in the ratios of the first derivatives of the current-voltage characteristics of the device in the superconducting and normal states. Further, it was pointed out that the non-linearities and critical points in this experimentally determined function were direct reflections of critical points in the product function $\alpha^2(\omega)F(\omega)$. (The details of this function were described in the first section of this Chapter where it was noted that $\alpha^2(\omega)$ was a smoothly varying function.) Consequently, and assuming no effects due to band structure, $F(\omega)$ will have exactly the same critical points as $\alpha^2(\omega)F(\omega)$ and in turn $N_T(\omega)$ will have critical points at these same positions in energy.

From considerations of equation (5-9) it may be noted that the addition of a second superconductor, with a known $N_T'(\omega)$ distribution factor, on the other side of the tunneling barrier does not present overly great problems for analysis. This problem of an additional superconductor on the other side of the barriers, with $N_T'(\omega)$ known for this material can be numerically treated. In fact, in the case that aluminum is that

other material, and it is advisable to consider thermal excitations above the energy gap,(as experimentally it is difficult to attain temperatures well below the T_c of aluminum) the addition of a temperature dependent Fermi distribution function into equation (5-9) is easily effected and the two superconducting densities of states can be convoluted to obtain the resultant current-voltage characteristic, $(\frac{dI}{dV})_S / (\frac{dI}{dV})_N$ versus V characteristic. Practically, the addition of a known superconductor on the other side of the junction has the experimental advantage in that it serves as a sharper probe at the gap edge with which to study the unknown superconductor than would a normal state material with temperature dependent Fermi distribution function.

(i) Aluminum as a Probe -

From the solution of the gap equations for aluminum utilizing the calculated $\alpha^2(\omega)F(\omega)$ of Figure 7-3 it is determined that the deviations from the B.C.S. predicted tunneling density of states,

$$N_T(\omega)_{B.C.S.} = N(0)\left(\frac{\omega}{(\omega^2 - \Delta_o^2)^{\frac{1}{2}}}\right)$$

are very slight compared to the alloys considered and at the maximum deviation point, which is well beyond the cut-off point for the alloys under study, the deviation from B.C.S. predictions is $\lesssim .02\%$. Hence, for the analysis of tunneling curves of devices of the type Aℓ-insulator-alloy, the $N_T(\omega)$ distribution parameter for the aluminum can be considered as a simple B.C.S. distribution, with thermal excitations and predictions

FIGURE 7.21

Comparison of calculated (dotted line) and experimental (solid line) $\left(\frac{dI}{dV}\right)_S \Big| \left(\frac{dI}{dV}\right)_N$ vs. V plot for

(a) Aℓ-I-$Pb_{.4}Tℓ_{.6}$ junction

(b) Aℓ-I-$Tℓ_{.8}Bi_{.2}$ junction at $1.1^{o}K$

V is measured from $\Delta_{oAℓ} + \Delta_{o}$ ALLOY

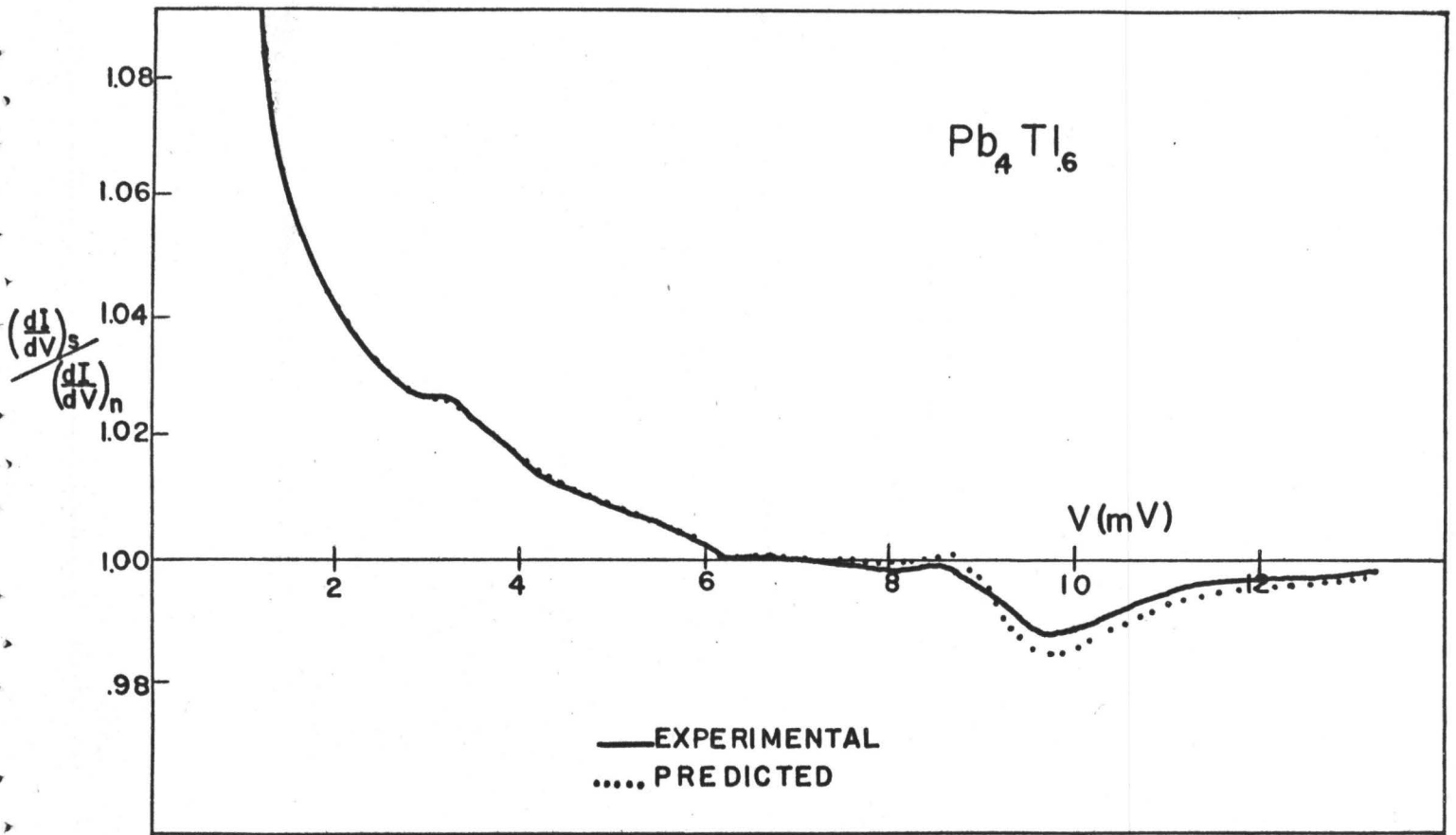
$Pb_4 Tl_{.6}$
$\left(\frac{dI}{dV}\right)_s / \left(\frac{dI}{dV}\right)_n$
1.08
1.06
1.04
1.02
1.00
.98
2
4
6
8
10
12
V (mV)
EXPERIMENTAL
PREDICTED

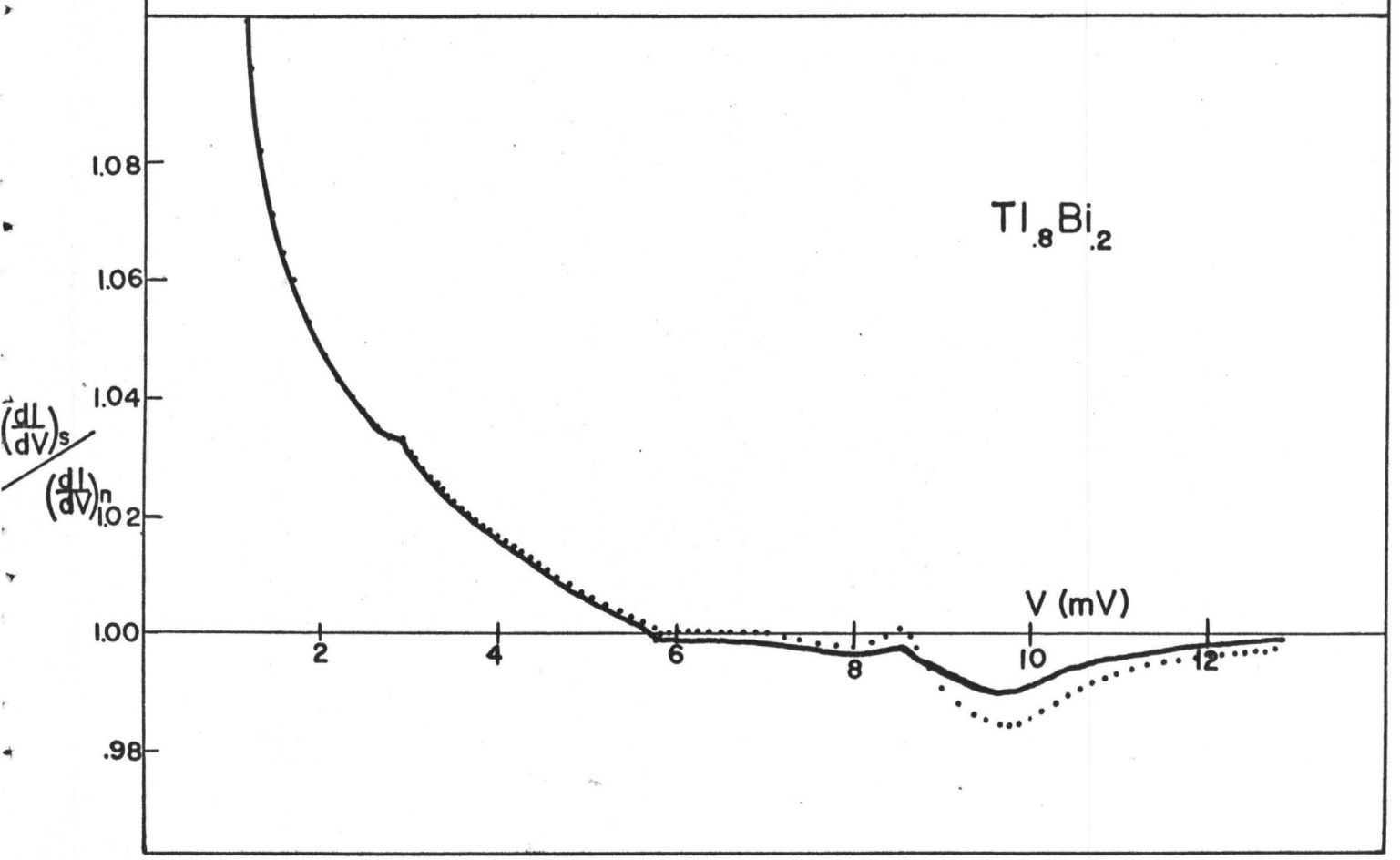
$Tl_{.8} Bi_{.2}$
$\left(\frac{dI}{dV}\right)_s / \left(\frac{dI}{dV}\right)_n$
1.08
1.06
1.04
1.02
1.00
.98
2
4
6
8
10
12
V (mV)

for the current-voltage characteristics of these particular fabrications may thus be obtained with recourse to equation (5-9). This prediction of the deviation in aluminum is in agreement with other investigators[85] who have carefully searched for these effects and have found them to be of this order. As we shall see, however, such deviations are indeed negligible in comparison to those observed for the alloys investigated in this Thesis.

(ii) $N_T(\omega)$ for the Alloys -

The gap equations were solved for those particular alloys that displayed a reliable and converging force constant model. The most reliable of the alloys considered in this respect were the two alloys having electron concentrations of 3.4/atom -- i.e. $Pb_{.4}Tl_{.6}$ and $Tl_{.8}Bi_{.2}$. In order to compare calculated tunneling characteristics with those of experiment, the determined $N_T(\omega)$ parameter for each alloy was convoluted with a B.C.S. $N_T(\omega)$ with thermal excitations at 1.1^oK representing the aluminum according to the prescription of equation (5-9). The results of such a comparison with the normalized results of a tunneling experiment for these two particular alloys are shown in Figure (7-21). The agreement between that predicted from a calculated $\alpha^2(\omega)F(\omega)$ and the actual results of a tunneling experiment is striking. It should also be recalled that excellent agreement was obtained with these particular alloys for the calculation of Δ_o.

This procedure was repeated for alloys with slightly less reliable force constant fits, namely, $Pb_{.6}Tl_{.4}$ and $Tl_{.9}Bi_{.1}$, and the results of such a calculation and comparison with experiment are illustrated in Figure 7-22.

FIGURE 7.22

Comparison of calculated (dotted line) and experimental (solid line) $\left(\frac{dI}{dV}\right)_S \Big| \left(\frac{dI}{dV}\right)_N$ vs. V plot for:

(a) Aℓ-I-$Pb_{.6}Tℓ_{.4}$

(b) Aℓ-I-$Tℓ_{.9}Bi_{.1}$ junctions at $1.1^{o}K$

V is measured from $\Delta_{o\ Aℓ} + \Delta_{o\ ALLOY}$

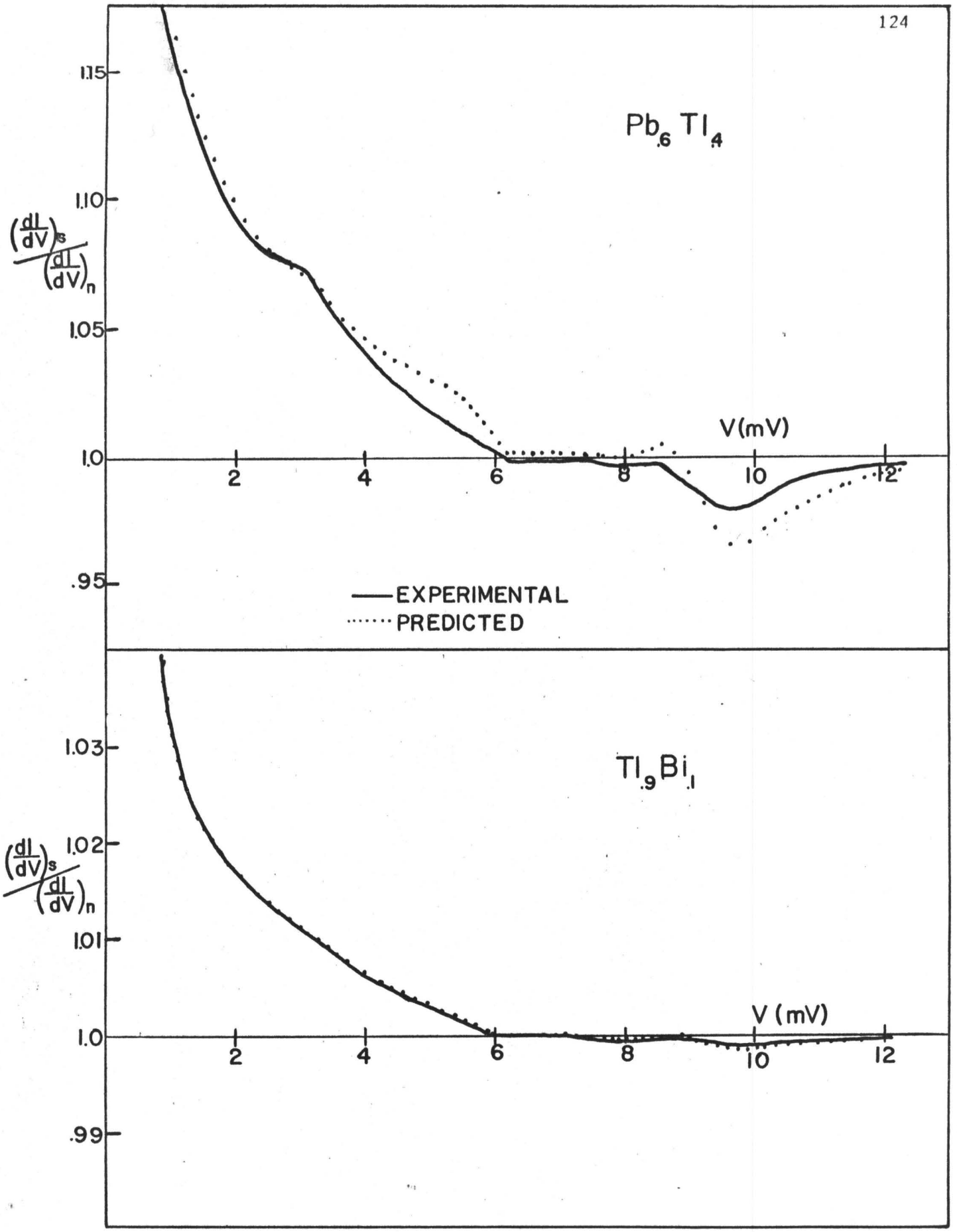
Pb.6 Tl.4
(dI/dV)s / (dI/dV)n
1.15
1.10
1.05
1.0
.95
V(mV)
2
4
6
8
10
12
EXPERIMENTAL
PREDICTED
Tl.9 Bi.1
(dI/dV)s / (dI/dV)n
1.03
1.02
1.01
1.0
.99
V (mV)
2
4
6
8
10
12

As expected, there are more discrepancies in these comparisons than in the first set of alloys considered, but nevertheless, the overall agreement is still good. In all of these alloys considered, however, there is a disagreement which should be noted, namely, in the fundamental dip due to the interaction of electrons with phonons of energy grouped around the longitudinal peak in the density of phonon states. This disagreement will be even more pronounced when we compare predicted and experimental plots of $\frac{d^2I}{dV^2}$ vs. V, the derivatives of the functions considered here.

It should also be pointed out that using the present detection system described in the previous Chapter, the difficulty in obtaining enough sensitivity to display the deviations from B.C.S. predictions for $Tl_{.9}Bi_{.1}$, and for materials with transition temperatures lower than this, becomes formidable. In order to obtain better sensitivity and resolution it would be necessary to employ a bridge circuit[73] which would enhance the signal to background ratio.

Another method of improving signal resolution would be to perform these experiments on symmetric junctions of the type alloy-insulator-alloy. One of the major problems associated with this type of junction is, however, in attaining constancy of concentration of the constituents of the alloy. The determination of concentration and homogeneity of the film is one of the major experimental problems in an investigation of this type and the addition of another film of the alloy and hence another variable, should be avoided.

It should also be emphasized that the curves plotted in Figures 7.21 and 7.22 are ratios $\left(\frac{dI}{dV}\right)_S \Big/ \left(\frac{dI}{dV}\right)_N$. Since the measured tunneling

curve in the normal state is not of the linear form that would be expected, $\left(\frac{dI}{dV}\right)_N$ is not a constant. Rather, it is found to be an asymmetric function slowly varying as a function of applied voltage with very slight indications of structure at various applied biases[51]. Clearly then, when determining the ratio

$$\left(\frac{dI}{dV}\right)_s \Big| \left(\frac{dI}{dV}\right)_N$$

this slowly varying term must be taken into account in the course of investigation. These normal state properties have been studied by Rowell and McMillan[86] as to whether or not the tunneling matrix element remains unchanged in the transition from the superconducting to normal states. Clear evidence has been obtained by the above investigators that in addition to non-linearities that could possibly be attributed to the change in shape of the tunnel barrier, well defined structure has been observed which was attributed to phonon emission in the oxide barrier during the tunneling process.

7.3-3 Second Derivative Comparisons -

An even more spectacular and revealing, if somewhat less physically meaningful method of comparison of experiment with predictions, is that of comparing calculated and experimentally obtained plots of $\frac{d\sigma}{dV}$ vs V, where $\sigma = \left(\frac{dI}{dV}\right)_s \Big| \left(\frac{dI}{dV}\right)_N$. Critical points in $N_T(\omega)$ or points of maximum or minimum slope are greatly amplified as a result of further differentiating.

In order to first determine the level of agreement that could be

FIGURE 7.23

A comparison of experimental (solid line) and calculated (dotted line) $\frac{d\sigma}{dV}$ vs. V plot for a Aℓ-I-Pb junction at $1.1^{o}K$.

$$\sigma = \left(\frac{dI}{dV}\right)_S \Big| \left(\frac{dI}{dV}\right)_N$$

V is measured from $\Delta_{o\ A\ell} + \Delta_{o\ Pb}$. The $\alpha^2(\omega)F(\omega)$ used was that of McMillan and Rowell[30].

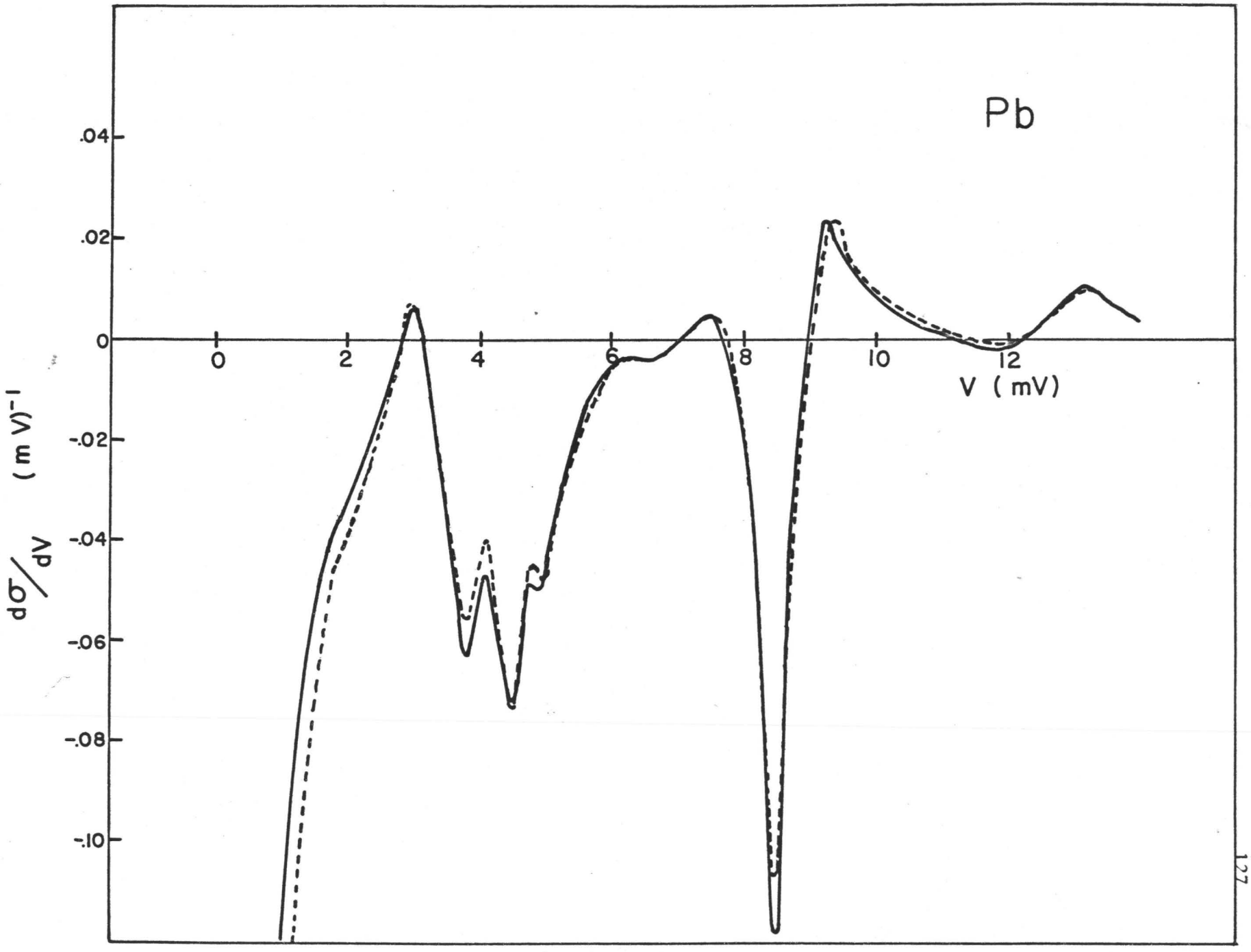
Pb
.04
.02
0
-.02
-.04
-.06
-.08
-.10
0
2
4
6
8
10
12
V (mV)
dσ/dV (m V)⁻¹

expected in such a comparison the experimentally determined $\alpha^2(\omega)F(\omega)$ function for lead[30] of Figure 5.5 was inserted into the gap equations and $N_T(\omega)$ determined. Then, in order to simulate an experiment, this $N_T(\omega)$ was convoluted with a tunneling density of states $N_T'(\omega)$ for aluminum at 1.1°K. $\frac{d\sigma}{dV}$ was then determined for such a hypothetical junction. In this way, a meaningful comparison could be carried out with the results of a tunneling experiment performed by the author on an Aℓ-I-Pb junction at 1.1°K and the results of such a comparison are illustrated in Figure 7.23.

It should be noted that the above comparison determination was performed with a view to applying a circular consistency check which would serve as a standard for comparison. A very small disagreement between calculated and experimental values of the tunneling density of states or more explicitly in $\left(\frac{dI}{dV}\right)_S \Big| \left(\frac{dI}{dV}\right)_N$, will result in a substantial disagreement in a plot of $\frac{d\sigma}{dV}$ vs. V so that we can very carefully determine agreement in this fashion.

In addition, it has been shown[55] that a peak in the phonon density of states, or more correctly in $\alpha^2(\omega)F(\omega)$, will result in a sharp drop in the effective tunneling density of states $N_T(\omega)$ (which is equivalent to a sharp drop in σ). Thus by further differentiating this curve, a sharp drop in σ will be manifested as a minimum in $\frac{d\sigma}{dV}$ and alternatively, a minimum in $\alpha^2(\omega)F(\omega)$ will show as a maximum in $\frac{d\sigma}{dV}$. Consequently, we can very easily identify maxima and minima in this type of tunneling plot with singularities, or critical points in the phonon distribution of the material in question. In this respect, the tunneling technique lends itself as an efficient and rapid tool for phonon spectroscopy in a superconductor.

(i) With these factors in mind, $\frac{d\sigma}{dV}$ vs. V was calculated for a Aℓ-I-$Pb_{.4}Tℓ_{.6}$ junction at 1.1°K employing a grid in $\alpha^2(\omega)F(\omega)$ of $Pb_{.4}Tℓ_{.6}$ somewhat indicative of the a.c. sensing signal experimentally applied to the device. A comparison of this calculated value and the experimentally determined value is given in Figure 7.24.

It may be seen that the agreement in the positions in energy of the critical points (maxima and minima) is extremely good and in some places the relative strengths of these different points show fair agreement -- although in other places, there are clearly large discrepancies. Nevertheless, as this is a derivative of the more physically meaningful $\left(\frac{dI}{dV}\right)_S \Big| \left(\frac{dI}{dV}\right)_N$ parameter, the agreement between experimental and predicted values is quite good.

This procedure is repeated for $Tℓ_{.8}Bi_{.2}$ where, (because the force constant model is felt to be reliable), good agreement is expected, and in $Tℓ_{.9}Bi_{.1}$ and $Pb_{.6}Tℓ_{.4}$ where fair agreement should exist. The results of such calculations and experiments are given in Figure 7.25, 7.26 and 7.27 respectively, where again it is seen that the positions of critical points energy-wise are in excellent agreement with calculations based on neutron scattering measurements. Further the relative strengths show agreement in some areas, and disagreement in others.

For purposes of completeness, the materials that display a suspect Born-von Karman analysis ($Pb_{.8}Tℓ_{.2}$ and Pb) are presented in Figures 7.28 and 7.29. Although the bulk properties of a superconductor are calculated in the case of these two materials with a fair degree of success, using the calculated $\alpha^2(\omega)F(\omega)$ parameter, good agreement between the predicted and experimental values of critical points is not expected.

FIGURE 7.24

Comparison of calculated (dotted line) and experimental (solid line) $\frac{d\sigma}{dV}$ vs. V for Aℓ-I-$Pb_{.4}Tℓ_{.6}$ junction at 1.1°K. V is measured from $\Delta_{o\ Aℓ} + \Delta_{o\ Pb_{.4}\ Tℓ_{.6}}$.

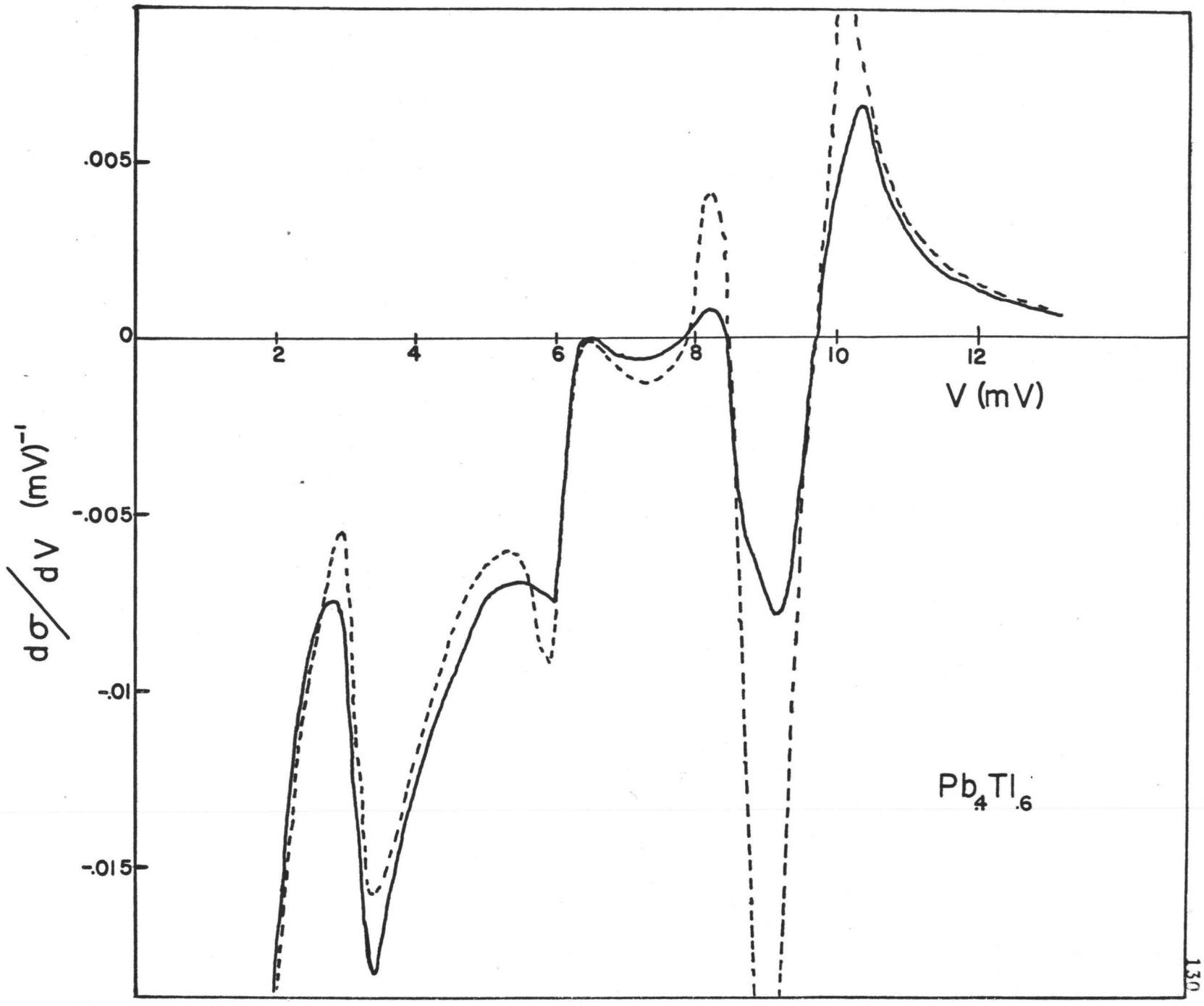
.005
0
-.005
-.01
-.015
2
4
6
8
10
12
V (mV)
dσ/dV (mV)⁻¹
Pb.4Tl.6

FIGURE 7.25

Comparison of calculated (dotted line) and experimental (solid line) $\frac{d\sigma}{dV}$ vs. V for Aℓ-I-$Tℓ_{.8}Bi_{.2}$ junction at 1.1°K. V is measured from $\Delta_{o\ Aℓ} + \Delta_{o\ Tℓ_{.8}Bi_{.2}}$.

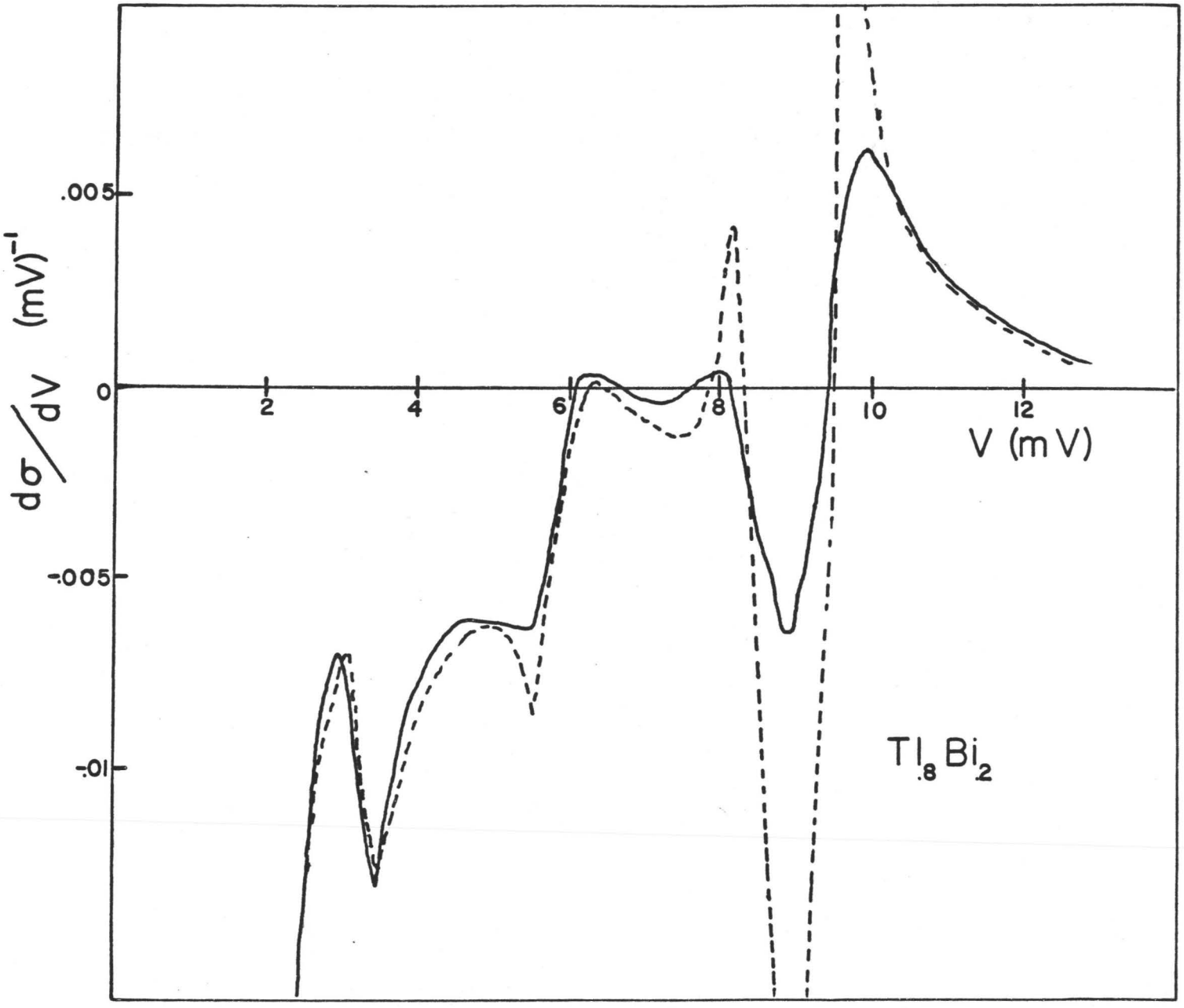
.005
0
-.005
-.01
dσ/dV (mV)⁻¹
2
4
6
8
10
12
V (mV)
Tl.8 Bi.2

FIGURE 7.26

Comparison of calculated (dotted line) and experimental (solid line) $\frac{d\sigma}{dV}$ vs. V for Aℓ-I-$Tℓ_{.9}Bi_{.1}$ junction at 1.1°K. V is measured from $\Delta_{o\ Aℓ} + \Delta_{o\ Tℓ_{.9}Bi_{.1}}$.

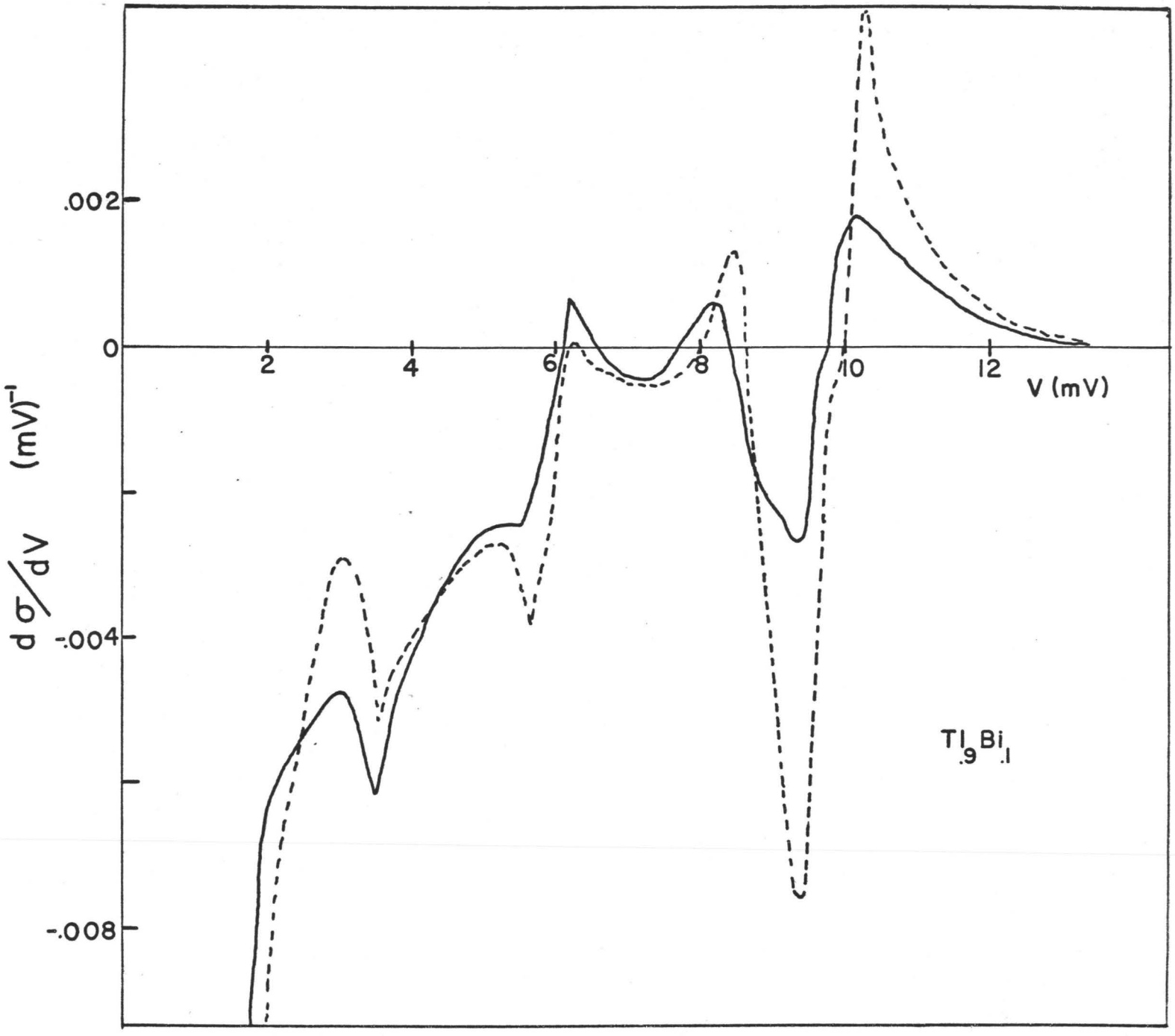
.002
0
-.004
-.008
2
4
6
8
10
12
V (mV)
dσ/dV (mV)⁻¹
Tl.9Bi.1

FIGURE 7.27

A comparison of calcualted (dotted line) and experimental (solid line) $\frac{d\sigma}{dV}$ vs. V for Aℓ-I-$Pb_{.6}Tℓ_{.4}$ at 1.1°K. V is measured from $\Delta_{o\ A\ell} + \Delta_{o\ Pb_{.6}Tℓ_{.4}}$.

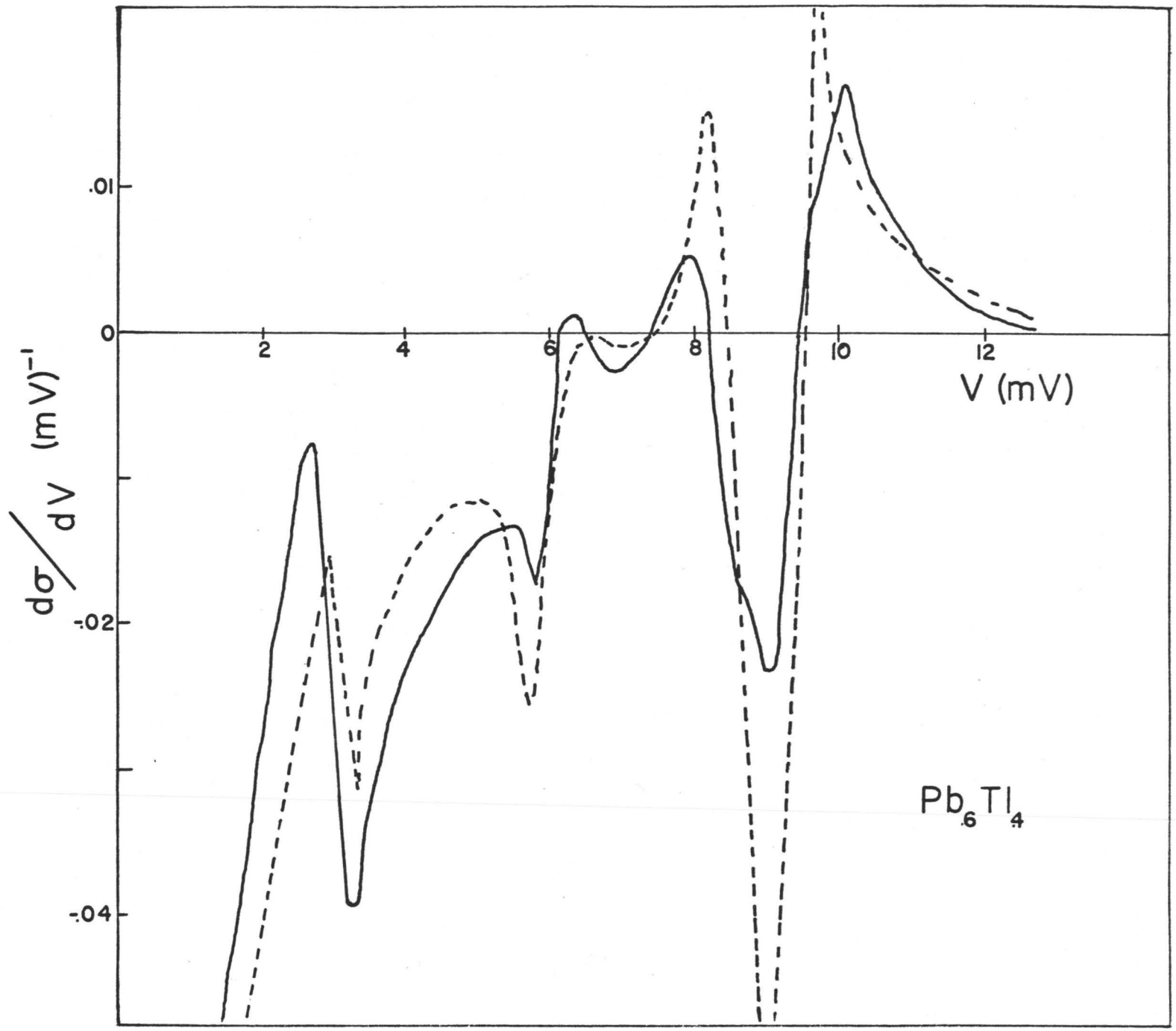
.01
0
-.02
-.04
2
4
6
8
10
12
V (mV)
dσ/dV (mV)⁻¹
Pb.6Tl.4

FIGURE 7.28

A comparison of calculated (dotted line) and experimental (solid line) $\frac{d\sigma}{dV}$ vs. V for Aℓ-I-$Pb_{.8}Tℓ_{.2}$ junction at 1.1°K. V is measured from $\Delta_{o\ A\ell} + \Delta_{o\ Pb_{.8}\ Tℓ_{.2}}$.

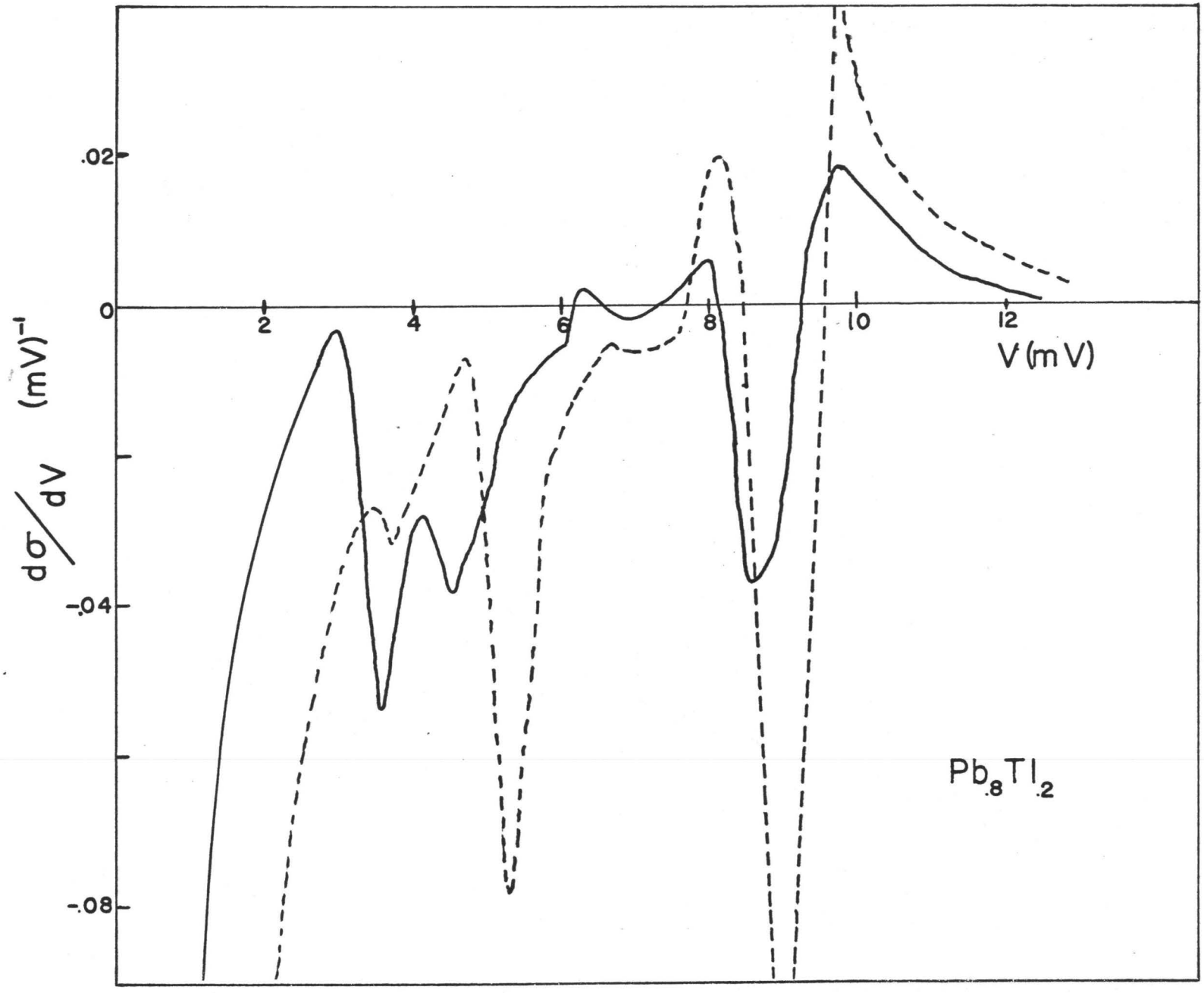
.02
0
-.04
-.08
2
4
6
8
10
12
V(mV)
dσ/dV (mV)⁻¹
Pb.8Tl.2

FIGURE 7.29

A comparison of calculated (dotted line) and experimental (solid line) $\frac{d\sigma}{dV}$ vs. V for Aℓ-I-Pb junction at 1.1°K. V is measured from $\Delta_{o\ A\ell} + \Delta_{o\ Pb}$.

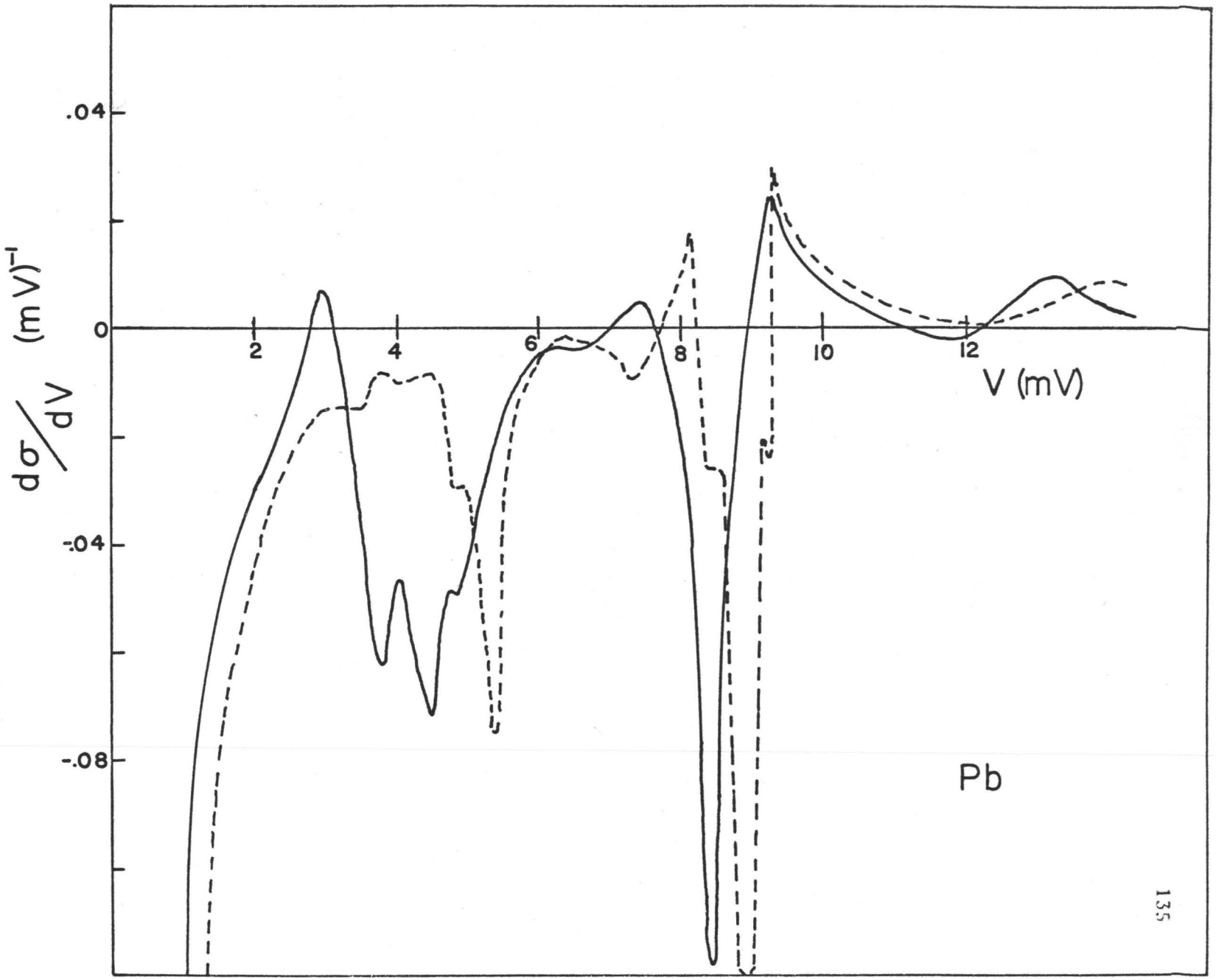
.04
0
-.04
-.08
dσ/dV (mV)⁻¹
2
4
6
8
10
12
V (mV)
Pb

Figure 7.29 is simply another manifestation of the disagreement cited in Figure 7.12. As was pointed out earlier, some of the critical points do, in fact, agree in both cases. Those that agree are related to critical points determined by neutron scattering experiments in the on-symmetry directions.

This comparison even further emphasizes the applicability of this tunneling method, for certain materials and alloys as a convenient method of critical point spectroscopy and as a guide to the more exacting neutron scattering experiment. As $\alpha^2(\omega)$ does not severely change the features of the phonon density of states $F(\omega)$ in $\alpha^2(\omega)F(\omega)$ the value of the Born-von Karman analysis can be easily assessed by this spectroscopic method of determination of the critical points. If a simple one-to-one comparison of critical points is not possible, a more extensive study of the two methods is necessary.

(ii) The disagreement in the relative strengths of the different peaks between those calculated and those experimentally observed cannot be ignored. In all the alloys considered, it was observed experimentally that there appeared to be an extensive amount of smearing in the region of the longitudinal peak.

One must first ascertain whether this smearing is due to something fundamental or simply a result of experimental smearing. The smearing is clearly not due to the finite size of the a.c. probe used to differentiate the tunneling characteristics as it appears to be energy dependent. In addition, a reduction of the size of the test signal has no effect on the

relative strengths of the different peaks. These experimental results have been seen by other observers[87] for some of these alloys and it appears from this reproducibility in different laboratories, that the smearing is not induced experimentally.

Recently, Zavaritskii[89] has reported tunneling experiments on lead thin films evaporated onto a substrate at 4.2°K where a somewhat similar effect was observed. It was noted that there was a substantial difference between the tunneling curves obtained on such samples, and those obtained from a sample prepared in the conventional manner with the substrate at room temperature. In addition, it was found that upon annealing the sample to room temperature, and then re-cooling, the characteristics assumed the form generally accepted as those of lead. The films prepared at low temperatures displayed a large amount of smearing in the distinctive peaks in the $\frac{d\sigma}{dV}$ plot and in fact, much of the fine detail was not there.

It is suggested that this phenomenon could be explained in terms of Lifshitz's[90] discussion of energy spectrum structure in disordered condensed systems. Lifshitz shows that in the vicinity of a boundary or cut-off point of the spectrum, if a perturbation to the ideal system is added (an impurity for example), a singularity that in the pure case may vary

$$\sim \sqrt{\omega - \omega_o}$$

where ω_o is the cut-off value, now assumes the form

$$\sim \exp \{ - \lambda \phi(c) \quad (\omega - \omega_o')^{-3/2} \}$$

where ω_o' is the new cut-off value given by $\omega_o' = \omega_o + V$ where V is the perturbation added, $\phi(c)$ is a function of the impurity concentration c which varies as ℓn c for low concentration, and λ is a constant. The absolute value of the constants in front of the exponential are difficult to determine but worthy of note is the fact that the functional form of this new type of discontinuity is suggestive of the "tail" at the high energy cut-off in the $\alpha^2(\omega)F(\omega)$ distribution shown in Figure 5.5 as determined by McMillan and Rowell[30]. In an ideal system this tail should not exist but a thin film is far from an ideal system and the perturbation caused by dislocations and small crystallite sizes could cause a singularity of the functional form described above.

This development of a tail at the high end of the energy spectrum is manifested also in the experimental $\frac{d\sigma}{dV}$ plots of the alloys presented in this work as the perturbation introduced takes the form of an impurity site. Lifshitz shows, in addition, that the insertion of a perturbation causes a smearing, not only at the cut-off of the spectrum, but throughout the energy spectrum and in particular, at critical points.

In the calculation of $\alpha^2(\omega)F(\omega)$ from a Born-von Karman force constant analysis, it should be emphasized that no provision is made for this disorder phenomenon. The material considered is assumed to be a pure material of some hypothetical element whose properties are those of the average of the constituents that make up the alloy. For example, the ionic mass of this material of $Pb_xTl_{(1-x)}$ is assumed to be:

$$M_{alloy} = xM_{Pb} + (1-x)\, M_{Tl}$$

Hence, the calculation assumes that the bonding between adjacent ions is of the type

$$Pb_xTl_{(1-x)} - Pb_xTl_{(1-x)} - Pb_xTl_{(1-x)}$$

while in fact they may be of the form:

$$Pb - Pb \quad \text{or} \quad Tl - Tl \quad \text{or} \quad Pb - Tl$$

Making this somewhat naive assumption, all finite lifetime effects for phonons, which certainly do exist in an alloy, are ignored.

Hence, disordered alloys may be expected to produce a broadening in the critical points due to random differences in the forces between various pairs of ions with the same geometrical arrangement. In essence, this randomness will produce a fuzziness in the dispersion curves which is inherent in an alloy system. While the ideal pure crystal will be expected to display sharp phonon dispersion curves, alloys will not.

Unfortunately at this time, the resolution of neutron scattering experiments is not sufficiently precise to determine the extent of this uncertainty, especially in the higher energy longitudinal branches where the errors quoted for the measurement of a neutron group are $\gtrsim$15% of the measured energy. Hence, until such resolution is increased to the point where the very pure materials show very narrow scatter from a central value, a measure of the uncertainty of the energy of a particular phonon is impossible. Hence, a Born-von Karman analysis of the dispersion curves of an alloy where it is assumed the curve is very well defined is, in some respects a "physically ideal" model while in actuality, disordered force constants must be taken into account.

CHAPTER VIII

CONCLUSIONS AND RECOMMENDATIONS

In this Thesis, a surprising amount of success has been achieved in determining the superconducting energy gap in lead, aluminum and thallium-lead-bismuth alloys from information now available on lattice vibrations in such materials, and the newly increased knowledge of the electron-ion pseudopotential form factor. The main quantity to be calculated in the above determinations is the phonon contribution to the Eliashberg gap equations which enters as the phonon density of states $F(\omega)$, modulated by an energy dependent electron-phonon coupling term usually denoted by $\alpha^2(\omega)$. From this product function, $\alpha^2(\omega)F(\omega)$, it has been possible to calculate the superconducting energy gap $\Delta(\Delta_o)$ of the above materials, much more carefully than has been possible in the past. None of the estimates presented here varied from the experimentally determined values by more than 10% in these materials. A small adjustment of the appropriate coulomb pseudopotential term $N(0)u_c$ in these equations, (which is not known very accurately at this time), would improve the agreement in each case. A more accurate evaluation should be performed of this coulomb repulsion term, which opposes the onset of superconductivity and is so important in the solution of the Eliashberg gap equations. It has also been shown that a small adjustment of the choice of the electron-ion form factor, so as to change the corresponding $\alpha^2(\omega)F(\omega)$ also has a

profound effect on the evaluation of $\Lambda(\Lambda_o)$.

As the Born-von Karman 8 nearest neighbour analysis of lead was shown to be suspect in certain regions due to critical points existing in off-symmetry directions that had not experimentally been measured, the agreement between measured and predicted values of $\Delta(\Delta_o)$ for this material was even better than perhaps expected.

In order to determine the validity of these predictions, a tunneling investigation of selected thallium-lead-bismuth alloys has been performed. As all the alloys had the same crystal structure (face centered cubic) and the atomic masses of the constituents were approximately equal, and since it was known from neutron scattering experiments that the phonon density of states $F(\omega)$ of this series of alloys did not change very drastically, changes in the electron-phonon interaction strength of these materials were primarily due to changes in the electron concentration which in turn affected the superconducting nature of the alloys. Agreement between predicted and experimentally observed $\Delta(\Delta_o)$ was extremely good for the entire series, even when the Born-von Karman calculation of $F(\omega)$ was not too reliable.

In addition, the tunneling experiments on these alloys allowed the comparison of critical points in the phonon energy spectrum between those obtained by neutron scattering experiments and a force constant analysis, and those obtained by tunneling. It was found that where reasonable confidence in the force constant model used to calculate $F(\omega)$ was felt, extremely good agreement in the positions of the critical points resulted. Also, fair agreement was experienced between the relative strengths of these critical points derived using the two methods. The

differences were felt to be due to the non-ideal nature of an alloy.

In the case of sodium and potassium, the critical temperatures (T_c) are estimated to be certainly less than 10^{-5} ^{o}K. This upper bound was obtained by progressively switching on the coulomb repulsion term $N(0)u_c$ and at each stage computing a corresponding critical temperature. This sequence of operations was terminated at a value of $N(0)u_c$ which was still much less than a realistic value[46] but which yielded a critical temperature sufficiently small that it was felt uninteresting to proceed further. To reduce this upper bound would have required more extensive computational complications which did not seem warranted.

Throughout this analysis no corrections were applied for the possible deviation of the electronic density of states at the Fermi surface from its free electron value. It was felt that any slight deviations from the free electron Fermi sphere would be averaged out when all possible scatterings were added up from any random point on the surface to any other random point. For any large deviations, this clearly is not true as some particular $\underline{q}$ values might be greatly enhanced over others.

It is important also to note that in all determinations of $\alpha^2(\omega)F(\omega)$, the critical points do not shift in energy although their relative strengths do. Also contrary to the expectation of Bennett[77], no new singularities are generated as a result of the cut-off at 2 k_F in the calculation of $\alpha^2(\omega)F(\omega)$. In the free electron approximation, $\alpha^2(\omega)$ is a smoothly varying, although by no means a constant function, as there is a divergence at low values of ω. Generally the main longitudinal peak region is more emphasized by the $\alpha^2(\omega)$ function than is the transverse region.

In light of the investigation described in this Thesis, it now seems possible that the tunneling method described can be used as an investigation tool for other materials.

Firstly, with improved sensing techniques and lower available temperatures in view of the predictions of $\alpha^2(\omega)F(\omega)$ for aluminum one could, using a symmetric junction Aℓ-I-Aℓ, investigate the possibility of determining experimentally the validity of this prediction. The limiting factor in such an investigation would be the sensitivity of the sensing device.

The effects of pressure on a simple superconductor, both from a theoretical and experimental point of view using the techniques outlined in this Thesis could also be investigated. Pressure on a material will bring about changes in the phonon spectrum and its critical points, and the strength of the electron phonon coupling term $\alpha^2(\omega)$. Experiments have recently been performed investigating the pressure dependence of superconductors using the tunneling technique[91] and preliminary results appear interesting. A comprehensive investigation of the effect of this variable would prove fruitful.

Also, a comprehensive study of the transition temperatures of noble transition elements and alloys has been carried out[92,93], over a wide range of materials and electron concentrations. It was found that the filling up of the d-band suppresses the superconducting transition temperature and in addition, materials with large magnetic susceptibilities were not superconducting above $0.015^{o}K$. A possible explanation of this correlation of parameters was given in terms of Berk and Schrieffer's model of ferromagnetic spin correlations[94]. These correlations effectively

enhance the electron-electron repulsion term $N(0)u_c$ (for example in Pd, this is many times the conventional coulomb pseudopotential) thus diminishing the probability of a material to go superconducting. Transition metals in which the phonons have been measured using inelastic neutron scattering experiments, possibly could be studied, and the strength of these various contributions could be determined by a combined experimental and theoretical approach. This investigation could strengthen the knowledge of a somewhat unknown subject.

APPENDIX A

In this Appendix, a standard method will be described to calculate the phonon density of states function $F(\omega)$, together with the modification to that method as required in the determination of the product function $\alpha^2(\omega)F(\omega)$. The method used is a Born-von Karman analysis[76] which is a phenomenological fit of interatomic force constant strengths to reproduce the measured dispersion curves. The actual Born-von Karman analysis for the materials considered was carried out by other investigators and the published [95,98] force constants are simply used in this analysis to determine the dispersion curves in the off-symmetry directions which are not measured. Proceeding in this fashion, one can determine the phonon frequencies for points over all the Brillouin zone and, by summing these, extract an estimate of the phonon density of states. As discussed in Chapter 7 this analysis can be slightly erroneous in some cases, as it is found in some materials that there are long-range forces, and thus this type of model does not converge with a realistic number of force constants.

A.1 BORN-VON KARMAN ANALYSIS:

From Chapter II we see that there is a restoring force in the lattice for displacements from equilibrium, much like a simple spring-restoring force in the simple harmonic oscillating spring. From equation (2-4) we can write the equation of motion for the ℓ th ion as:

$$- M \frac{d^2 U_\alpha(\ell)}{dt^2} = \sum_{\ell'\beta} \Phi_{\alpha\beta}(\ell\ell') U_\beta(\ell') \qquad \text{------(A-1)}$$

where M = mass of ion, $U_\alpha(\ell)$ is the α-direction component of the excursion from equilibirum of the ℓ'th ion and $\Phi_{\alpha\beta}(\ell\ell')$ is the force in the αth direction on this ion due to a unit displacement of the ℓ'th ion in the β direction. Because of the periodicity of the lattice, these atomic force constants (A.F.C.) do not depend explicitly on the atoms ℓ or ℓ' but only on the distance $R_{\ell\ell'}$ between them. For each type of neighbour (i.e. first nearest neighbour or second nearest neighbour) there are a certain number of these independent constants. Consider, for example a force-centered cubic lattice, and the first nearest neighbours of the atom in the (0, 0, 0) position. There are twelve of these nearest neighbours located on the faces and their co-ordinates are given by:

$\frac{a}{2}(110)$, $\frac{a}{2}(101)$, $\frac{a}{2}(011)$, $\frac{a}{2}(\bar{1}10)$, $\frac{a}{2}(\bar{1}01)$----- etc.

There are, at first glance 3 x 3 constants for each atom and hence 3 x 3 x 12 constants altogether. Because of the high symmetry of the cubic system, one can immediately eliminate most of these and reduce the number of independent force constants to 3. Thus;

$$\Phi_{xx}(110) = \Phi_{yy}(110) = \Phi_{zz}(101) = \text{------} \equiv -\alpha_1$$

$$\Phi_{xy}(110) = \Phi_{xz}(101) = \text{------} \equiv -\gamma_1$$

$$\Phi_{zz}(110) = \Phi_{yy}(101) = \Phi_{xx}(101) = \text{------} = -\beta_1$$

If we now consider the second nearest neighbours of the point (0,0,0), it can be seen that there are six of these whose co-ordinates are given by:

$$\frac{a}{2}\ (2,0,0),\ \frac{a}{2}\ (0,2,0),\ \frac{a}{2}\ (0,0,2),\ \frac{a}{2}\ (\bar{2},0,0),\ \frac{a}{2}\ (0,\bar{2},0),\ \frac{a}{2}\ (0,0,\bar{2})$$

Again from symmetry considerations, the number of independent force constants can be reduced to two and these are denoted by:

$$\Phi_{xx}(200) = \Phi_{yy}(020) = \text{------} \equiv -\alpha_2$$

$$\Phi_{yy}(200) = \Phi_{zz}(200) = \text{------} = -\beta_2$$

This analysis can easily be extended to the general case of nth nearest neighbours with co-ordinates $\frac{a}{2}$ (u, v, w). In the most general case, $u \neq v \neq \omega$ and there are 48 nearest neighbours with 6 independent force constants permitted by symmetry.

From the equation of motion (A-1), as previously described in Chapter 2, a trial wave solution can be attempted of the form

$$\underline{U}(\ell) = \frac{1}{\sqrt{M}}\ \underline{\varepsilon}\ (\underline{q},\ \lambda)\ \exp i\{\underline{q}\ .\ \underline{R}(\ell) - \omega(\underline{q}\ \lambda)\ t\ \} \qquad \text{------(A-2)}$$

where $\underline{\varepsilon}\ (\underline{q}\ \lambda)$ is the polarization vector of the normal mode $\omega(\underline{q},\lambda)$ and $\underline{R}(\ell)$ is the equilibrium position of the ℓ'th atom. Inserting equation (A-2) into equation (A-1) and multiplying both sides by $e^{-q.\underline{R}(\ell)}$ yields

$$\omega^2(\underline{q},\ \lambda)\ \varepsilon_\alpha\ (\underline{q}\ \lambda) = \sum_\beta \frac{1}{M}\ \left[\sum_{\ell'} e^{-i\underline{q}\underline{R}(\ell)} \Phi_{\alpha\beta}\ (\ell,\ell')\ e^{i\underline{q}.\underline{R}(\ell)}\right] \varepsilon_\beta(\underline{q},\ \lambda) \qquad \text{------(A-3)}$$

It can be shown, however, that the quantity in the square brackets above does not depend on ℓ. It is a function of $\underline{q}$ only and is called the Dynamical matrix

$$D_{\alpha\beta}(\underline{q}) = \sum_{m} \frac{1}{M} e^{-i\underline{q}\underline{R}_m} \Phi_{\alpha\beta}(m, 0) \qquad \text{------(A-4)}$$

Equation (A-3) may thus be written in the form:

$$\omega^2 (\underline{q}, \lambda) \varepsilon_\alpha(\underline{q}, \lambda) = \sum_{\beta} D_{\alpha\beta} (\underline{q}) \varepsilon_\beta (\underline{q}, \lambda). \qquad \text{------(A-5)}$$

which is just a simple eigenvalue problem for the 3 x 3 matrix $D(\underline{q})$. Thus, given the dynamical matrix at any point $\underline{q}$ in the Brillouin zone, it is a simple mathematical problem to determine the three eigenvalues $\omega(q, \lambda)$, $\lambda = 1, 3$ and corresponding eigenvectors which form an orthonormal set. Further, and from (A-5), it is clear that for any given $\underline{q}$, $D(\underline{q})$ is easily constructed from the force constants $\Phi_{\alpha\beta}(\ell,\ell')$.

Phonons can be measured using the inelastic neutron scattering technique. In this way one normally determines the dispersion curves along high symmetry directions in the first Brillouin zone. It is also common practice to vary the force constants $\Phi_{\alpha\beta}(m, 0)$ so as to obtain the best possible fit to the dispersion curves for a specified number of nearest neighbours. The number of parameters needed to achieve good agreement depends, of course, on how structured the measured dispersion curves are. In sodium and potassium, for instance, where the dispersion curves show little detailed structure, a fifth nearest neighbour fit gives essentially exact agreement with the data. To obtain good agreement

in aluminum, which is a slightly more complicated case, one must go out to 8 nearest neighbours. In lead, where large Kohn anomalies[99,100] are observed, eight nearest neighbours gives only a reasonable overall fit. A good fit in this case would require more parameters. Nevertheless, such fits are very useful since from the force constants one can calculate in principle many interesting properties; for example, the resistivity of a material[101] or the superconducting energy gap.

Up to this point, all the constraints imposed on these force constants are due to the symmetry of the crystal structure. If one also considers the nature of the force system between neighbours, it can be shown that[76] if one limits the type of force considered to that of a central force depending only on the magnitude $|r|$ of the distance apart, additional constraints can be imposed onto these force constants. These additional constraints are listed in references cited[28], however, a most general force constant analysis as outlined above considering only the symmetric nature of the system is most desirable.

An additional constraint can be imposed upon these force constants if the crystal is in equilibrium; i.e. the lattice constant distances must be such as to minimize the total potential energy in the system.

In Table A-1 are listed the atomic force constants for pure lead and for the Tℓ-Pb-Bi alloys at 100°K as tabulated by Ng[98] for 8 nearest neighbours. In Table A-2 are listed the atomic force constants for aluminum[97], sodium[95] and potassium[96]. The treatment for Aℓ is to 8 nearest neighbours, while sodium and potassium it is to 5 nearest neighbours.

TABLE A-1

ATOMIC FORCE CONSTANTS FOR Bi-Pb-Tℓ ALLOYS AT 100°K

IN UNITS OF DYNES/CM

AFC	Pb	$Pb_{.8}Tℓ_{.2}$	$Pb_{.6}Tℓ_{.4}$	$Pb_{.4}Tℓ_{.6}$	$Bi_{.2}Tℓ_{.8}$	$Bi_{.1}Tℓ_{.9}$
α_1	3933	4055	4603	4944	4679	4984
β_1	-1280	-1111	-1333	-1532	-1448	-1485
γ_1	4929	5270	5445	5540	5198	6161
α_2	1617	976	407	43	151	65
β_2	309	103	-128	-148	-129	107
α_3	-266	-252	-97	193	104	-26
β_3	41	59	-92	-150	-133	-44
γ_3	349	147	53	-4	-37	-72
δ_3	-58	-4	45	-8	-61	-66
α_4	757	566	382	141	251	-3
β_4	105	-68	-9	-6	-60	-74
γ_4	376	-51	-100	123	337	12
α_5	-288	-35	-64	-142	-156	12
β_5	-341	-217	-26	67	40	-7
γ_5	-347	-240	-21	93	64	-10
δ_5	20	68	-14	-79	-73	7
α_6	34	50	-25	-81	1	11
β_6	-177	8	43	23	117	15
α_7	-59	-97	-10	97	51	38
β_7	133	101	31	-38	-81	17
γ_7	30	40	26	-5	20	-25
δ_7	33	13	9	10	-7	4
ϵ_7	50	20	14	14	-10	7
ζ_7	100	39	27	29	-21	13
α_8	679	197	44	-114	-34	-131
β_8	185	88	-35	-7	39	78

TABLE A-2

ATOMIC FORCE CONSTANTS FOR ALUMINUM (f.c.c.) SODIUM (b.c.c.) AND POTASSIUM (b.c.c.) IN UNITS OF OF DYNES/CM

AFC Aℓ (at 80°K)		AFC Na (at 90°K)		AFC K(9°K)	
α_1	10107	α_1	1178	α_1	786
β_1	-1337	β_1	1320	β_1	895
γ_1	11444				
α_2	2452	α_2	472	α_2	432
β_2	-529	β_2	104	β_2	29
α_3	-625	α_3	-38	α_3	-41
β_3	-182	β_3	-.4	β_3	12
γ_3	-148	γ_3	-65	γ_3	-53
δ_3	-296				
α_4	271	α_4	52	α_4	2
β_4	321	β_4	-7	β_4	-4
γ_4	-50	γ_4	3	γ_4	.75
		δ_4	14	δ_4	2.25
α_5	461	α_5	17	α_5	6
β_5	227	β_5	33	β_5	4
γ_5	198				
δ_5	888				
α_6	142				
β_6	-109				
α_7	-64				
β_7	-94				
γ_7	-111				
δ_7	12				
ϵ_7	18				
ζ_7	36				
α_8	-534				
β_8	-116				

FIGURE A-1

Irreducible $1/48^{th}$ segment of the Brillouin zone for

(a) face centered cubic system

(b) body centered cubic system

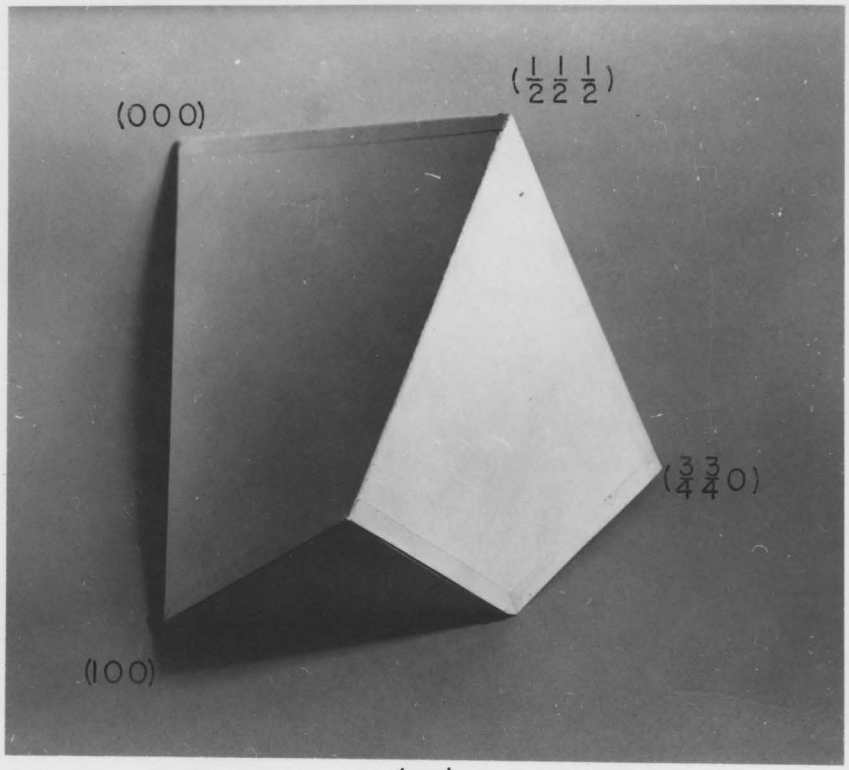
(000)
$(\frac{1}{2}\frac{1}{2}\frac{1}{2})$
$(\frac{3}{4}\frac{3}{4}0)$
(100)

(a)

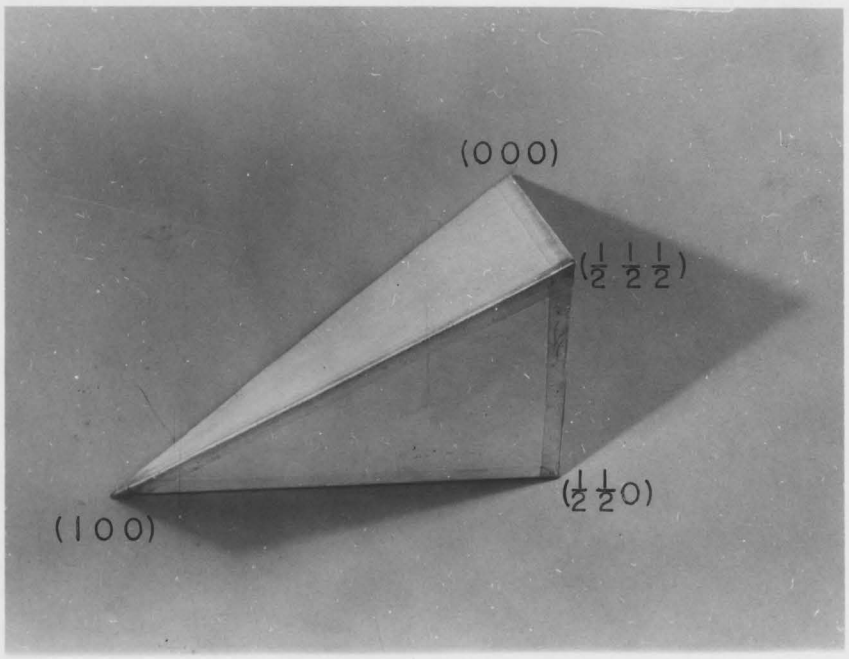
(000)
$(\frac{1}{2}\frac{1}{2}\frac{1}{2})$
$(\frac{1}{2}\frac{1}{2}0)$
(100)

(b)

Having now briefly outlined the general method of the force constant analysis, we are now in a position to calculate the phonon density of states function $F(\omega)$ and the product function $\alpha^2(\omega)F(\omega)$. In a cubic system, the Brillouin zone can be represented by an irreducible $1/48^{th}$ segment of the zone. The complete zone, and hence all of reciprocal space can be generated from this irreducible zone. For a face-centered cubic crystal system, reciprocal space is represented by a body-centered cubic system and the $1/48^{th}$ segment for this system is defined by the planes:

$$\begin{aligned} q_x &= 1.0 \\ q_z &= 0.0 \\ q_x &= q_y \\ q_y &= q_z \\ q_x + q_y + q_z &= \frac{3}{2} \end{aligned} \qquad \text{------(A-6)}$$

where q is in reduced units of $\frac{2\pi}{a_L}$ and a_L is the lattice distance. A schematic diagram of this irreducible zone is shown in Figure (A-1).

Similarily, a body centered cubic system has a face centered cubic reciprocal space, and this $1/48^{th}$ segment is defined by:

$$\begin{aligned} q_z &= 0.0 \\ q_x &= q_y \\ q_y &= q_z \\ q_x + q_y &= 1 \end{aligned} \qquad \text{------(A-7)}$$

This zone is illustrated in Figure A-1. The method of calculation follows the method of Gilat and Raubenheimer[102], where the irreducible $1/48^{th}$ segment is divided into a finer mesh of equally spaced points. At each point in this mesh the phonon energies $\omega(\underline{q}, \lambda)$ $\lambda = 1, 3$, are calculated in addition to their polarization vectors $\underline{\varepsilon}(\underline{q}, \lambda)$, and the gradients of these dispersion curves at that point

$$\frac{\partial\omega(\underline{q}, \lambda)}{\partial q_\alpha} \qquad \text{where} \qquad \lambda = 1, 3 \qquad \alpha = 1, 3$$

The dispersion curve is linearly extrapolated to the edge of cube defined by the fine mesh into which the $1/48^{th}$ segment is divided, using the calculation of the gradient as a recipe. The density of states is then obtained by adding together the contributions from all the different small cubes and all branches. In order for linear extrapolation to be adequate, the mesh points (at which calculations are to be performed), should be sufficiently fine.

This phonon density of states function for the material is defined by:

$$F(\omega) = \frac{1}{N} \sum_{\lambda} \int \frac{d^3\underline{q}}{(2\pi)^3} \delta(\omega - \omega'(\underline{q}\,\lambda)) \qquad \text{------(A-8)}$$

where the integration is over the entire first Brillouin zone.

Recalling our definition of the product function $\alpha^2(\omega)F(\omega)$ from equations (4-15) and (2-26), we see that:

$$\alpha^2(\omega)F(\omega) = \frac{N(0)}{8\pi k_F^{\,2}\, MN} \sum_{\lambda} \int_{<2k_F} d^3\underline{q}\, \frac{|\underline{\varepsilon}(\underline{q}\lambda) \cdot \underline{q}|^2}{|\underline{q}|\ \omega'(\underline{q}\lambda)} \times |\langle \underline{k_F}+\underline{q}|\hat{w}|\underline{k_F}\rangle|^2 \delta(\omega-\omega'(\underline{q}\lambda)) \qquad \text{------(A-9)}$$

where the matrix element $< \underline{k}_F+\underline{q} \mid w \mid \underline{k}_F >$ for scattering from one point on the Fermi surface to another is taken to depend only on the momentum transfer $\underline{q}$, and is denoted $w(\underline{q})$. The integration in q space is now over a sphere of radius $2k_F$. This is the maximum possible q-transfer between a phonon and an electron on the Fermi sphere. In integrating over this sphere, which penetrates out beyond the first Brillouin zone for most materials, we see that Umklapp processes are being considered. Using a prescribed functional form for $w(\underline{q})$ the calculation can now proceed by simply extending the volume to be considered to a $1/48^{th}$ of a sphere of radius $2k_F$. In materials such as lead, where a sphere of radius $2k_F$ covers many of these irreducible zones, the computational time is clearly a factor to be considered. Proceeding in this straightforward fashion, to calculate $\alpha^2(\omega)F(\omega)$ one would require 10 - 15 times that computational time required for the determination of $F(\omega)$.

In order to keep this to a minimum, and because of the obvious repeatability of the dispersion curves out into the second zone and beyond, it is convenient to construct the sphere of $2k_F$ from units of the irreducible $1/48^{th}$ segment of the Brillouin zone. The phonon energies and polarization vectors of a given point in this zone need only be calculated once and, by a suitable co-ordinate transformation, all points in reciprocal space can be represented. Thus, the use of this transformation represents a large time-saving tool in the calculation of $\alpha^2(\omega)F(\omega)$.

The co-ordinate transformations required to map this irreducible zone out to fill up all of reciprocal space for face centered cubic and body centered cubic structures are given in Table A-3. The extent of these transformations is adequate for all the materials considered in

TABLE A-3a

TRANSFORMATIONS REQUIRED TO MAP $1/48^{th}$ OF THE FIRST BRILLOUIN ZONE OUT INTO FURTHER ZONES. FACE CENTERED CUBIC.

RECIPROCAL LATTICE POINT	TRANSFORMATIONS	RECIPROCAL LATTICE POINT	TRANSFORMATIONS
(000)	$q'_x = q_x$ $q'_y = q_y$ $q'_z = q_z$	(200)	$q'_x = 2 - q_x$ $q'_y = q_y$ $q'_z = q_z$
(111)	$q'_x = 1-q_z$ $q'_y = 1-q_y$ $q'_z = 1-q_x$	(200)	$q'_x = 2 - q_y$ $q'_y = q_x$ $q'_z = q_z$
(111)	$q'_x = 1+q_z$ $q'_y = 1-q_y$ $q'_z = 1-q_x$	(200)	$q'_x = 2 - q_z$ $q'_y = q_x$ $q'_z = q_y$
(111)	$q'_x = 1+q_y$ $q'_y = 1-q_z$ $q'_z = 1-q_x$	(200)	$q'_x = 2 + q_z$ $q'_y = q_x$ $q'_z = q_y$
(111)	$q'_x = 1+q_y$ $q'_y = 1+q_z$ $q'_z = 1-q_x$	(200)	$q'_x = 2 + q_y$ $q'_y = q_x$ $q'_z = q_z$
(111)	$q'_x = 1+q_x$ $q'_y = 1+q_y$ $q'_z = 1+q_z$	(200)	$q'_x = 2 + q_x$ $q'_y = q_y$ $q'_z = q_z$
(111)	$q'_x = 1+q_x$ $q'_y = 1+q_y$ $q'_z = 1-q_z$		
(111)	$q'_x = 1+q_x$ $q'_y = 1+q_z$ $q'_z = 1-q_y$		
(111)	$q'_x = 1 + q_x$ $q'_y = 1-q_z$ $q'_z = 1-q_y$		

TABLE A-3a (Continued)'

RECIPROCAL LATTICE POINT	TRANSFORMATIONS	RECIPROCAL LATTICE POINT	TRANSFORMATIONS
(220)	$q'_x = 2-q_y$ $q'_y = 2-q_x$ $q'_z = q_z$	(311)	$q'_x = 3 - q_z$ $q'_y = 1 - q_y$ $q'_z = 1 - q_x$
(220)	$q'_x = 2-q_z$ $q'_y = 2-q_x$ $q'_z = q_y$	(311)	$q'_x = 3 - q_y$ $q'_y = 1 - q_z$ $q'_z = 1 - q_x$
(220)	$q'_x = 2+q_z$ $q'_y = 2-q_x$ $q'_z = q_y$	(311)	$q'_x = 3 - q_x$ $q'_y = 1 - q_z$ $q'_z = 1 - q_y$
(220)	$q'_x = 2+q_y$ $q'_y = 2-q_x$ $z'_z = q_z$	(311)	$q'_x = 3 - q_x$ $q'_y = 1 + q_z$ $q'_z = 1 - q_y$
(220)	$q'_x = 2-q_z$ $q'_y = 2-q_y$ $q'_z = q_x$	(311)	$q'_x = 3 - q_x$ $q'_y = 1 + q_y$ $q'_z = 1 - q_z$
(220)	$q'_x = 2+q_z$ $q'_y = 2-q_y$ $q'_z = q_x$	(311)	$q'_x = 3 - q_x$ $q'_y = 1 - q_y$ $q'_z = 1 + q_z$
		(311)	$q'_x = 3 - q_y$ $q'_y = 1 + q_z$ $q'_z = 1 - q_x$

TABLE A-3b

TRANSFORMATIONS REQUIRED TO MAP $1/48^{th}$ OF THE FIRST BRILLOUIN ZONE OUT TO FURTHER ZONES. BODY CENTERED CUBIC.

RECIPROCAL LATTICE POINT	TRANSFORMATIONS	RECIPROCAL LATTICE POINT	TRANSFORMATIONS
(000)	$q'_x = q_x$ $q'_y = q_y$ $q'_z = q_z$	(110)	$q'_x = 1 + q_x$ $q'_y = 1 - q_z$ $q'_z = q_y$
(110)	$q'_x = 1 - q_y$ $q'_y = 1 - q_x$ $q'_z = q_z$	(110)	$q'_x = 1 + q_x$ $q'_y = 1 + q_z$ $q'_z = q_y$
(110)	$q'_x = 1 - q_z$ $q'_y = 1 - q_x$ $q'_z = q_y$	(110)	$q'_x = 1 + q_y$ $q'_y = 1 - q_z$ $q'_z = q_x$
(110)	$q'_x = 1 + q_z$ $q'_y = 1 - q_x$ $q'_z = q_y$	(110)	$q'_x = 1 + q_y$ $q'_y = 1 + q_z$ $q'_z = q_x$
(110)	$q'_x = 1 + q_y$ $q'_y = 1 - q_x$ $q'_z = q_z$	(200)	$q'_x = 2 - q_x$ $q'_y = q_y$ $q'_z = q_z$
(110)	$q'_x = 1 + q_x$ $q'_y = 1 - q_y$ $q'_z = q_z$	(200)	$q'_x = 2 - q_y$ $q'_y = q_x$ $q'_z = q_z$
(110)	$q'_x = 1 + q_x$ $q'_y = 1 + q_y$ $q'_z = q_z$	(200)	$q'_x = 2 + q_y$ $q'_y = q_x$ $q'_z = q_z$
(110)	$q'_x = 1 - q_z$ $q'_y = 1 - q_y$ $q'_z = q_x$	(200)	$q'_x = 2 - q_z$ $q'_y = q_x$ $q'_z = q_y$
(110)	$q'_x = 1 + q_z$ $q'_y = 1 - q_y$ $q'_z = q_x$	(200)	$q'_x = 2 + q_z$ $q'_y = q_x$ $q'_z = q_y$

TABLE A-3b (Continued)

RECIPROCAL LATTICE POINT	TRANSFORMATIONS	RECIPROCAL LATTICE POINT	TRANSFORMATIONS
(200)	$q'_x = 2 + q_x$ $q'_y = q_y$ $q'_z = q_z$		
(211)	$q'_x = 2 + q_z$ $q'_y = 1 - q_y$ $q'_z = 1 - q_x$		
(211)	$q'_x = 2 - q_z$ $q'_y = 1 - q_y$ $q'_z = 1 + q_x$		
(211)	$q'_x = 2 - q_y$ $q'_y = 1 - q_z$ $q'_z = 1 - q_x$		
(211)	$q'_x = 2 - q_x$ $q'_y = 1 - q_z$ $q'_z = 1 - q_y$		
(211)	$q'_x = 2 - q_y$ $q'_y = 1 + q_z$ $q'_z = 1 - q_x$		
(211)	$q'_x = 2 - q_x$ $q'_y = 1 + q_z$ $q'_z = 1 - q_y$		
(211)	$q'_z = 2 - q_x$ $q'_y = 1 + q_y$ $q'_z = 1 - q_z$		
(211)	$q'_x = 2 - q_x$ $q'_y = 1 + q_y$ $q'_z = 1 + q_z$		

this Thesis. It is to be noted, however, that one would be required to extend these transformations further out into reciprocal space, if materials with k_F values greater than that for lead were to be considered.

Having this transformation available, it is now simply necessary, (a) to determine $\underline{\varepsilon}(\underline{q}\lambda)$ and $\omega(\underline{q}\lambda)$ for the irreducible $1/48^{th}$ segment of the first Brillouin zone as in the calculation of $F(\omega)$, (b) apply the transformation until $\underline{q}$ becomes greater than $2k_F$, and (c) add up all contributions.

In order to now determine $\alpha^2(\omega)F(\omega)$ from equation (A-9) it is now simply necessary to determine the form of the electron-ion from factor $\omega(\underline{q})$. The different calculations of this function have been discussed in detail by Harrison[79] and where available, $\omega(\underline{q})$ takes the Heine-Abarenkov[34] form as tabulated by Harrison. For the alloys considered here and for which this data was not available, a form supplied by Taylor[81] appeared reliable. Where neither of these was available, an interpolated value between those reliable was utilized.

REFERENCES

1. H. K. Onnes,Commun. Phys. Lab. Univ. Leiden, No. 119b (1911)
2. See e.g. G. Rickayzen, Theory of Superconductivity, Interscience Publishers, New York,(1965).
3. B. T. Matthias, T. H. Geballe and V. B. Compton, Revs. Mod. Phys. 35, 1 (1963).
4. N. B. Hannay, T. H. Geballe, B. T. Matthias, K. Andres, P. Schmidt and D. MacNair, Phys. Rev. Lett., 14, 225 (1965).
5. J. F. Schooley, W. R. Hosler, E. Ambler, J. H. Becker, M. L. Cohen and C. S. Koona, Phys. Rev. Lett., 14, 305 (1965).
6. C. J. Gorter and H. B. G. Casimir, Phys. Z., 35, 963 (1934).
7. W. Meissner and R. Ochsenfeld, Naturwiss, 21, 787 (1933).
8. H. London and F. London, Proc. Roy. Soc. (London), A149, 71 (1935); Physica 2, 341 (1935).
9. F. London, Phys. Rev., 74, 562 (1948).
10. See e.g. J. R. Schrieffer, Theory of Superconductivity, Chapter VIII W. A. Benjamin Inc., New York,(1964).
11. B. S. Deaver and W. M. Fairbank, Phys. Rev. Lett., 7, 43 (1961).
12. R. Doll and M. Nabauer, Phys. Rev. Lett., 7, 51 (1961).
13. A. B. Pippard and T. E. Faber, Prog. Low Temp. Phys., I, 159 (1955).
14. M. A. Biondi, A. T. Forrester, M. P. Garfunkel, and C. B. Satterthwaite, Rev. Mod. Phys, 30, 1109 (1958).

15. E. Maxwell, Phys. Rev., 78, 477 (1950).

16. C. A. Reynolds, B. Serin and L. B. Nesbitt, Phys. Rev., 84, 691 (1951).

17. H. Fröhlich, Phys. Rev., 79, 845 (1950).

18. L. D. Landau, Zhur. Eksp. i Teoret. Fiz., 30, 1058 (1956). (English translation, Soviet Phys.-JETP, 3, 920 (1957)).

19. L. D. Landau, Zhur, Eksp. i Teoret. Fiz., 35, 97 (1958). (English translation, Soviet Phys. - JETP, 8, 70 (1959))

20. L. N. Cooper, Phys. Rev., 104, 1189 (1956).

21. J. Bardeen, L. N. Cooper and J. R. Schrieffer, Phys. Rev., 108, 1175 (1957).

22. Y. Nambu, Phys. Rev., 117, 648 (1960).

23. G. M. Eliashberg, Soviet Phys. JETP, 11, 696 (1960).

24. J. R. Schrieffer, Theory of Superconductivity, (W. A. Benjamin, Inc., New York, (1964)).

25. I. Giaever, Phys. Rev. Letters, 5, 147, 464 (1960).

26. I. Giaever, H. R. Hart, Jr. and K. Megerle, Phys. Rev., 126, 941 (1962).

27. J. M. Rowell, P. W. Anderson and D. E. Thomas, Phys. Rev. Letters, 10, 334 (1963).

28. For an excellent review of the present techniques of inelastic neutron scattering and of the present knowledge about phonons in metals see an article by B. N. Brockhouse, E. D. Hallman, and S. C. Ng in Magnetic and Inelastic Scattering of Neutrons by Metals, Edited by T. J. Rowland and P. A. Beck, Gordon and Breach, to be published.

29. J. R. Schrieffer, D. J. Scalapino, J. W. Wilkins, Phys. Rev. Letters, 10, 336 (1963).

30. W. L. McMillan and J. M. Rowell, Phys. Rev. Letters, 19, 108 (1965).

31. L. Schiff, Quantum Mechanics, McGraw Hill, New York, (1955).

32. See, for example J. M. Ziman, Electrons and Phonons, Clarendon Press, Oxford (1960).

33. Here we have closely followed the treatment by W. A. Harrison, Pseudopotentials in the Theory of Metals, W. A. Benjamin, Inc., New York (1966).

34. V. Heine and I. Abarenkov, Phil. Mag., 9, 451 (1964).

35. H. Fröhlich, Proc. Roy. Soc. Lond., A215, 291 (1952).

36. J. Bardeen and D. Pines., Phys. Rev., 99, 1140 (1955).

37. See e.g., E. A. Lynton, Superconductivity, Methuen and Co. Ltd, London (1961), Page 113.

38. N. N. Bogoliubov, Nuovo Cimento, 7, 794 (1958).

39. J. Valatin, Nuovo Cimento, 7, 843 (1958).

40. Y. Nambu, Phys. Rev. 117, 648 (1960).

41. L. P. Gor'kov, Soviet Phys. JETP, 7, 505 (1958).

42. F. J. Dyson, Phys. Rev., 75, 486 (1949).

43. A. B. Migdal, Soviet Physics JETP, 1, 996 (1958).

44. D. J. Scalapino, J. R. Schrieffer, and J. W. Wilkins, Phys. Rev., 148, 263 (1966).

45. N. N. Bogoliubov, V. V. Tolmachev, and D. V. Shirkov, A New Method in the Theory of Superconductivity, Consultant's Bureau, New York, (1959).

46. P. Morel and P. W. Anderson, Phys. Rev., 125, 1263 (1962).

47. G. Gamow, Zeit f. Physik, 51, 204 (1928).

48. R. H. Fowler and L. W. Nordheim, Proc. Roy Soc. (London) A119, 173 (1928).

49. J. Bardeen, Phys. Rev. Letters, 6, 57 (1961); 9, 147 (1962)

50. M. H. Cohen, L. M. Falicov, and J. C. Phillips, Phys. Rev. Letters, 8, 316 (1962).

51. W. L. McMillan and J. M. Rowell, Tunneling and the Strong Coupling Superconductor, to appear in a book on Superconductivity edited by R. D. Parks.

52. B. N. Brockhouse, T. Arase, G. Caglioti, K. R. Rao, A. D. B. Woods, Phys. Rev., 128, 1099 (1962).

53. L. Van Hove, Phys. Rev., 89, 1189 (1953).

54. J. M. Rowell and L. Kopf, Phys. Rev., 137, A907 (1965).

55. D. J. Scalapino and P. W. Anderson, Phys. Rev., 133, A921 (1964).

56. J. M. Rowell, W. L. McMillan and P. W. Anderson, Phys. Rev. Letters, 14, 633 (1965).

57. L. Holland, Vacuum Deposition of Thin Films, John Wiley and Sons, Inc. New York, (1956).

58. I. Dietrich, Z. Naturforsch, 17A, 94 (1962).

59. N. V. Zavaritskii, Soviet Phys. JETP, 18, 1260 (1964).

60. D. G. Walmsley, Ph.D. Thesis, McMaster University, (1965), unpublished.

61. H. J. Levinstein and J. E. Kunzler, LT 10 Conference, Moscow (1966).

62. N. Cabrera and N. F. Mott Reports on Progress in Phys., 12, 163 (1949).

63. A similar result was reported by I. Giaever, 2nd International Conference on Tunneling Phenomena in Solids, Riso, Denmark (1967).

64. B. D. Josephson, Phys. Letters, 1, 251 (1962).

65. B. D. Josephson, Revs. Mod. Phys., 36, 216 (1964).

66. M. H. Cohen and D. H. Douglass, Jr., Phys. Rev. Letters, 19, 118 (1967).

67. Myron Strongin, O. F. Kammerer, D. H. Douglass, Jr., and M. H. Cohen, Phys. Rev. Letters, 19, 121, (1967).

68. D. G. Walmsley, C. K. Campbell, R. C. Dynes, Can. J. Phys, in Press.

69. In order to produce symmetric junctions M-I-M, many investigators have formed oxides on lead films. The author has obtained a high degree of success on lead and lead-bismuth alloy films. See, C. K. Campbell, R. C. Dynes, and D. G. Walmsley, Can. J. Phys., 44, 2601, (1966).

70. J. Strong, H. V. Neher, A. E. Whitford, C. H. Cartwright, and R. Hayward, Procedures in Experimental Physics, Prentice-Hall, Inc. New York (1938).

71. The author is indebted to Mr. H. Walker who carried out these analyses.

72. C. H. Morgan, and B. McKay, B.Eng. Thesis, McMaster University (1966), unpublished.

73. J. G. Adler and J. E. Jackson, Rev. Sci. Inst., 37, 1049 (1966).

74. F. G. Brickwiedde, H. van Dijk, M. Durieux, J. R. Clement and J. K. Logan, National Bureau of Standards, Washington, Monograph 10, (1960).

75. For further details see J. M. Ziman, Electrons and Phonons, Clarendon Press, Oxford (1960).

76. M. Born and K. Huang, Dynamical Theory of Crystal Lattices, Oxford University Press (1954).

77. A. J. Bennett, Phys. Rev., 140, A1902 (1967).

78. R. Stedman, L. Almquist, G. Nilsson, Phys. Rev., 162, 549 (1967).

79. W. A. Harrison, Pseudopotentials in the Theory of Metals, W. A. Benjamin, Inc., New York (1966).

80. R. C. Dynes, J. P. Carbotte, and E. J. Woll, Jr., Solid State Comm., in Press.

81. D. W. Taylor and R. C. Dynes, Bull. Am. Phys. Soc., 13, 451 (1968).

82. T. M. Wu, Phys. Rev. Letters, 19, 508 (1967).

83. J. P. Carbotte and R. C. Dynes, Phys. Letters, 25A, 685 (1967). The value quoted in this Thesis for Δ_o is in slight disagreement with that quoted in this reference. A more careful solution of the gap equations yields the value quoted in the Thesis Δ_o = .190 meV.

84. J. P. Carbotte and R. C. Dynes, to be published.

85. S. B. Woods and J. S. Rogers, LT 10 Tenth International Conference on Low Temperatures, Moscow (1966).

86. J. M. Rowell and W. L. McMillan, Bull. Am. Phys. Soc., 12, 77 (1967)

87. T. Claeson, Solid State Comm., 5, 119 (1967).

88. J. G. Adler, J. E. Jackson and T. A. Will, Phys. Lett., 24A, 407 (1967).

89. N. V. Zavaritskii, JETP Letters, 6, 155, (1967).

90. I. M. Lifshitz, Soviet Phys. Uspekhi, 7, 549 (1965).

91. J. P. Franck and W. J. Keeler, Phys. Rev. Letters, 20, 379 (1968).

92. K. Andres and M. A. Jensen, Phys. Rev., 165, 533 (1968).

93. M. A. Jensen and K. Andres, Phys. Rev., 165, 545 (1968).

94. N. F. Berk and J. R. Schrieffer, Phys. Rev. Letters, 17, 433 (1966).

95. For Na A. D. B. Woods, B. N. Brockhouse, R. H. March and A. T. Stewart, Phys. Rev., 128, 1112 (1962).

96. For K see R. A. Cowley, A. D. B. Woods and G. Dolling, Phys. Rev., 150, 487 (1966).

97. For Aℓ see G. Gilat and R. M. Nicklow, Phys. Rev., 143, 487 (1966).

98. for Pb and the alloys considered, see (28) and S. C. Ng, Ph.D. Thesis, McMaster University, Hamilton, Ontario, Canada (unpublished).

99. W. Kohn, Phys. Rev. Letters, 2, 393 (1959).

100. E. J. Woll and W. Kohn, Phys. Rev., 126, 1693 (1962).

101. J. P. Carbotte and R. C. Dynes, Phys. Letters, 25A, 532 (1967).

102. G. Gilat and L. J. Raubenheimer, Phys. Rev., 144, 390 (1966).